

POLITECNICO DI TORINO

Master of Science in Mechanical Engineering

Master Degree Thesis



EXPERIMENTAL ANALYSIS AND FEM SIMULATION OF VIBRATING PLATES AND ACOUSTIC GUITAR SOUNDBOARD

Supervisor

Professor Alessandro Fasana

Candidate

Castaldo Giorgio

April 2018

Alla mia famiglia, a Francesca, ai miei amici
che mi sono stati accanto in questo lungo percorso.

TABLE OF CONTENTS

LIST OF FIGURES AND TABLES	ix
ABSTRACT.....	xiii

PART I

1 PLATE VIBRATIONS	1
1.1 PLATE EIGENPROBLEM.....	1
1.2 NATURAL FREQUENCIES AND MODE SHAPES	3
1.3 ANALYTICAL MODEL	6
1.3.1 SIMPLY SUPPORTED PLATE	7
1.3.2 CLAMPED-FREE PLATE	11
1.3.3 FREE PLATE.....	15
2 FINITE ELEMENTS SIMULATION	17
2.1 SIMPLY SUPPORTED PLATE	18
2.2 CLAMPED-FREE PLATE	21
2.3 FREE PLATE	24
3 PLATE SPECIMEN CHARACTERISTICS	26
3.1 PRELIMINARY CONSIDERATIONS	26
3.2 DENSITY AND YOUNG MODULUS ESTIMATION	27
4 LABORATORY EXPERIENCES	29
4.1 EQUIPMENT AND MAIN PROCEDURE.....	29
4.2 LABORATORY TESTS.....	32
4.2.1 CHLADNI PLATES EXPERIENCE	32
4.2.2 PSD COMPUTATION - ACCELEROMETERS MEASUREMENTS	39
4.2.3 PSD COMPUTATION - LASER MEASUREMENTS.....	43
5 PROCEDURE FOR STUDENTS EXPERIENCE	47

PART II

1 GUITAR ANATOMY AND PHYSICS	53
1.1 STRINGS	53
1.2 COUPLED RESONATORS	54
1.3 SOUNDBOARD	56
1.4 SOUNDBOARD BRACING	57
1.4.1 LAYOUT	57
1.4.2 SECTION SHAPE AND DIMENSIONS	58
1.4.3 LONGITUDINAL PROFILE	58
2 FEM SIMULATIONS	59
2.1 MODE SHAPES	61
2.1.1 FROM BLANK TO BRACED SOUNDBOARD	61
2.1.2 MATERIAL REMOVAL	64
2.2 NATURAL FREQUENCIES	67
2.3 CONSIDERATIONS	70
3 EXPERIMENTAL MEASUREMENTS	71
3.1 BLANK SOUNDBOARD	71
3.1.1 EXPERIMENTAL LAYOUT AND CONSIDERATIONS	71
3.1.2 TRANSFER FUNCTION	74
3.2 BRACED SOUNDBOARD	77
3.3 LIGHTENED AND SCALLOPED BRACED SOUNDBOARD	83
3.4 FINAL RESULTS AND CONSIDERATIONS	87
4 CONCLUSIONS AND POSSIBLE APPLICATIONS	89
BIBLIOGRAPHY	93

LIST OF FIGURES – Part I

- Figure 1.1 (a) plate element, system of reference; (b) - forces and moments acting on the plate element. [1]
- Figure 1.2 - Some mode shapes at high frequencies of a completely free square plate. [2]
- Figure 1.3 – The three B.C. configurations analyzed. [2]
- Figure 1.4 - Mode shapes for SSSS plate
- Figure 1.5 – Comparison between plate (a) and beam (b) mode shapes, (b) . [2]
- Figure 1.6 – Mode shapes for FCFC plate
- Figure 1.7 – Beam mode shapes for clamped-clamped and free-free cases
- Figure 1.8 – Experimental mode shapes. [2]
- Figure 2.1 – FE model of the plate.
- Figure 2.2 – SSSS boundary conditions.
- Figure 2.3/2.5 – Mode shapes changes due to added concentrated mass, SSSS case.
- Figure 2.6 – FCFC boundary conditions
- Figure 2.7/2.11 – Mode shapes changes due to added concentrated mass, FCFC case.
- Figure 2.12 – FFFF Mode shapes.
- Figure 3.1 – Young modulus estimation graphic.
- Figure 4.1/4.7 – Laboratory equipment and materials.
- Figure 4.8 – Reproduction of Chladni’s original demonstrative set of plates.
- Figure 4.9 – Example of Chladni patterns in guitar soundboards, from Wikipedia.
- Figure 4.10 – Comparison between predicted and experimental shapes.
- Figure 4.11 – A detail of the central constrain.
- Figure 4.12/4.20 – FEM mode shapes and their corresponding experimental picture.
- Figure 4.21 – Mode shapes obtained with a violin bow.
- Figure 4.22 – Drawing of accelerometers positions.
- Figure 4.23/4.27 – Power spectral density graphics from accelerometers measurement.
- Figure 4.28 – FEM and picture of a ‘twin’ mode shape.
- Figure 4.29 – Picture of the laser head support structure.
- Figure 4.30/4.33 – Power spectral density graphics from laser measurement.

LIST OF TABLES – Part I

- Table 1.1 - λ_{ij} dependence on ν for different aspect ratios. [2]
- Table 1.2 – λ_{ij} parameter for six modes, for different aspect ratios, SSSS plate. [2]
- Table 1.3 – parameters for approximated natural frequency formula. [2]
- Table 1.4 – comparison between exact and approximated frequencies, SSSS plate.
- Table 1.5 - λ_{ij} parameter for six modes, for different aspect ratios, FCFC plate. [2]
- Table 1.6 - comparison between exact and approximated frequencies, FCFC plate.
- Table 1.7 – Beam mode shapes formulas for different boundary conditions. [2]
- Table 1.8 - λ_{ij} parameter for six modes, for different aspect ratios, FFFF plate. [2]
- Table 1.9 - comparison between exact and approximated frequencies, FFFF plate.
- Table 1.10 – Comparison between SSSS, FCFC and FFFF natural frequencies
- Table 2.1 – Natural frequencies comparison between analytical and numerical results, SSSS plate.
- Table 2.2 – Natural frequencies comparison between analytical and numerical results, FCFC plate.
- Table 2.3 – Natural frequencies comparison between analytical and numerical results, FFFF plate.
- Table 3.1 – Materials data.
- Table 3.2 – Materials performance comparison.
- Table 3.3 – Young modulus estimation table.
- Table 4.1 – Comparison between numerical and experimental natural frequencies.
- Table 5.1 – FEM mode shapes and natural frequencies to be reproduced experimentally by students.

References:

- [1] From Genta G, *Vibration of structures and machines*, Springer, 1999.
- [2] From Blevins, Robert D., *Formulas for natural frequencies and mode shapes*, Van Nostrand Reinhold Company, 1979.

LIST OF FIGURES – Part II

- Figure 1.1 – String mode shapes.
- Figure 1.2 – Guitar bridge and saddle detail.
- Figure 1.3 – Helmholtz resonator equivalent model [3].
- Figure 1.4 – Scheme of guitar parts as resonators [3].
- Figure 1.5 – 2 and 3 d.o.f. mass-spring equivalent models [3].
- Figure 1.6 – Modes of the soundboard-cavity air-back system [3].
- Figure 1.7 – Main guitar body shapes, from Wikipedia.
- Figure 1.8 – Different bracing layouts.
- Figure 1.9 – Bracing cross section shape, from *Principles of guitar dynamics and design* by Ervin Somogyi, <http://www.esomogyi.com>
- Figure 1.10 – Examples of straight and scalloped braced soundboards.
- Figure 2.1 – Soundboard dimensions for the FEM model.
- Figure 2.2 – Braced soundboard FEM model.
- Figure 2.3/2.5 – Different steps of the FEM model, from blank to scalloped.
- Figure 2.6 – FEM mode shapes of free blank soundboard.
- Figure 2.7/2.8 – FEM mode shapes of partially braced free soundboard.
- Figure 2.9 – FEM mode shapes of fully braced free soundboard.
- Figure 2.10/ 2.12 – Comparison between blank and partially braced shapes, fixed soundboard.
- Figure 2.13/ 2.14 – FEM mode shapes of fully braced, fixed soundboard.
- Figure 2.15 – FEM mode shapes of fully scalloped, free soundboard.
- Figure 2.16/ 2.21 – Comparison, in more steps, between mode shapes of straight and scalloped braced, fixed soundboard.
- Figure 3.1 – Blank soundboard.
- Figure 3.2 a) – Probe and hammer used in the measurements.
- Figure 3.2 b) – Reference points on the blank soundboard.
- Figure 3.3 a) – The experimental setup in the anechoic chamber.
- Figure 3.3 b) – A phase of the measuring process.
- Figure 3.4/3.6 – Transfer function plots for measurements on blank soundboard.
- Figure 3.7/3.8 – Steps in the building of the braced soundboard.

Figure 3.9 – Reference points on the braced soundboard.

Figure 3.10/3.15 – Transfer function plots for measurements on braced soundboard.

Figure 3.16 – Detail of the scalloped braced soundboard.

Figure 3.17/3.19 – Transfer function plot for measurements on scalloped soundboard.

Figure 3.20 – A comparison of the transfer functions for the three stages.

LIST OF TABLES – Part II

Table 1.1 – Guitar strings fundamental frequencies.

Table 2.1 – Natural frequencies comparison in the free soundboard configuration.

Table 2.2 - Natural frequencies comparison in the fixed soundboard configuration.

Table 3.1 – Natural frequencies of most evident resonances for the three cases.

References:

[3] From Rossing, Thomas D., *The science of string instruments*, Springer, 2010.

ABSTRACT

The aim of this study is, in its first part, the description of the dynamic behavior of metal plates, with the computation of natural frequencies and mode shapes; the problem has been approached with different methods, each of them highlighting a particular perspective.

The main points of part I are:

- The presentation of the theoretical background of the vibrating plate, to understand the phenomenon, the main physical quantities involved, and the mathematical equations ruling vibrations.
- An analytical computation, through equations previously demonstrated, of natural frequencies and mode shapes for a set of different cases.
- A Finite Elements study, both for confirming the previous point, and to provide results for cases that are too complex for the closed-form solution.
- The detailed description of the design, building and set up procedure of the laboratory test rig to verify the model, and the discussion of the obtained results.
- The definition of a didactic experience, to be conducted by students in the DEXPILAB laboratories, with the relative operative procedure and safety norms.

A practical application of this first study has been carried out in the second part of the thesis, where it has been used to design, and build, the top soundboard of a string instrument, a guitar, providing it with the desired acoustic properties.

In particular, this second part consists of:

- A description of the physics of the instrument, highlighting the link between the way it is designed and built, and the dynamic properties that one should achieve.
- The modelling, through FEM, of the instrument soundboard to understand the importance of the reinforcement ribs pattern in the dynamic behavior.
- The practical construction of a braced soundboard, tuned step by step with a specific technique, and simultaneously analyzed with laboratory measurements.

ABSTRACT

Lo scopo di questo studio, nella sua prima parte, è la descrizione del comportamento dinamico di piastre metalliche, con il calcolo delle frequenze naturali e delle forme modali; il problema è stato affrontato con diversi metodi, ciascuno per sottolinearne un particolare aspetto.

I punti principali della prima parte sono:

- La presentazione dell'aspetto teorico della vibrazione delle piastre, per comprendere il fenomeno, le equazioni che lo governano e le principali grandezze fisiche coinvolte.
- Il calcolo analitico, attraverso le equazioni dimostrate precedentemente, delle frequenze naturali e delle forme modali per diversi casi.
- Un'analisi agli elementi finiti, sia per confermare il punto precedente, sia per fornire risultati per i casi troppo complessi per una soluzione analitica in forma chiusa.
- La descrizione dettagliata della progettazione, costruzione e configurazione di un banco sperimentale per verificare il modello, e discutere i risultati ottenuti.
- La definizione di un'esperienza didattica per gli studenti, da svolgere nei laboratori DEXPILAB del Politecnico, con la relativa procedura operativa e norme di sicurezza.

Un'applicazione pratica è stata sviluppata nella seconda parte della tesi, per progettare e costruire la tavola armonica di uno strumento a corde, in particolare una chitarra acustica, garantendo le proprietà acustiche desiderate.

In particolare, la seconda parte consiste di:

- La descrizione della fisica dello strumento, sottolineando il legame tra ciascun componente e le proprietà dinamiche e acustiche complessive.
- La modellazione FEM della tavola armonica dello strumento, per comprendere l'importanza della catenatura di rinforzo nel comportamento dinamico.
- La costruzione pratica di una tavola armonica rinforzata, accordata con una tecnica specifica, e contemporaneamente analizzata con misure di laboratorio.

PART I

1 PLATE VIBRATIONS

1.1 PLATE EIGENPROBLEM [1]

In the study of plates, the following assumption will be made:

1. thickness is small compared to the edges, less than 1/10 of the minimum one, and constant.
2. Homogeneous, isotropic, linearly elastic material.
3. Rotary inertia and shear deformation are neglected, flexural deformation is small compared to thickness, and midsurface in undeformed condition remains such during deformation; this is the so-called Kirchhoff plate, as opposed to Mindlin plate, in which shear is not neglected, due to higher thickness.
4. In-plane load is zero, unlike membranes, in which this load acts like a restoring force, while material elasticity is not considered.

The description of the physical model with related pictures and equations are taken from Genta G, *Vibration of structures and machines*.

If we consider a portion of plate with edges dx , dy and thickness h (Fig. 1.1a), forces and moments it undergoes are represented (Fig. 1.1b):

parallel to y axis

- Shear forces (per unit length) F_y
- Bending moment (per unit length) M_y
- Twisting moment (per unit length) M_{yx}

parallel to x axis:

- Shear forces (per unit length) F_x
- Bending moment (per unit length) M_x
- Twisting moment (per unit length) M_{xy}

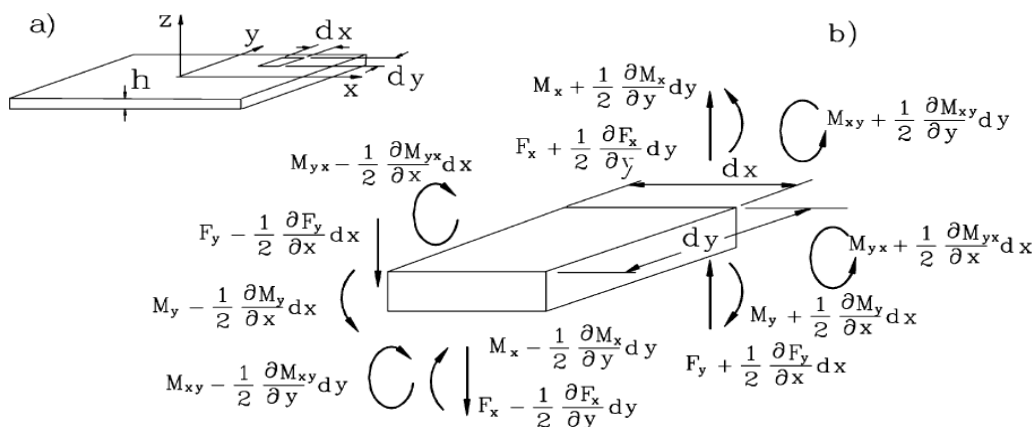


Figure 1.1 (a) - plate element, system of reference; (b) - forces and moments acting on the plate element

Balancing forces and moments, and considering an external force distribution $f_z(x, y, t)$ the translational and rotational equilibrium equations are obtained

$$\left\{ \begin{array}{l} \rho h \frac{d^2 u_z}{dt^2} dx dy = \frac{F_x}{\partial x} dx dy + \frac{F_y}{\partial y} dx dy + f_z dx dy \\ \frac{\partial M_{xy}}{\partial x} + \frac{\partial M_x}{\partial y} + \partial F_x = 0 \\ \frac{\partial M_y}{\partial x} + \frac{\partial M_{xy}}{\partial y} - \partial F_y = 0 \end{array} \right. \quad (1.1)$$

From previous equilibrium equations, it follows:

$$\rho h \frac{d^2 u_z}{dt^2} = \frac{\partial^2 M_y}{\partial x^2} + \frac{\partial^2 M_{xy}}{\partial x \partial y} - \frac{\partial^2 M_x}{\partial y^2} + f_z \quad (1.2)$$

The relationship between moments and deformation can be expressed as follows. The bending moment M_y is obviously linked to curvature in xz plane but a contribution of the yz plane deformation is present, too: unlike in beams, where the cross section in the analyzed plane xz would be free to contract on the direction perpendicular to the plane yz, due to Poisson effect, here in plates this motion is prevented by adjacent material, creating a M_x moment acting in yz plane. Therefore, if we define the bending stiffness of the plate as $B = \frac{Eh^3}{12(1-\nu^2)}$ and approximate curvatures with second derivatives of displacements $\frac{\partial^2 u_z}{\partial x^2}$ and $\frac{\partial^2 u_z}{\partial y^2}$, moments expressions are:

$$\left\{ \begin{array}{l} M_y = -B \left(\frac{\partial^2 u_z}{\partial x^2} + \nu \frac{\partial^2 u_z}{\partial y^2} \right) \\ M_x = B \left(\frac{\partial^2 u_z}{\partial y^2} + \nu \frac{\partial^2 u_z}{\partial x^2} \right) \\ M_{xy} = -B(1-\nu) \frac{\partial^2 u_z}{\partial x \partial y} \end{array} \right. \quad (1.3)$$

Equation of motion (1.2), with these moments expressions (1.3), becomes

$$\frac{\rho h}{B} \frac{\partial^2 u_z}{\partial t^2} + \frac{\partial^4 u_z}{\partial x^4} + 2 \frac{\partial^4 u_z}{\partial x^2 \partial y^2} + \frac{\partial^4 u_z}{\partial y^4} = \frac{f_z}{B} \quad (1.4)$$

Since we are interested in the eigenvalue problem, we will consider the homogeneous equation of motion neglecting external force distribution f_z .

Assuming solution as the product of a harmonic function $\eta(t)$, and one of space alone $q(x, y)$

$$u_z(x, y, t) = q(x, y)\eta(t) \quad (1.5)$$

and assuming the time function $\eta(t)$ is harmonic, the equation of motion (1.4) finally gives the eigenproblem equation, a 4th order, partial derivative differential equation.

$$\omega^2 \frac{\rho h}{B} q(x, y) + \frac{\partial^4 q(x, y)}{\partial x^4} + 2 \frac{\partial^4 q(x, y)}{\partial x^2 \partial y^2} + \frac{\partial^4 q(x, y)}{\partial y^4} = 0 \quad (1.6)$$

1.2 NATURAL FREQUENCIES AND MODE SHAPES [2]

The analytical part of this study will often resort to picture, formulas and tables from Blevins, Robert D., *Formulas for natural frequencies and mode shapes*.

Given i and j , integer numbers of flexural halfwaves in x and y directions respectively, the deformation can be expressed, according to the expansion theorem, as the sum of modal deformations:

$$u = \sum_i \sum_j A_{ij} q_{ij} \sin(2\pi f_{ij} t + \phi_{ij}) \quad (1.7)$$

So, for any i and j for which a vibration mode exists, we can define:

1. Amplitude A_{ij}
2. Mode shape q_{ij}
3. Natural frequency f_{ij}
4. Phase angle ϕ_{ij}

Natural frequencies

The exact natural frequencies of the plate are given by the expression

$$f_{ij} = \frac{\lambda_{ij}^2}{2\pi a^2} \left[\frac{Eh^3}{12\gamma(1-\nu^2)} \right]^{1/2} \quad (1.8)$$

where λ_{ij} parameter depends on mode indices i and j , plate geometry and aspect ratio, boundary conditions, and weakly on Poisson ratio ν .

$$\lambda_{ij} = \lambda_{ij} \left(\frac{a}{b}, b.c., \nu \right) \quad (1.9)$$

Tables with λ_{ij} values will be used later on for computations.

An approximated closed form solution for frequencies exists, too, obtained using Rayleigh energy method and assuming beam mode shapes:

$$f_{ij} = \frac{\pi}{2} \left[\frac{G_1^4}{a^4} + \frac{G_2^4}{b^4} + \frac{2J_1 J_2 + 2\nu(H_1 H_2 - J_1 J_2)}{a^2 b^2} \right]^{1/2} \left[\frac{Eh^3}{12\gamma(1-\nu^2)} \right]^{1/2} \quad (1.10)$$

where coefficients G , H and J for each couple of edges (index 1 when referring to sides of length b , index 2 for sides of length a) are tabulated as function of B.C. and mode indexes i and j . The error made using this approximation is below 5%, but with clamped or supported edges, it is much lower since the beam mode shapes are very accurate for these types of boundary condition (see paragraph below).

Mode shapes

Since a general analytical form for mode shapes of a plate with generic boundary condition doesn't exist, an approximation involving a series of beam mode shapes, \tilde{q}_m and \tilde{q}_n , is used:

$$q_{ij}(x, y) = \sum_m \sum_n \tilde{q}_m(x) \tilde{q}_n(y) \quad (1.11)$$

For boundary conditions with certain patterns, the first term alone

$$q_{ij}(x, y) \approx \tilde{q}_m(x)\tilde{q}_n(y) \quad (1.12)$$

is sufficient to approximate the mode shapes; some peculiar cases are:

1. If the plate has two opposite free edges, there will be a mode in which $\tilde{q}_n \approx 1$, i.e. the half wave in that direction is basically flat.
2. If two opposite edges are simply supported, the beam mode shape in this direction will be exactly $\tilde{q}_n(x) = \sin\left(\frac{i\pi x}{a}\right)$, resulting in the plate mode shape

$$q_{ij}(x, y) = \sin\left(\frac{i\pi x}{a}\right)\tilde{q}_m(y) \quad (1.13)$$

3. Similarly, if all the four edges are simply supported, the mode shape is

$$q_{ij} = \sin\left(\frac{i\pi x}{a}\right)\sin\left(\frac{j\pi y}{b}\right) \quad (1.14)$$

As the boundary conditions become less regular, for example if there is not even a couple of opposite supported edges, the expression (1.12) is no longer enough to describe the mode shapes, and a higher order expansion of (1.11) is needed. A typical example is the completely free plate, where the deformations along directions x and y intermingle in more complex patterns; an example is provided below (Fig. 1.2), further considerations about the completely free vibrating plate will follow.

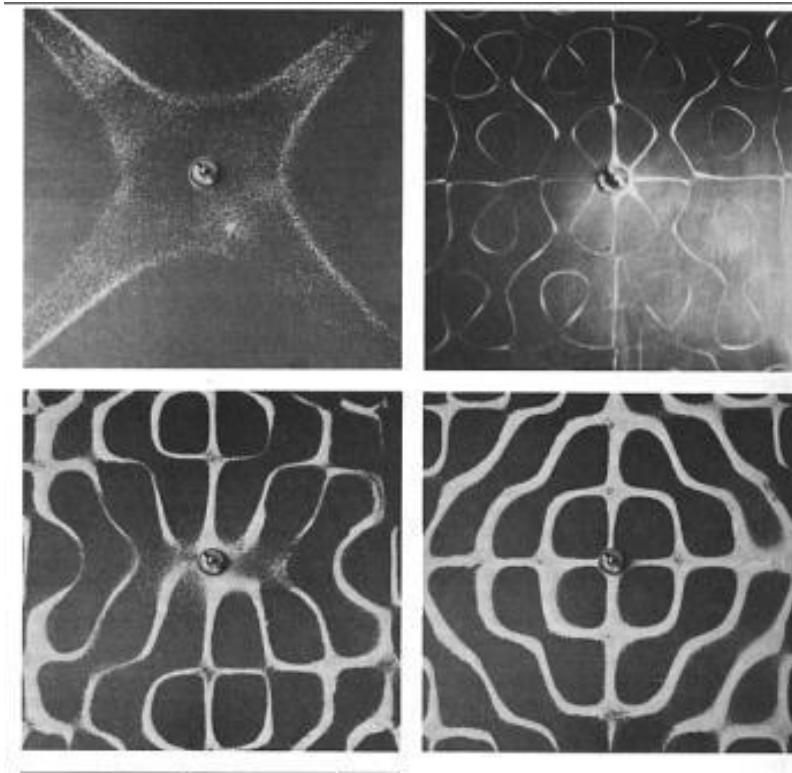


Figure 1.2 - Some mode shapes at high frequencies of a completely free square plate.

Other considerations

λ_{ij} parameter depends on ν only if there is at least one free edge, anyway dependence is weak.

Table 1.1 - λ_{ij} dependence on ν for different aspect ratios.

$\frac{a}{b}$	λ_{11}^2		
	$\nu = 0.0$	$\nu = 0.3$	$\nu = 0.5$
0.4	9.870	9.760	9.451
1.0	9.870	9.631	9.079
2.5	9.870	9.484	8.704

Rotary inertia and shear deformation have been neglected in this plate model; if they are taken into account, and it is necessary to describe accurately thicker plates (like in the Mindlin model), natural frequencies are lowered since, considering these additional stresses, the body acts as more deformable.

1.3 ANALYTICAL MODEL

On the basis of the theoretical model described above, natural frequencies and modal shapes have been computed analytically, implementing a procedure on MATLAB. The computation has been carried out for three different boundary condition constraint configurations (Fig 1.3)

1. plate simply supported on all four edges ('SSSS' configuration);
2. plate with a couple of clamped opposite edges, and the other couple free ('FCFC' configuration);
3. completely free plate ('FFFF configuration).

Analytical computation, and FE analysis later on, will be done on a 1,25 mm thick, 300 mm x 300 mm aluminum plate. Plates of different materials and dimension have been considered in the experimental part, and their choice will be discussed and motivated in chapter 3.

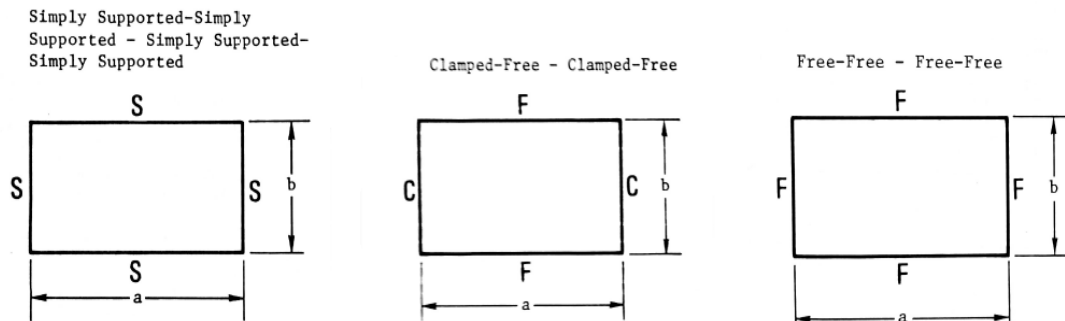


Figure 1.3 – The three B.C. configurations analyzed.

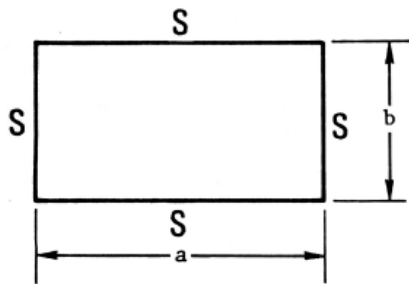
1.3.1 SIMPLY SUPPORTED PLATE

Natural frequencies

Exact natural frequencies can be computed using equation (1.8), where the λ parameter can be found on tables once boundary conditions and aspect ratio are fixed; the parameter is provided only for first six modes (Tab 1.2).

Table 1.2 – parameter for six modes, for different aspect ratios.

16. Simply Supported-Simply Supported - Simply Supported-Simply Supported



$\frac{a}{b}$	Mode Sequence					
	1	2	3	4	5	6
0.4	11.45 (11)	16.19 (12)	24.08 (13)	35.14 (14)	41.06 (21)	45.80 (22)
2/3	14.26 (11)	27.42 (12)	43.86 (21)	49.35 (13)	57.02 (22)	78.96 (23)
1.0	19.74 (11)	49.35 (21)	49.35 (12)	78.96 (22)	98.70 (31)	98.70 (13)
1.5	32.08 (11)	61.69 (21)	98.70 (12)	111.0 (31)	128.30 (22)	177.7 (32)
2.5	71.56 (11)	101.16 (21)	150.5 (31)	219.6 (41)	256.6 (12)	286.2 (22)

$$\lambda_{ij}^2 = \pi^2 \left[i^2 + j^2 \left(\frac{a}{b} \right)^2 \right]$$

Since we would like to know more than only six frequencies, the approximated formula (1.10) should be resorted to; parameters G, H and J depend on boundary conditions on pair of opposite edges, and can be computed using tables according to the current configuration (case 4 on table X.Y below) for both edges pairs:

Table 1.3

Boundary Conditions on Opposite Edges	Mode Index (a) (n)	$G^{(a)}$	$H^{(a)}$	$J^{(a)}$
1. Free-Free	1	0	0	0
	2	0	0	1.216
	3	1.506	1.248	5.017
	$n (n > 3)$	$n - \frac{3}{2}$	$\left(n - \frac{3}{2}\right) \left[1 - \frac{2}{\left(n - \frac{3}{2}\right)^n}\right]$	$\left(n - \frac{3}{2}\right)^2 \left[1 + \frac{6}{\left(n - \frac{3}{2}\right)^n}\right]$
2. Simply Supported-Free	1	0	0	0.3040
	2	1.25	1.165	2.756
	3	2.25	4.346	7.211
	$n (n > 1)$	$n - \frac{3}{4}$	$\left(n - \frac{3}{4}\right)^2 \left[1 - \frac{1}{\left(n - \frac{3}{4}\right)^n}\right]$	$\left(n - \frac{3}{4}\right)^2 \left[1 + \frac{3}{\left(n - \frac{3}{4}\right)^n}\right]$
3. Clamped-Free	1	0.597	-0.0870	0.471
	2	1.496	1.347	3.284
	3	2.500	4.658	7.842
	$n (n > 2)$	$n - \frac{1}{2}$	$\left(n - \frac{1}{2}\right)^2 \left[1 - \frac{2}{\left(n - \frac{1}{2}\right)^n}\right]$	$\left(n - \frac{1}{2}\right)^2 \left[1 + \frac{2}{\left(n - \frac{1}{2}\right)^n}\right]$
4. Simply Supported-Simply Supported	1	1	1	$J = H$
	2	4	4	
	3	9	9	
	n	n^2		
5. Clamped-Simply Supported	1	1.25	1.165	$J = H$
	2	2.25	4.346	
	3	3.25	9.528	
	n	$n + \frac{1}{4}$	$\left(n + \frac{1}{4}\right)^2 \left[1 - \frac{1}{\left(n + \frac{1}{4}\right)^n}\right]$	
6. Clamped-Clamped	1	1.506	1.248	$J = H$
	2	2.5	4.658	
	3	3.5	10.02	
	$n (n > 1)$	$n + \frac{1}{2}$	$\left(n + \frac{1}{2}\right)^2 \left[1 - \frac{2}{\left(n + \frac{1}{2}\right)^n}\right]$	

(a) $G = G_1, H = H_1, J = J_1$, and mode index = i when boundary conditions are applied to sides of length b . $G = G_2, H = H_2, J = J_2$, and mode index = j when boundary conditions are applied to sides of length a . Ref. 11-61.

Exact and approximated natural frequencies, with their relative error, is summarized in the Table 1.4:

Table 1.4

F exact [Hz]	F approx [Hz]	Relative error
67,46	67,45	-0,004%
168,64	168,63	-0,004%
168,64	168,63	-0,004%
269,83	269,82	-0,004%
337,28	337,27	-0,004%
337,28	337,27	-0,004%
-	438,45	-
-	438,45	-
-	573,36	-
-	573,36	-
-	607,08	-

As expected, the error between approximated and exact values is almost negligible for this kind of boundary condition, since the assumed beam shapes, from which the parameters G , H , J are obtained, are exact for this B.C. configuration.

Mode shapes

As mentioned before, the regularity of B.C. allows an easy computation, resulting in mode shapes that are, in x direction and y direction, simply those of a beam supported on both sides; mathematically, eigenvectors are exactly those predicted by (1.14), i.e.

$$q_{ij} = \sin\left(\frac{i\pi x}{a}\right) \sin\left(\frac{j\pi y}{b}\right) \quad (1.14)$$

Mode shapes for modes i, j from 1 to 3 are pictured below (Fig 1.4); the number of halfwaves in x and y directions can easily be spotted.

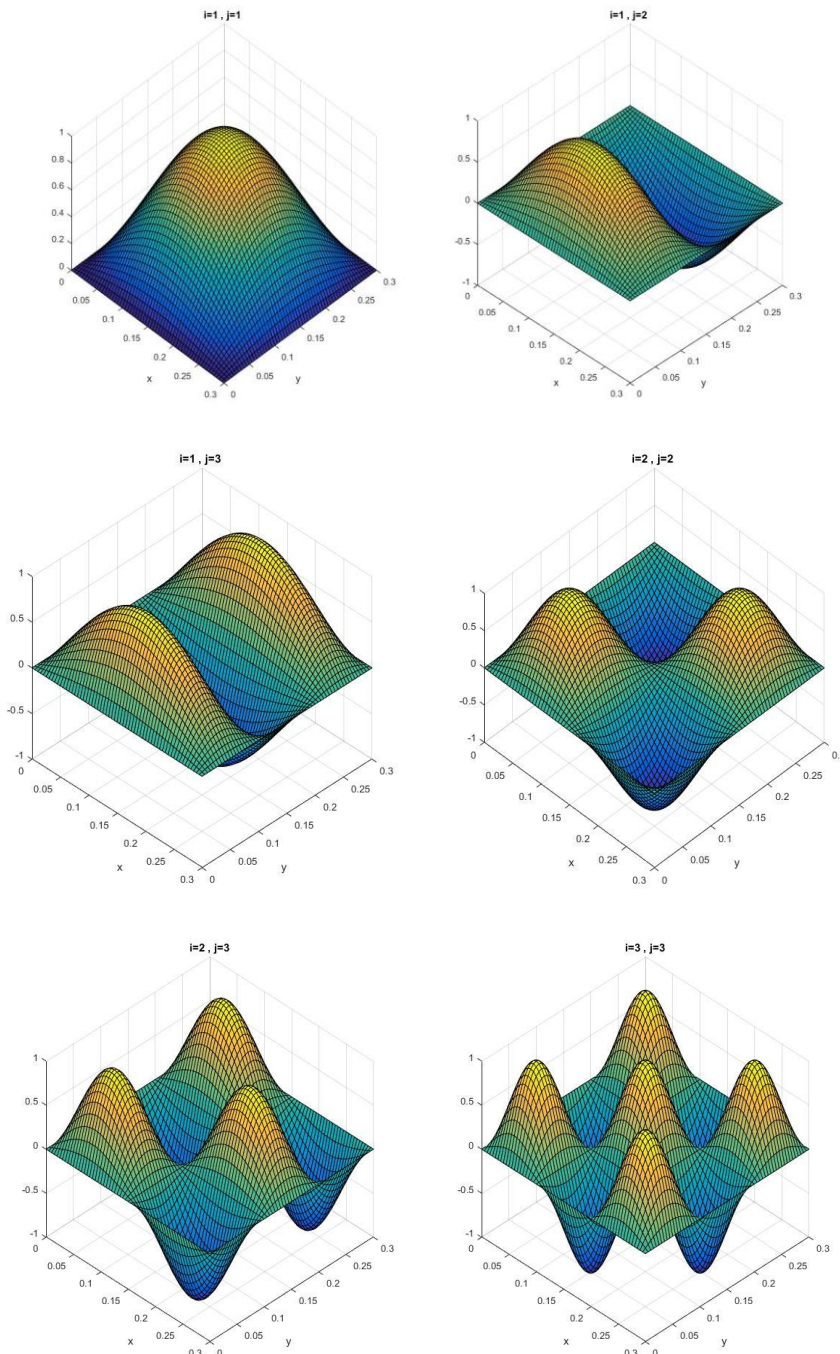


Figure 1.4

The beam mode shapes are even more evident if we look at the plate from a direction parallel to one of the edges: in the Figure 1.5 a) below for mode (3,2) there are three halfwaves along x direction and two along y direction, while Fig 1.5 b) shows beam mode shapes for the pinned-pinned case.

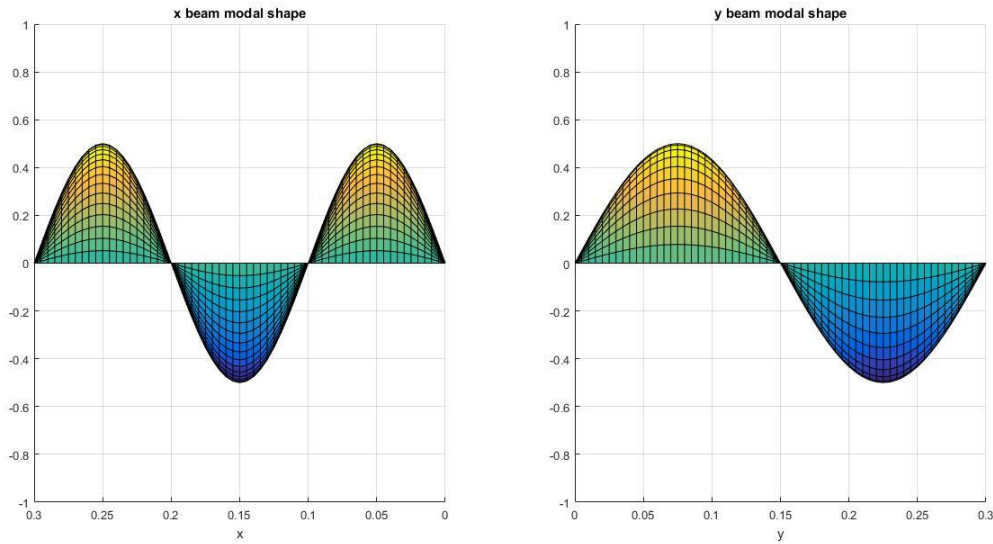


Figure 1.5 a)

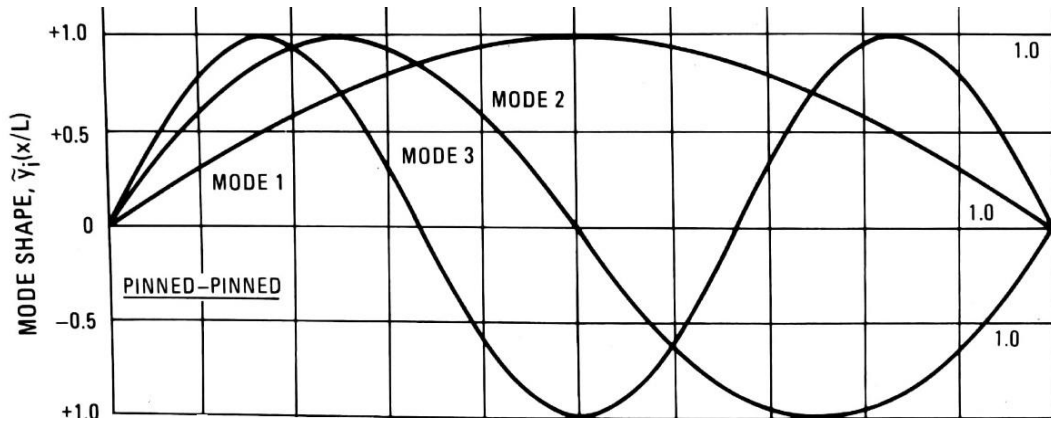


Figure 1.5 b)

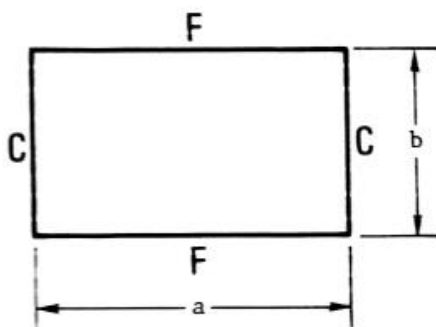
1.3.2 CLAMPED-FREE PLATE

Natural frequencies

Resorting again to equation (1.8), and finding the λ parameter on the specific table (Tab 1.5) for this boundary conditions and the usual aspect ratio, the first six frequencies can be computed.

Table1.5

8. Clamped-Free - Clamped-Free



$\frac{a}{b}$	Mode Sequence					
	1	2	3	4	5	6
0.4	22.35 (11)	23.09 (12)	25.67 (13)	30.63 (14)	38.69 (15)	49.86 (16)
2/3	22.31 (11)	24.31 (12)	31.70 (13)	46.82 (14)	61.57 (21)	64.34 (22)
1.0	22.27 (11)	26.53 (12)	43.66 (13)	61.47 (21)	67.55 (22)	79.90 (14)
1.5	22.21 (11)	30.90 (12)	61.30 (21)	70.96 (13)	74.26 (22)	118.3 (23)
2.5	22.13 (11)	41.69 (12)	61.00 (21)	92.38 (22)	119.9 (31)	157.8 (32)

$\nu = 0.3$

For the approximated formula, parameters now discriminate between G_1, H_1, J_1 for the clamped-clamped opposite edges (case 6 on the table 1.3), and G_2, H_2, J_2 for the free-free pair edges (case 1).

Both exact and approximated frequencies are reported:

Table1.6

F exact [Hz]	F approx [Hz]	Relative error
77,13	76,49	-0,821%
90,66	90,36	-0,333%
149,20	149,72	0,349%
210,06	210,79	0,350%
230,84	230,36	-0,204%
273,04	270,19	-1,043%
-	300,45	-
-	384,90	-
-	413,15	-
-	416,72	-
-	420,13	-

the error between approximated and exact values is still very low, but anyway two orders of magnitude higher than in the SSSS configuration, because, given the lower regularity of the boundary condition, the beam mode shapes are now less accurate.

Mode shapes

Mode shapes can still be found using (1.12), but the functions $\tilde{q}_m(x)$ and $\tilde{q}_n(y)$ now are not simple sines, and can be found on beam mode shapes tables (Tab X.Y);

$$q_{ij}(x, y) \approx \tilde{q}_m(x)\tilde{q}_n(y) \quad (1.7)$$

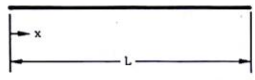
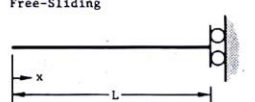
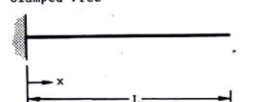
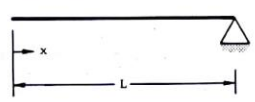
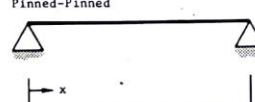
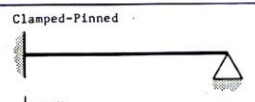
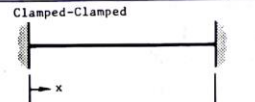
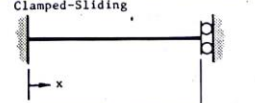
Table 1.7

Table 8-1. Single-Span Beams.

Notation: x = distance along span of beam; m = mass per unit length of beam;

E = modulus of elasticity;

I = area moment of inertia of beam about neutral axis (Table 5-1); L = span of beam; see Table 3-1 for consistent sets of units

Natural Frequency (hertz); $f_i = \frac{\lambda_i^2}{2\pi L^2} \left(\frac{EI}{m} \right)^{1/2}$; $i=1,2,3,\dots$			
Description (a)	λ_i ; $i=1,2,3,\dots$	Mode Shape, $\tilde{y}_i \left(\frac{x}{L} \right)$	σ_i ; $i=1,2,3,\dots$
1. Free-Free 	4.73004074 7.85320462 10.9956078 14.1371655 17.2787597 $(2i + 1)\frac{\pi}{2}$; $i > 5$	$\cosh \frac{\lambda_i x}{L} + \cos \frac{\lambda_i x}{L}$ $-\sigma_i \left(\sinh \frac{\lambda_i x}{L} + \sin \frac{\lambda_i x}{L} \right)$	0.982502215 1.000777312 0.999966450 1.000001450 0.999999937 ≈ 1.0 for $i > 5$ See Ref. 8-2
2. Free-Sliding 	2.36502037 5.49780392 8.63937983 11.78097245 14.92256510 $(4i - 1)\frac{\pi}{4}$; $i > 5$	$\cosh \frac{\lambda_i x}{L} + \cos \frac{\lambda_i x}{L}$ $-\sigma_i \left(\sinh \frac{\lambda_i x}{L} + \sin \frac{\lambda_i x}{L} \right)$	0.982502207 0.999966450 0.999999933 0.999999993 0.999999993 1.0 ; $i > 5$
3. Clamped-Free 	1.87510407 4.69409113 7.85475744 10.99554073 14.13716839 $(2i - 1)\frac{\pi}{2}$; $i > 5$	$\cosh \frac{\lambda_i x}{L} - \cos \frac{\lambda_i x}{L}$ $-\sigma_i \left(\sinh \frac{\lambda_i x}{L} - \sin \frac{\lambda_i x}{L} \right)$	0.734095514 1.018467319 0.999224497 1.000033553 0.999998550 ≈ 1.0 ; $i > 5$ See Ref. 8-2
4. Free-Pinned 	3.92660231 7.06858275 10.21017612 13.35176878 16.49336143 $(4i + 1)\frac{\pi}{4}$; $i > 5$	$\cosh \frac{\lambda_i x}{L} + \cos \frac{\lambda_i x}{L}$ $-\sigma_i \left(\sinh \frac{\lambda_i x}{L} + \sin \frac{\lambda_i x}{L} \right)$	1.000777304 1.000001445 1.000000000 1.000000000 1.000000000 1.0 ; $i > 5$
5. Pinned-Pinned 	$i\pi$	$\sin \frac{i\pi x}{L}$	--
6. Clamped-Pinned 	3.92660231 7.06858275 10.21017612 13.35176878 16.49336143 $(4i + 1)\frac{\pi}{4}$; $i > 5$	$\cosh \frac{\lambda_i x}{L} - \cos \frac{\lambda_i x}{L}$ $-\sigma_i \left(\sinh \frac{\lambda_i x}{L} - \sin \frac{\lambda_i x}{L} \right)$	1.000777304 1.000001445 1.000000000 1.000000000 1.000000000 1.0 ; $i > 5$
7. Clamped-Clamped 	4.73004074 7.85320462 10.9956079 14.1371655 17.2787597 $(2i + 1)\frac{\pi}{2}$; $i > 5$	$\cosh \frac{\lambda_i x}{L} - \cos \frac{\lambda_i x}{L}$ $-\sigma_i \left(\sinh \frac{\lambda_i x}{L} - \sin \frac{\lambda_i x}{L} \right)$	0.982502215 1.000777312 0.999966450 1.000001450 0.999999937 1.0 ; $i > 5$ See Ref. 8-2
8. Clamped-Sliding 	2.36502037 5.49780392 8.63937983 11.78097245 14.92256510 $(4i - 1)\frac{\pi}{4}$; $i > 5$	$\cosh \frac{\lambda_i x}{L} - \cos \frac{\lambda_i x}{L}$ $-\sigma_i \left(\sinh \frac{\lambda_i x}{L} - \sin \frac{\lambda_i x}{L} \right)$	0.982502207 0.999966450 0.999999933 0.999999993 0.999999993 1.0 ; $i > 5$

Different mode shapes are pictured below (Fig 1.6); beam mode shapes for the clamped-clamped beam in x direction, and for the free-free one in y direction, can still be noticed easily; Fig 1.7 shows the beam modes for free-free and clamped-clamped B.C.

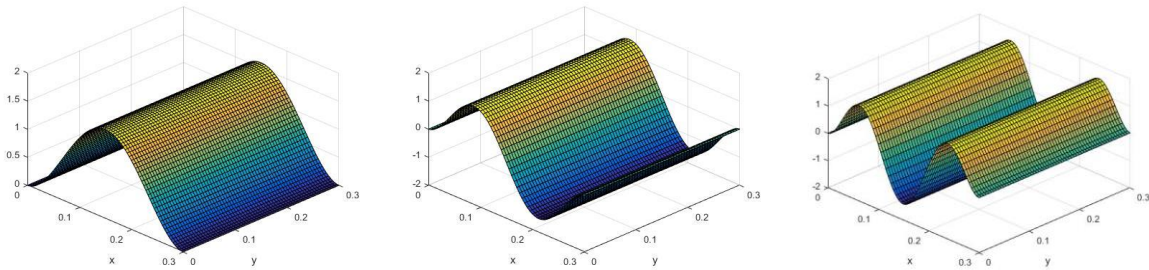


Fig 1.6 a) – Mode shapes 1, 4 and 8. As in 1.2, If the plate has two opposite free edges there is a mode in which $\tilde{q}_n \approx 1$, i.e. the half wave in that direction is basically flat. Halfwaves numbers in the clamped-clamped direction can be seen easily.

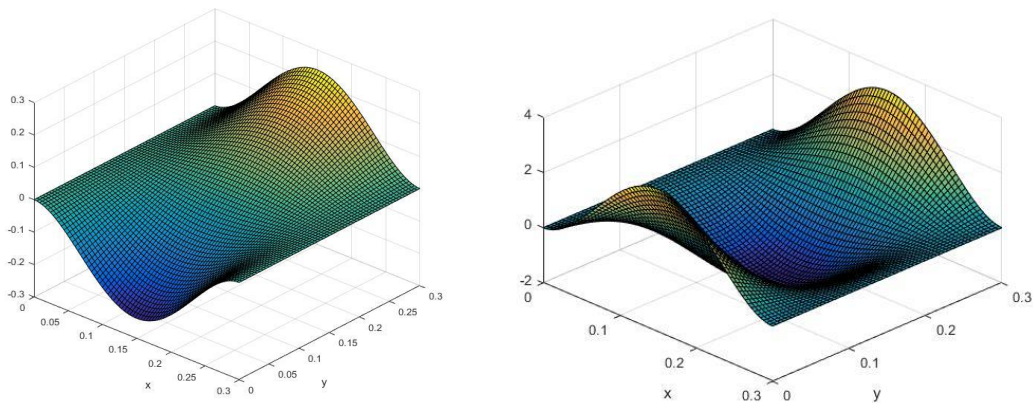


Figure 1.6 b) – Second and third mode shapes. Beam mode shapes with one halfwave along clamped-clamped direction combine with beam mode shapes along the free-free direction, with one and two halfwaves (respectively left and right).

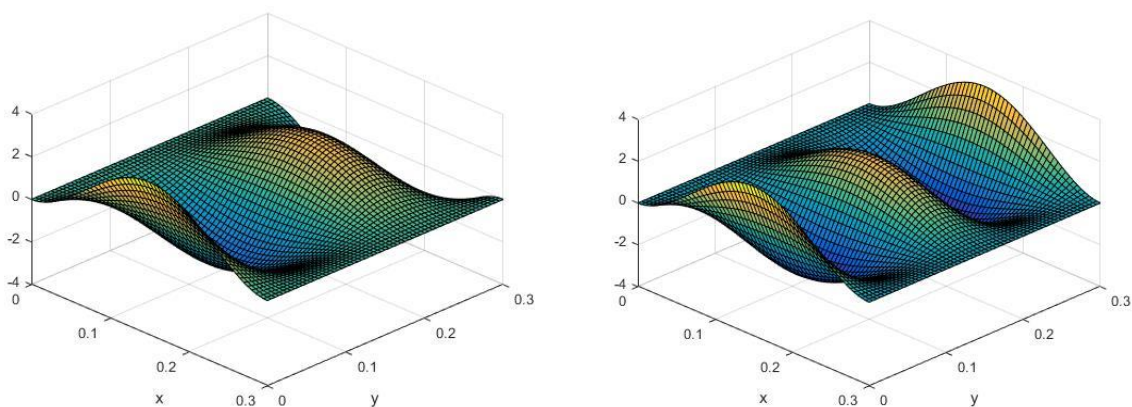


Figure 1.6 c) – Mode shapes 6 and 11, with still one halfwave along clamped-clamped direction, and three or four (respectively left and right) along the free-free direction

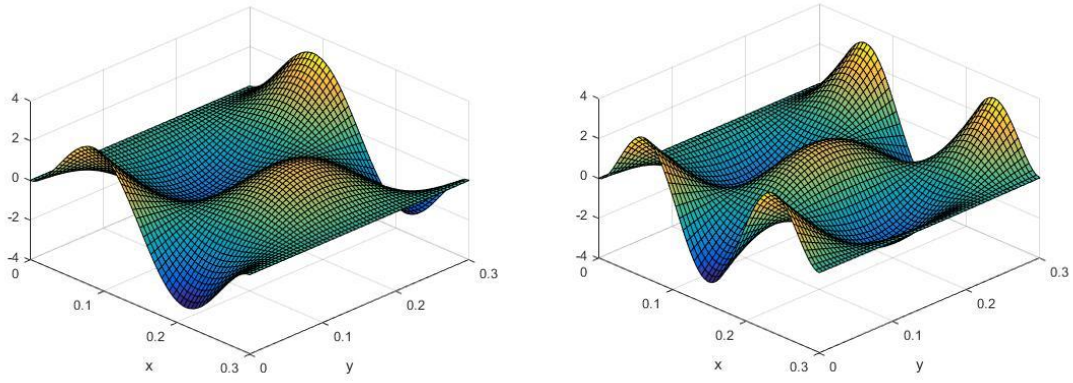


Figure 1.6 d) – Shapes 7 and 12. As mode indexes increases, shapes become more complex but still they simply come from beam shapes overlapping.

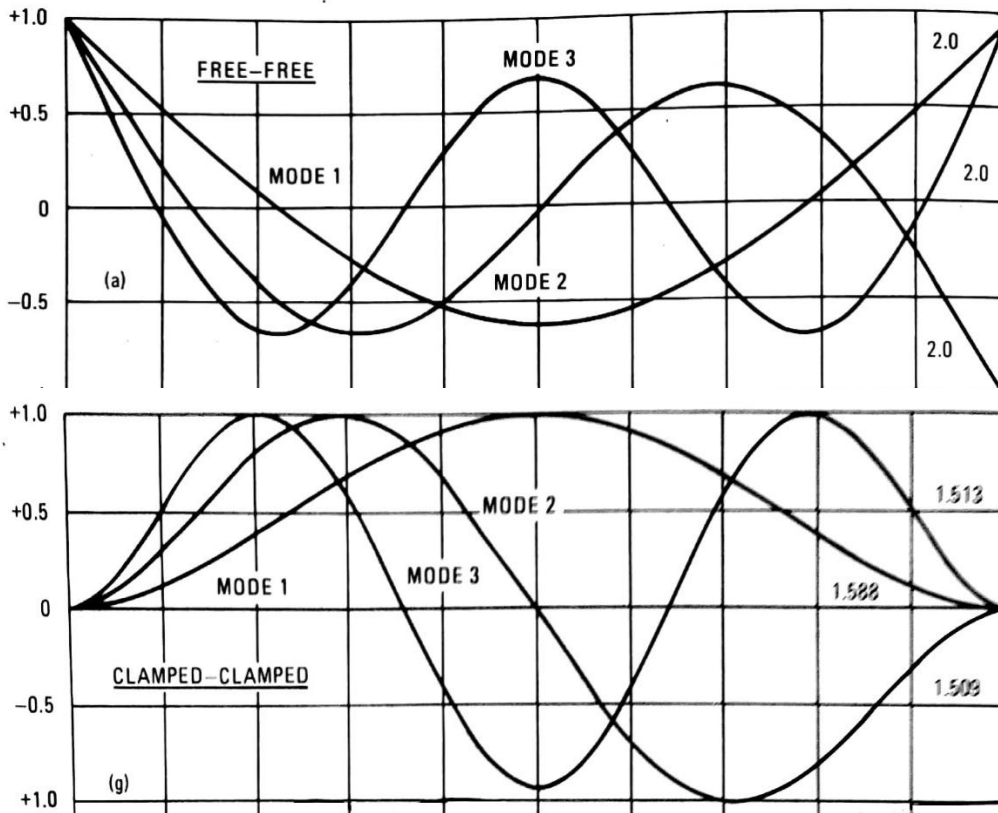


Figure 1.7 – Beam mode shapes for the current boundary conditions; they can be recognized in plate mode shapes above.

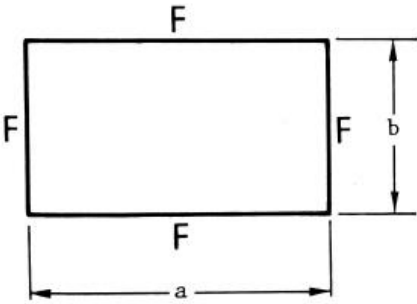
1.3.3 FREE PLATE

Natural frequencies

The λ parameter for the FFFF configuration is on the proper table (Tab 1.8):

Table 1.8

$$\text{Natural Frequency (hertz)} f_{ij} = \frac{\lambda_{ij}^2}{2\pi a^2} \left[\frac{Eh^3}{12\gamma(1 - \nu^2)} \right]^{1/2} ; i=1,2,3\dots; j=1,2,3\dots$$

Description	λ_{ij}^2 and (ij)						
	Mode Sequence						
	$\frac{a}{b}$	1	2	3	4	5	6
1. Free-Free - Free-Free 	0.4	3.463 (13)	5.288 (22)	9.622 (14)	11.44 (23)	18.79 (15)	19.10 (24)
	2/3	8.946 (22)	9.602 (13)	20.74 (23)	22.35 (31)	25.87 (14)	29.97 (32)
	1.0	13.49 (22)	19.79 (13)	24.43 (31)	35.02 (32)	35.02 (23)	61.53 (41)
	1.5	20.13 (22)	21.60 (31)	46.65 (32)	50.29 (13)	58.20 (41)	67.49 (23)
	2.5	21.64 (31)	33.05 (22)	60.14 (41)	71.48 (32)	117.5 (51)	119.4 (42)
	$\nu = 0.3$; (ij) = (11), (12), (21) are rigid body modes. Also see Ref. 11-82.						

For the approximated formula, parameters G, H and J can be found on the usual table (case 1 for both edges couples). Results are shown below.

Table 1.9

F ex [Hz]	F approx [Hz]	Relative error
46,10	47,47	2,985%
67,63	76,49	13,111%
83,48	76,49	-8,372%
119,67	123,09	2,853%
119,67	123,09	2,853%
210,26	210,79	0,252%
-	210,79	-
-	226,36	-
-	254,69	-
-	254,69	-
-	369,24	-

The error in now considerably higher because these boundary conditions do not allow an accurate analytical description.

A comparison between the free boundary conditions highlights, as we expected, lower frequencies as the plate becomes less constrained.

Table 1.10

SSSS [Hz]	FCFC [Hz]	FFFF [Hz]
67,45	76,49	47,47
168,63	90,36	76,49
168,63	149,72	76,49
269,82	210,79	123,09
337,27	230,36	123,09
337,27	270,19	210,79
438,45	300,45	210,79
438,45	384,90	226,36
573,36	413,15	254,69
573,36	416,72	254,69
607,08	420,13	369,24

Mode shapes

The plate behavior is no longer a simple superimposition of beam modes, as they start to interact with each other in a more complex way; if computed as it has been done with other cases, i.e. with (1.12) and using the free-free beam mode shapes, many modes cannot be described, as a comparison with experimental results can show (Fig 1.8). Since the analytical instruments cannot solve this problem, it will be treated using finite elements and then through the experimental test.

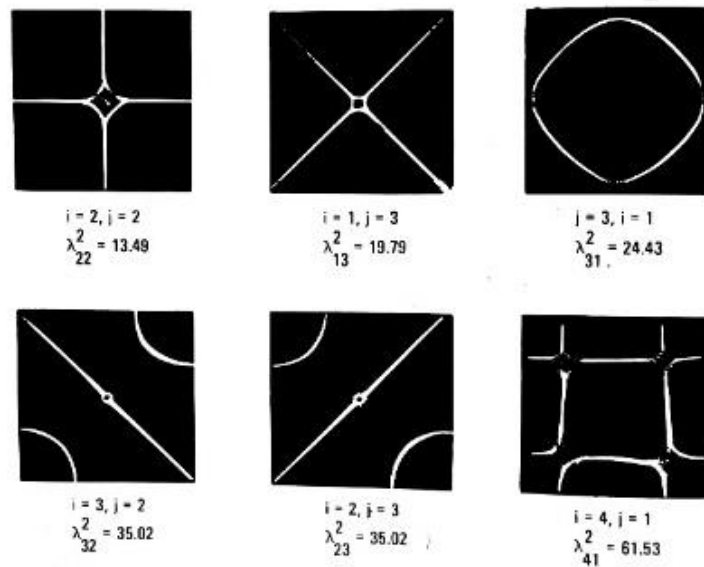


Figure 1.8 – First six modes, experimentally obtained.

2 FINITE ELEMENTS SIMULATION

Continuum systems can be studied analytically only in a few simple cases, when the geometry and boundary conditions are simple enough; as the problem becomes more complex, the only feasible approach becomes discretization i.e. its reduction to a finite, yet possibly very high, number of degree of freedom system. Different techniques of discretization have been developed, just to mention some of them:

- Assumed-modes methods, where mode shapes are assumed to be finite in number and approximated with arbitrary shapes (Rayleigh).
- Lumped parameters methods, in which both continuum mass and stiffness are replaced by a set of point masses, with inertial properties alone, and elastic ‘fields’ that only have stiffness properties.

The increasingly high computation power of modern computers made these methods outdated, in favor of finite elements method (FEM), the most used discretization method nowadays. The continuum body is divided into many small deformable solids, called elements, and their deformation is approximated with assumed shape functions, while the displacement of its vertices, the nodes, acts as degree of freedom. The discretization will result in a system of ordinary differential equations, which, although large, can be solved more easily than the partial derivative differential equation of the original continuum model.

Even if the plate in our analysis is one of those very simple structure that could be studied analytically (as we did before, for both the simply supported and clamped cases), the presence of a less predictable boundary condition like in the completely free configuration, or the addition of concentrated accelerometers masses, create a system that is no longer under the strict hypothesis of the theoretical model, and therefore can only be studied using a finite elements simulation.

In particular, the software SOLIDWORKS SIMULATION has been used at this purpose; all the three configurations of the plate have been implemented:

- the SSSS and FCFC plates will be now studied with the added mass, to observe how frequency and mode shapes are affected;
- the mode shapes of the FFFF plate, for which the analytical study was too complex because of boundary conditions, will now be computed; the configuration with added accelerometers mass will be treated, as well.

2.1 SIMPLY SUPPORTED PLATE

The plate has been modeled according to correct dimensions and thickness (Fig 2.1); the mesh, with automatic choice of tetrahedral elements, has been created and slightly refined to achieve a better precision.

Distributed accelerometers masses have been added, in particular two masses of 6 grams each, on a 7,5 mm diameter circular area; one accelerometer is near a vertex, the other at the midpoint of an edge.

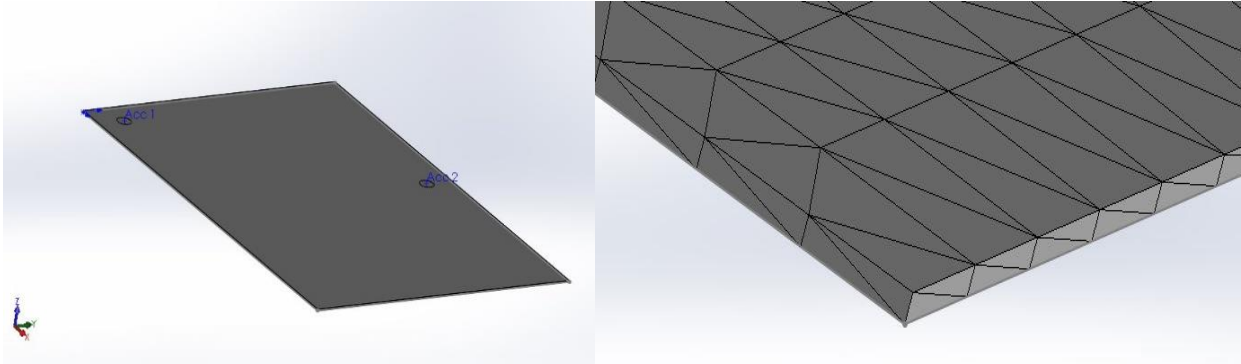


Figure 2.1 – Model and mesh detail.

Proper constraints have been added (Fig 2.2), to model the simply supported boundary conditions; each edge of the lower surface has been constrained imposing null vertical displacement.

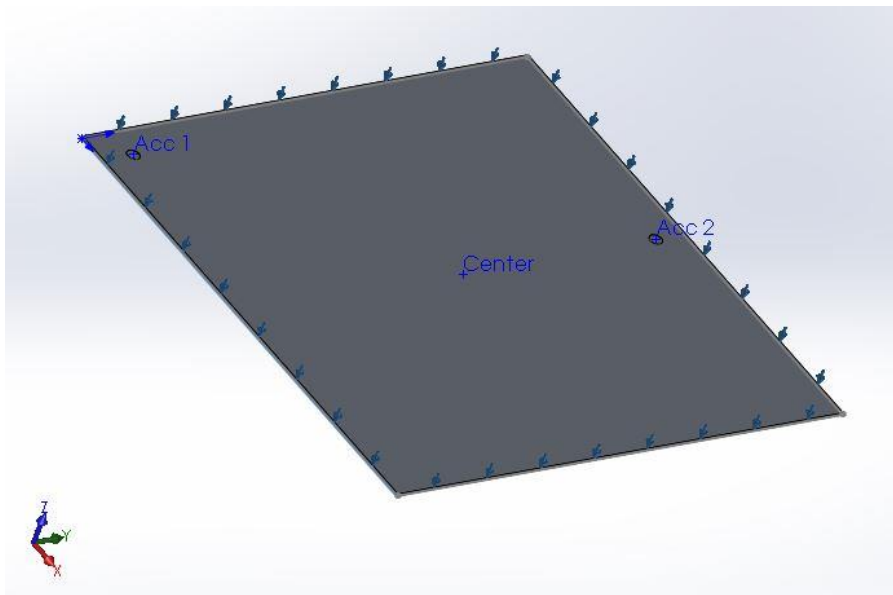


Figure 2.2 – SSSS boundary conditions.

First, the simulation without the added masses has been run, to check its exactness through frequencies and mode shapes, known from the analytical computation; finally, masses have been reintroduced; both frequencies and mode shapes for these two cases are compared below:

Table 2.1 – Natural frequencies comparison; frequencies are in [Hz], error and shift are expressed in percentage.

SSSS					
Mode Order	Analytical (MATLAB)	Simulation (SW)	Relative error	Simulation, added masses	Change due to added mass
1	67,5	67,5	0,05%	67,4	-0,18%
2	168,6	168,8	0,12%	167,7	-0,68%
3	168,6	168,9	0,18%	168,8	-0,05%
4	269,8	270,8	0,37%	270,5	-0,12%
5	337,3	338,0	0,22%	332,4	-1,68%
6	337,3	338,1	0,24%	337,7	-0,12%
7	438,4	440,6	0,48%	436,2	-0,99%
8	438,4	441,3	0,66%	440,3	-0,24%
9	573,4	575,0	0,29%	557,3	-3,09%
10	573,4	575,3	0,34%	574,4	-0,16%
11	607,1	612,7	0,92%	603,6	-1,49%
12	674,5	679,3	0,71%	673,0	-0,92%
13	674,5	679,4	0,72%	679,2	-0,02%
14	843,2	852,0	1,05%	802,0	-5,87%
15	843,2	854,6	1,36%	845,6	-1,06%

Some considerations can be drawn from the differences between the two configurations:

- The simulation error for frequencies is below 1%, proving that this boundary condition allows a precisely predictable behavior of the plate; mode shapes are those found analytically (Fig 2.3).

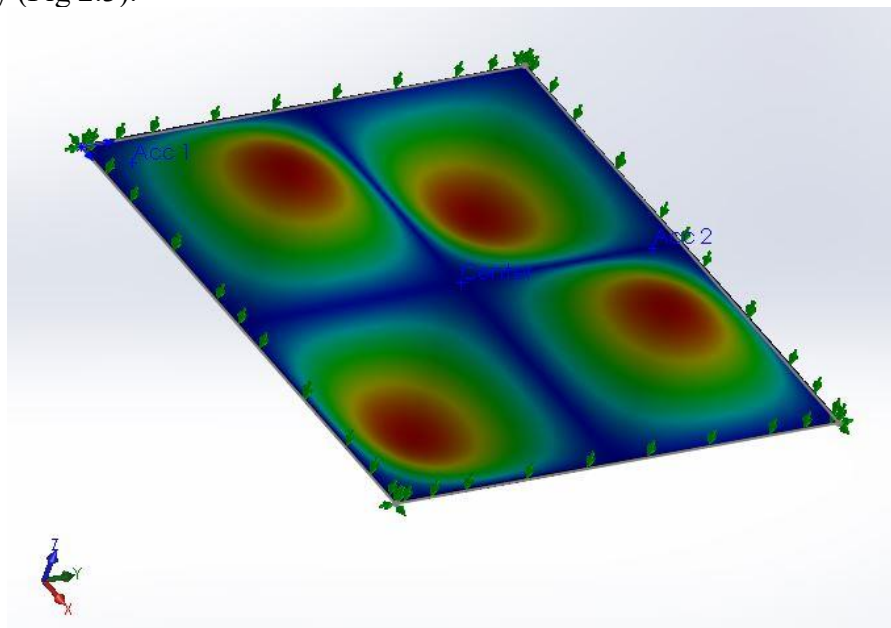


Figure 2.3 – Mode shape 2,2.

- The added masses, even if small compared to the plate mass, lightly lower the natural frequency of the system; moreover, mode shapes change, losing their symmetry because of the masses position; some of them change slightly (Fig 2.4), other significantly (Fig 2.5), in particular mode shapes for which accelerometers are not on nodal lines.

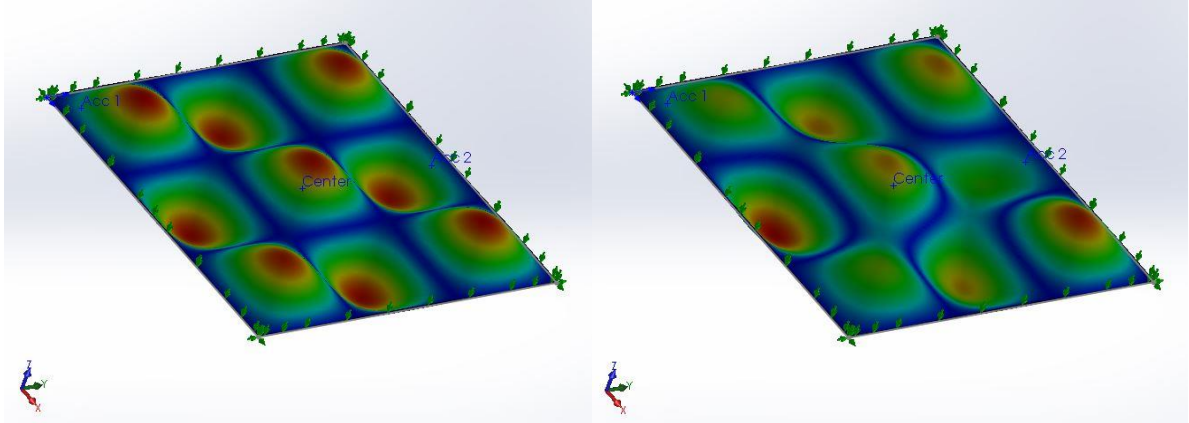


Figure 2.4 – Mode shape 3,3 is slightly affected from additional masses; nodal lines become less defined and symmetric.

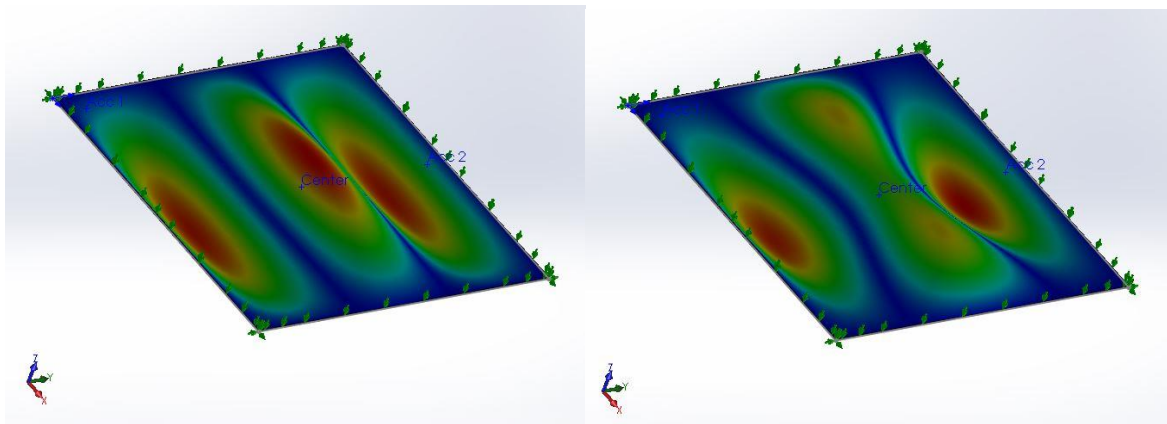


Fig 2.5–Mode shape 3,1 changes more: there are still three areas moving in counter-phase, but their shape changed because of the mass distribution.

2.2 CLAMPED-FREE PLATE

The two short edges have been constrained in each direction, to simulate the clamped boundary condition, while there are no constraints on the other couple of edges (Fig 2.6).

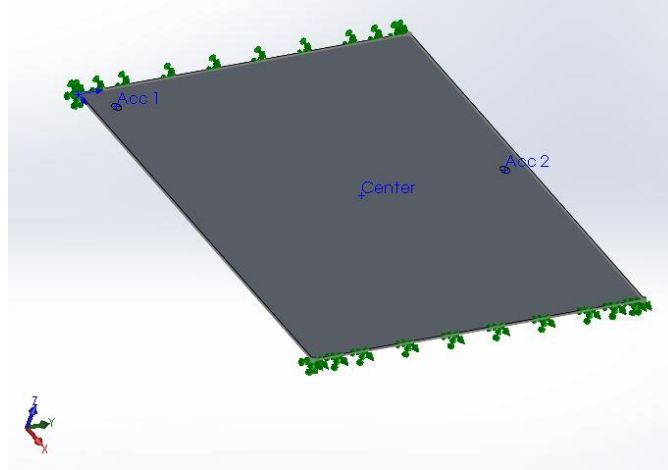


Figure 2.6 – FCFC Boundary condition.

The frequencies and mode shapes are compared below:

Table 2.2 - Natural frequencies comparison; frequencies are in [Hz], error and shift are expressed in percentage.

FCFC					
Mode Order	Analytical (MATLAB)	Simulation (SW)	Relative error	Simulation, added masses	Change due to added mass
1	76,5	75,9	-0,78%	73,1	-3,63%
2	90,4	90,0	-0,39%	86,2	-4,28%
3	149,7	148,6	-0,73%	143,8	-3,25%
4	210,8	209,5	-0,59%	209,4	-0,07%
5	230,4	229,7	-0,30%	229,4	-0,13%
6	270,2	272,7	0,93%	267,6	-1,86%
7	300,4	299,7	-0,26%	299,3	-0,12%
	384,9				
	413,2				
8	416,7	411,7	-1,21%	397,7	-3,39%
9	420,1	426,4	1,48%	426,2	-0,04%
10	435,0	434,2	-0,20%	421,8	-2,85%
11		468,4		466,4	-0,42%
12	512,4	512,5	0,02%	501,1	-2,22%
13	629,6	618,5	-1,78%	618,1	-0,06%
14	630,5	646,9	2,61%	636,3	-1,64%

- It is important to notice that some of the frequencies predicted by the analytical computation are not found in the simulation, and vice versa.
- At the frequencies predicted by both methods, the accuracy of the simulation is still very good but slightly lower compared to SSSS case, due to less strict constraints.

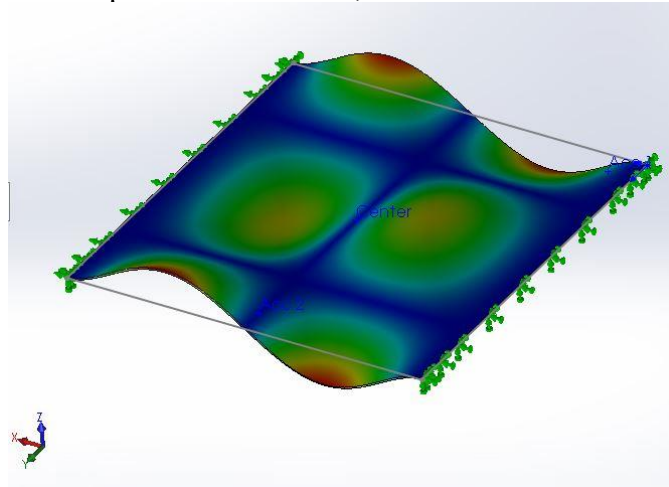


Figure 2.7 – One of the mode shapes already computed analytically

- For the same reason, the shift in frequencies due to the added masses is higher.
- Accelerometer 1 is near a fixed edge, so its influence in mode shapes is almost null; accelerometer 2 mass affects mainly mode shapes that do not have a node in that point.

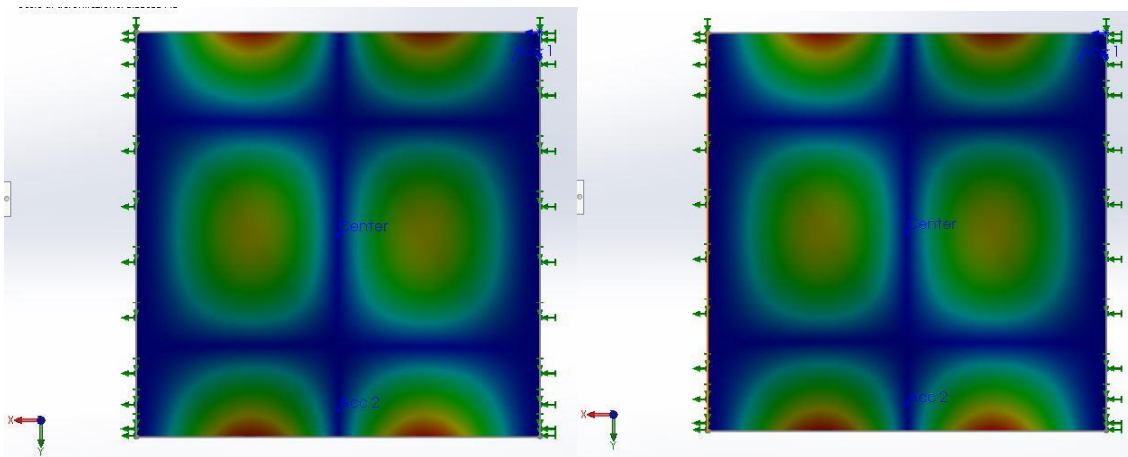


Figure 2.8 – Unaffected mode shape.

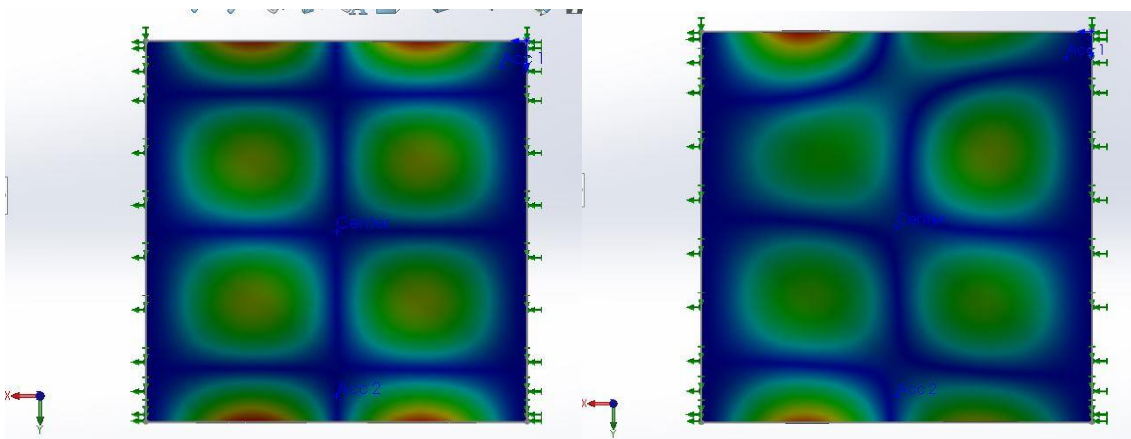


Figure 2.9 – Mode shape only slightly modified, since both accelerometers are above nodal lines.

- Other mode shapes are strongly affected by the masses: for example, the two distinct mode shapes in figure 2.10 present a different number of halfwaves along free-free direction; when masses are added, two new mode shapes (Fig 2.11) substitute them, having a structure resembling a mix of the first two.

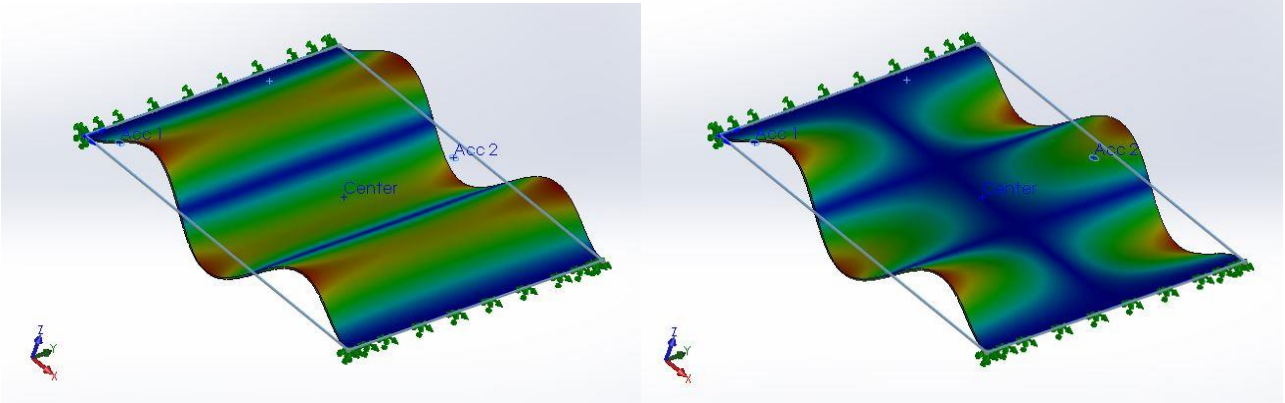


Figure 2.10

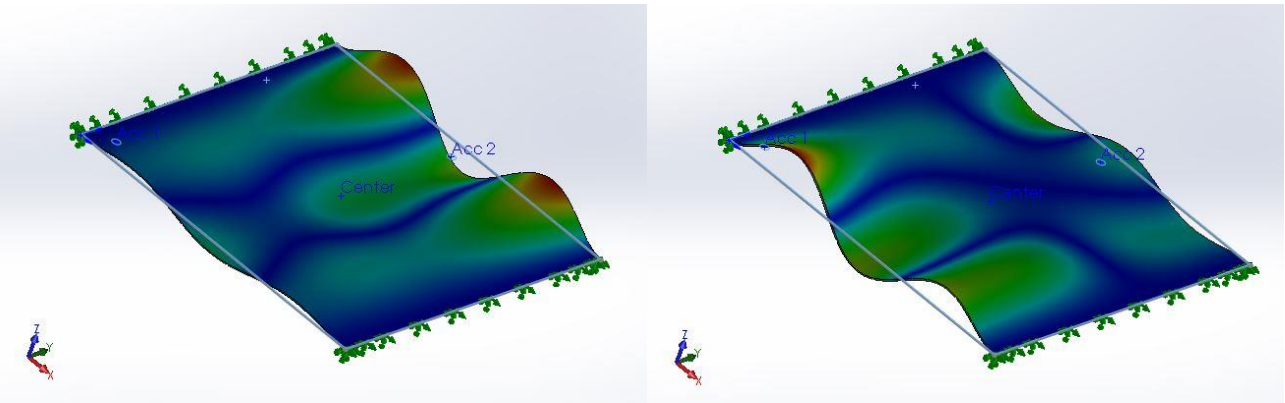


Figure 2.11

2.3 FREE PLATE

The plate is now totally free, no constraints have been added; the frequency comparison is:

Table 2.3 - Natural frequencies comparison; frequencies are in [Hz], error and shift are expressed in percentage.

FFFF					
Mode Order	Analytical (MATLAB)	Simulation (SW)	Relative error	Simulation, added massess	Change due to added mass
1	47,5	45,1	-4,97%	43,3	-4,09%
2	76,5	65,8	-13,97%	63,8	-3,11%
3	76,5	83,4	9,07%	80,5	-3,48%
4	123,1	117,7	-4,34%	110,2	-6,44%
5	123,1	117,8	-4,29%	116,4	-1,17%
6	210,8	208,4	-1,12%	199,4	-4,34%
7	210,8	208,5	-1,10%	208,0	-0,24%
8	226,4	217,3	-3,99%	211,7	-2,58%
9	254,7	235,2	-7,65%	235,1	-0,04%
10	254,7	265,1	4,09%	258,6	-2,44%
11	369,2	362,4	-1,85%	348,6	-3,82%
12	369,2	363,7	-1,50%	361,1	-0,72%
13	413,2	399,0	-3,44%	396,2	-0,70%
14	413,2	419,4	1,50%	412,5	-1,63%
15	453,6	451,3	-0,52%	437,7	-3,01%

The FE simulation allows to find mode shapes that we were unable to compute in the analytical part; some modes are shown in Fig 2.12.

- Frequency are predicted way less accurately, as the increased error shows.
- Some mode shapes still highlight trigonometric function standing waves (figure 6 and 9 in the following page), other seems to have a polar symmetry (figure 3 and 8), while other shapes clearly do not follow basic functions, and become more and more complex and less predictable as frequencies increases.

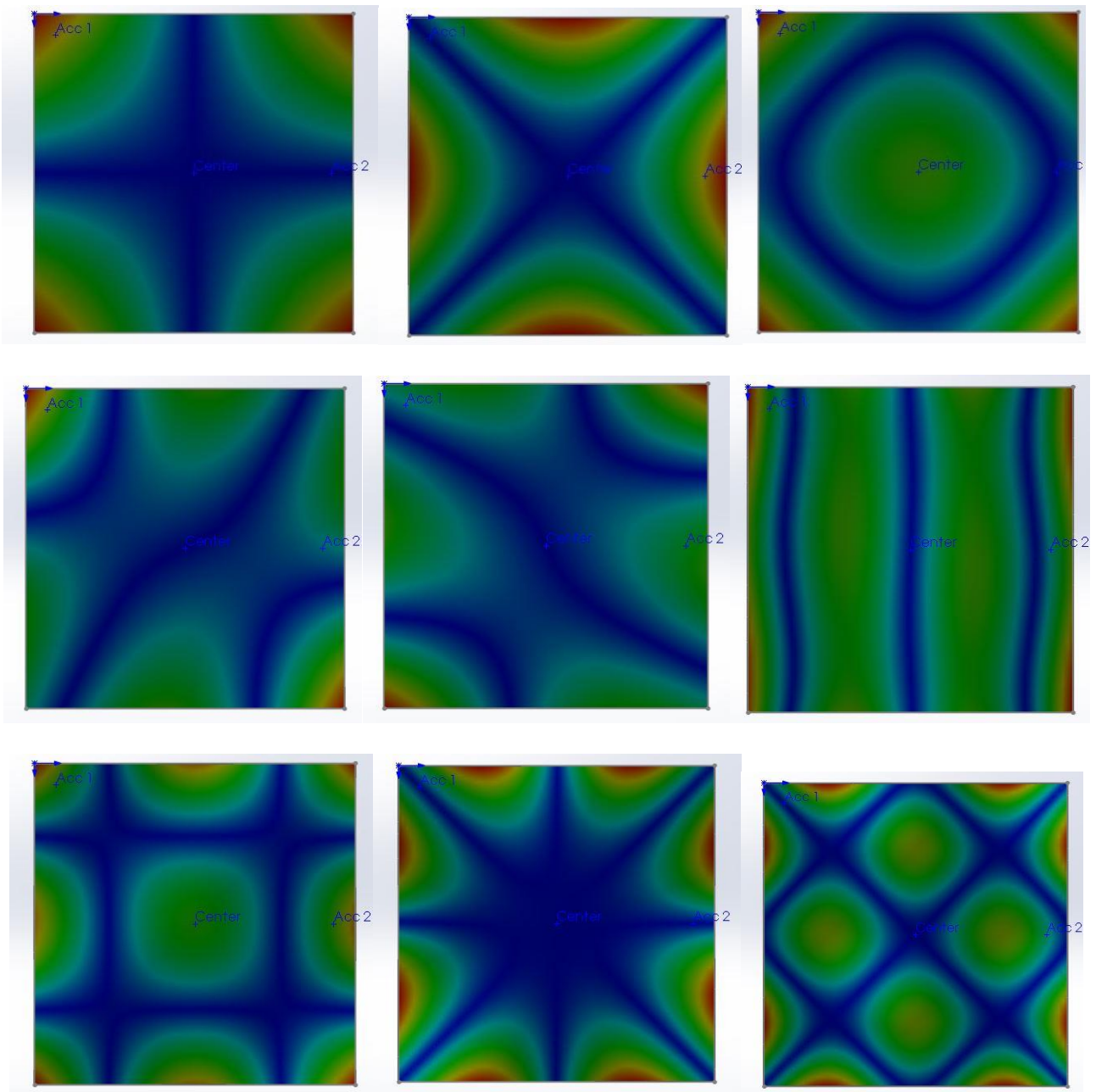


Figure 2.12 – Nine mode shapes, ordered progressively.

3 PLATE SPECIMEN CHARACTERISTICS

3.1 PRELIMINARY CONSIDERATIONS

The need to build a model for the laboratory experience, gives some limitations as far materials, dimensions and frequency range is concerned:

- Material should be common to find, not brittle not to be dangerous during the test.
- The combination of material, stiffness, edge dimensions should provide a specimen that is not too heavy for the shaker, but still stiff enough not to bend under its own weight: small deflections are not only a hypothesis of the theoretical model, but also a practical need since sand used to highlight nodal lines (see chapter 4) would fall off.
- Natural frequencies of the plate that we want to compute, should fall into a range with an upper limit not too high, to guarantee acoustic comfort during the experience; of course, this range should be smaller than the one we can reach with the shaker, too.

To roughly estimate the specimen dimension, static and dynamic behavior, the weight, the value of the 20th frequency of interest, and the maximum vertical displacement under self-weight have been computed, the formers with MATLAB while the latter through FEM simulation, for a variety of geometrical configuration, different reasonable thicknesses and common materials:

Table 3.1 – Materials data.

	Steel	Aluminum	PMMA
Density[Kg/m3]	7800	2700	1190
E [Gpa]	210	69	2,7

Results are summarized in Tab 3.2.

Table 3.2

Rectangular 200x300											
mass [kg]				max vertical displacement [mm]				20th frequency FFFF [Hz]			
Thickness [mm]	Steel	Aluminum	PMMA	Thickness [mm]	Steel	Aluminum	PMMA	Thickness [mm]	Steel	Aluminum	PMMA
1	0,468	0,162	0,071	1	0,28	0,28	3,77	1	890	880	267
1,5	0,702	0,243	0,107	1,5	0,12	0,12	1,70	1,5	1340	1315	400
2	0,936	0,324	0,143	2	0,07	0,07	0,96	2	1790	1740	540
3	1,404	0,486	0,214	3	0,03	0,03	0,43	3	2680	2630	800
Squared 200x200											
mass [kg]				max vertical displacement [mm]				20th frequency FFFF [Hz]			
Thickness [mm]	Steel	Aluminum	PMMA	Thickness [mm]	Steel	Aluminum	PMMA	Thickness [mm]	Steel	Aluminum	PMMA
1	0,312	0,108	0,048	1	0,09	0,09	1,23	1	1360	1320	400
1,5	0,468	0,162	0,071	1,5	0,04	0,04	0,56	1,5	2000	190	600
2	0,624	0,216	0,095	2	0,02	0,02	0,32	2	2700	2640	800
3	0,936	0,324	0,143	3	0,01	0,01	0,14	3	4000	3950	1190
Squared 250x250											
mass [kg]				max vertical displacement [mm]				20th frequency FFFF [Hz]			
Thickness [mm]	Steel	Aluminum	PMMA	Thickness [mm]	Steel	Aluminum	PMMA	Thickness [mm]	Steel	Aluminum	PMMA
1	0,488	0,169	0,074	1	0,21	0,21	3,02	1	870	850	250
1,5	0,731	0,253	0,112	1,5	0,09	0,09	1,37	1,5	1300	1260	380
2	0,975	0,338	0,149	2	0,05	0,05	0,77	2	1740	1700	500
3	1,463	0,506	0,223	3	0,02	0,02	0,35	3	2610	2500	760

Weights above 750 grams, deflections above 1 mm, and frequency above 2000 Hz have been highlighted, because they should be avoided. Since aluminum and steel have similar frequencies and displacements, the former has been chosen for its lower density, to avoid a heavy specimen to be mounted on the shaker; PMMA has been considered too, to compare the behavior of two different materials. About thickness, a compromise between weight, maximum deformation and stiffness can be reached using 1.5 mm aluminum plates, and 2 mm PMMA plates.

3.2 DENSITY AND YOUNG MODULUS ESTIMATION

Both materials were purchased in a hardware store, aluminum having a 1,25 mm thickness and PMMA a 1.8 mm thickness, and different dimension. Since a technical data sheet was not available, both density and elastic modulus had to be computed or estimated.

Because Plexiglass proved to be less stable and predictable already in preliminary tests, only aluminum will be considered from this point on.

Density can be easily obtained dividing the weight of one of the plates, obtained by a precision scale in the laboratory, by its volume.

$$\rho_{Al} = \frac{m}{V} = \frac{0,233 \text{ kg}}{0,270 \text{ m} * 0,270 \text{ m} * 0,00125 \text{ m}} = 2555 \frac{\text{kg}}{\text{m}^3}$$

Young modulus has been estimated using natural frequencies: once the frequencies are known from the experimental part, several simulations have been run with variable E value; the closest value is the one which minimize the error between actual and simulated frequencies, i.e. 60 GPa, as can be seen from tables and graphic below.

Table 3.3

Actual Frequency	FEM Frequency							
	E [GPa]	68	66	64	62	60	58	56
555		588	579	571	562	553	543	534
695		727	716	705	694	683	671	659
715		770	758	747	735	723	711	699
755		814	802	790	777	765	752	739
1008		1024	1009	994	978	962	946	930
1132		1190	1172	1154	1136	1118	1099	1079

Actual Frequency	FEM Frequency Error							
	E [GPa]	68	66	64	62	60	58	56
555		5,9%	4,3%	2,9%	1,3%	-0,4%	-2,2%	-3,8%
695		4,6%	3,0%	1,4%	-0,1%	-1,7%	-3,5%	-5,2%
715		7,7%	6,0%	4,5%	2,8%	1,1%	-0,6%	-2,2%
755		7,8%	6,2%	4,6%	2,9%	1,3%	-0,4%	-2,1%
1008		1,6%	0,1%	-1,4%	-3,0%	-4,6%	-6,2%	-7,7%
1132		5,1%	3,5%	1,9%	0,4%	-1,2%	-2,9%	-4,7%

Mean abs Error	4,681%	3,317%	2,395%	1,492%	1,476%	2,234%	3,677%
----------------	--------	--------	--------	--------	--------	--------	--------

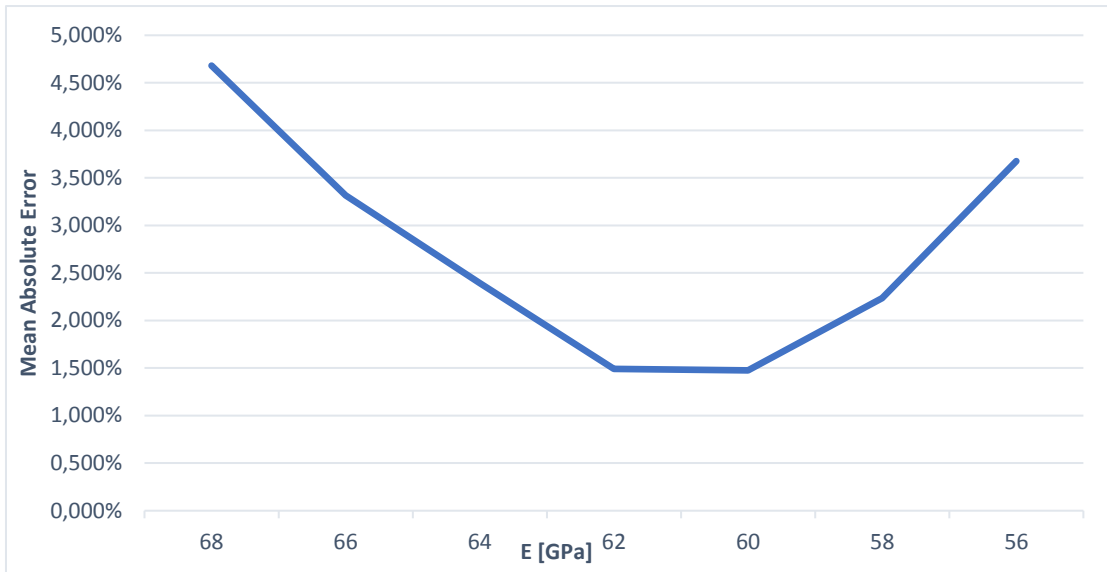


Figure 3.1

Finding a dynamic property resorting to vibration analysis is a commonly used technique, for example when looking for a new material property (together with more traditional methods like tensile test), or to find the stiffness of a component that is too complex to be analytically studied.

4 LABORATORY EXPERIENCES

4.1 EQUIPMENT AND MAIN PROCEDURE [3]

An experimental test rig has been realized, to practically demonstrate the vibration phenomenon, reproduce and measure it. The used equipment is:

- Polymethyl methacrylate (PMMA, commonly Plexiglass) and aluminum plates, of different dimensions, rectangular 200x300 mm, and squared with 200, 250, 270, 300 mm edge. (Fig 4.1)
- TIRA TV50018 shaker and its power amplifier (Fig 4.2)
- OROS OR38 multichannel analyzer, and a notebook running its NVgate software (Fig 4.3)
- Two high frequency accelerometers (Fig 4.4)
- Wavetek frequency generator (Fig 4.5)
- A laser sensor Keyence LK-G3000 (Fig 4.6) with a support structure (Fig 4.7)
- Safety headphones.

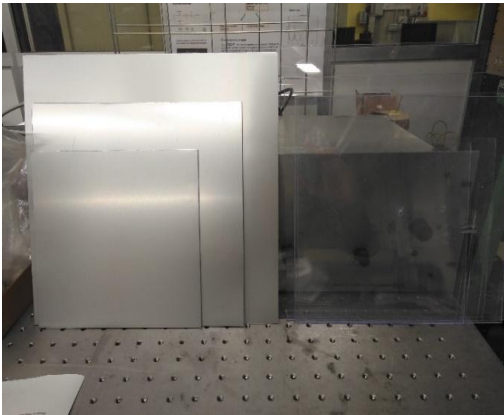


Figure 4.1

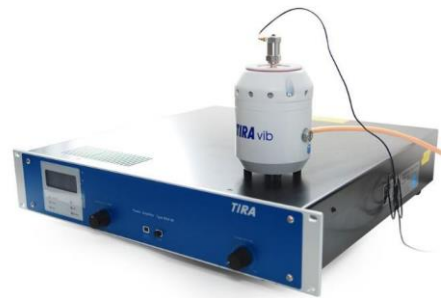


Figure 4.2



Figure 4.3



Figure 4.4



Figure 4.5

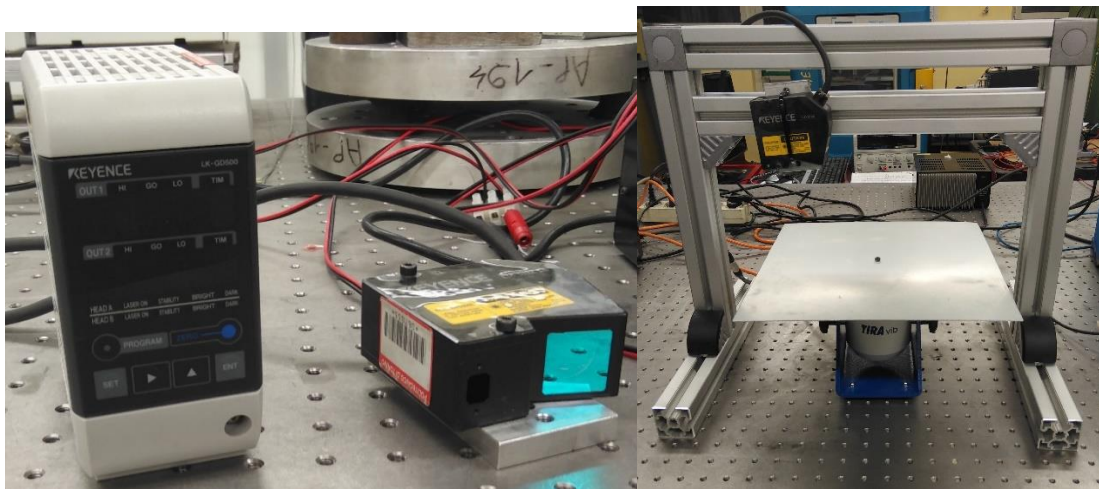


Figure 4.6

The complete setup is illustrated in Fig (4.7)

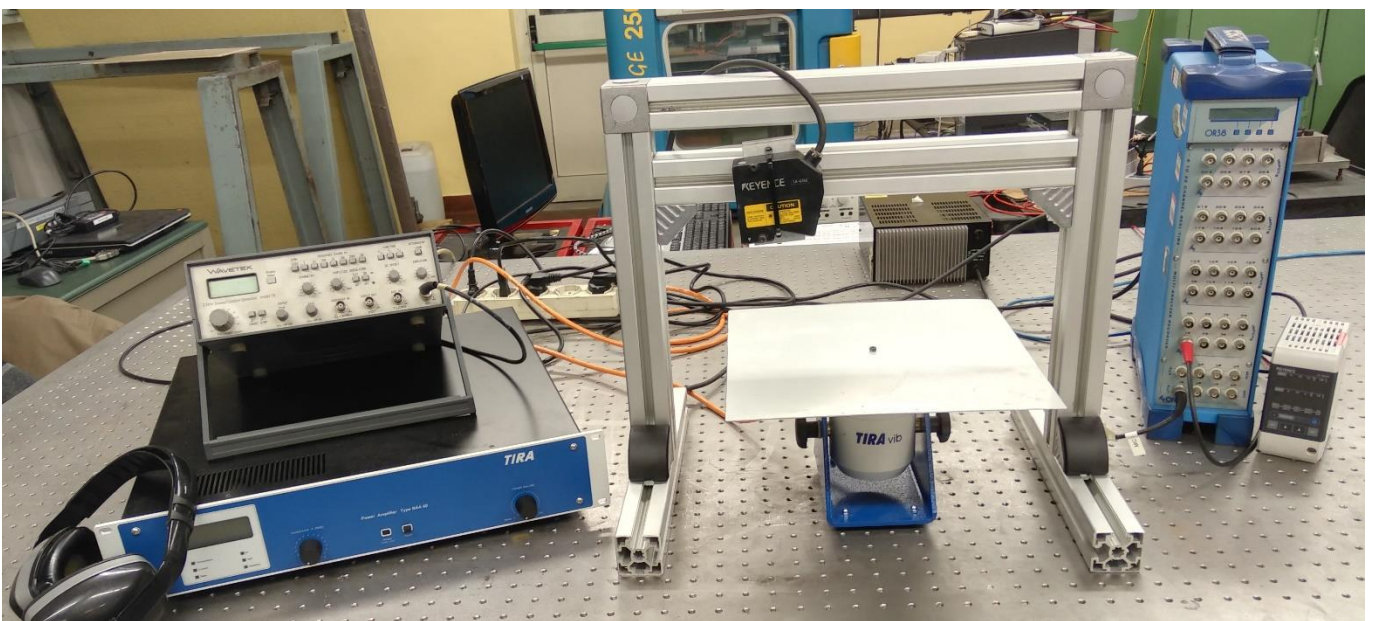


Figure 4.7

The test rig operates in the following way:

- The exciting signal is generated by the frequency generator and adjusted manually; in alternative the analyzer is used, if a sine sweep or random signal with a given frequency content are needed.
- The exciting signal is driven through the amplifier, and then finally reaches the shaker, where the specimen under investigation is fixed through a M4 screw and nut.
- Accelerometers are attached to the plate with wax, and their wires are connected to the analyzer input ports.
- If the laser sensor is used instead, the laser head is fixed to the adjustable structure and suspended at a given distance from the measuring point; the head is connected to its control unit, and finally plugged into the analyzer input port as well.
- The acquisition software allows data processing, and their exportation as MATLAB file for further analysis and considerations.

Helpful advices about signal analysis and experimental measurements have been provided from Fasana A., Marchesiello S., *Meccanica delle vibrazioni*, and from Professor Fasana himself.

4.2 LABORATORY TESTS

All laboratory experiences have been executed on aluminum plates, which showed much smaller deflections and a better stability, compared to PMMA.

Moreover, only the totally free configuration has been considered, since both the supported and the clamped constraints are difficult to be realized with sufficient accuracy on multiple edges of such length; since the FFFF plate is the only one without a complete analytical description, FEM simulation will be used to predict the experimental results and make comparison between them.

Different tests have been made in laboratory:

1. Chladni figures experiment, i.e. highlighting nodal lines of mode shapes using sand or other powdered materials.
2. Measurements of acceleration, to compute the power spectral density (PSD) of the specimen.
3. Measurements of displacement with the laser sensor, to compare the spectrum with the one obtained with accelerometers.

4.2.1 CHLADNI PLATES EXPERIENCE

Ernst Chladni (1756-1827), a German physicist, is mostly known for his experiment on vibrating plates: spreading some powdered material, such as flour or salt, on a plate clamped in its center, and then exciting it with a violin bow, different resonance frequencies and relative mode shapes are excited, together with a distinct and strong sound, depending on the point where the excitation is applied, and how fast; since every mode shape has its own nodal lines, i.e. points that are not displaced and separate two areas of the plate moving in counter-phase, the powder is carried away from moving areas, and settles on nodal lines, that can now be visualized (Fig 4.8). The experiment was repeated for different plate shapes, dimensions, thicknesses, materials, highlighting the dependence of frequencies and mode shapes from these variables.



Figure 4.8 - Reproduction of the original Chladni layout.

The importance of this experiment is not in the vibration field alone, but also in the discovery of the link, not clear by that time, between sound and vibration; Chladni himself build musical instrument based on his discoveries, and still nowadays acoustic instruments with a soundboard are designed using these knowledges and procedures (Fig 4.9), as will be explored in Part II.

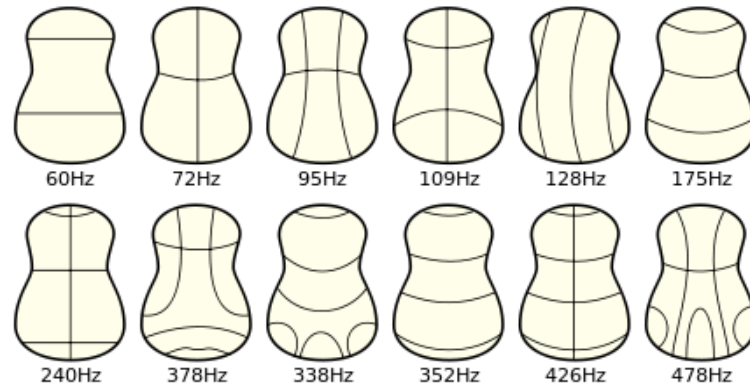


Figure 4.9

A more ‘technical’ version of this experience has been realized in the laboratory, substituting the violin bow with the more accurate electrodynamic shaker.

Squared aluminum plate, 300 x 300 mm

Comparing the totally free plate shapes and frequencies, obtained from the FEM simulation, with experimental results, led to some incongruences: the real model was stiffer, with higher frequencies; some numerical shapes were similar to the real ones, but not exactly the same in nodal line position (Fig 4.10 A), other shapes were expected but could not be found in practice (Fig 4.10 B), while on the contrary unexpected patterns were encountered (Fig 4.10 C)

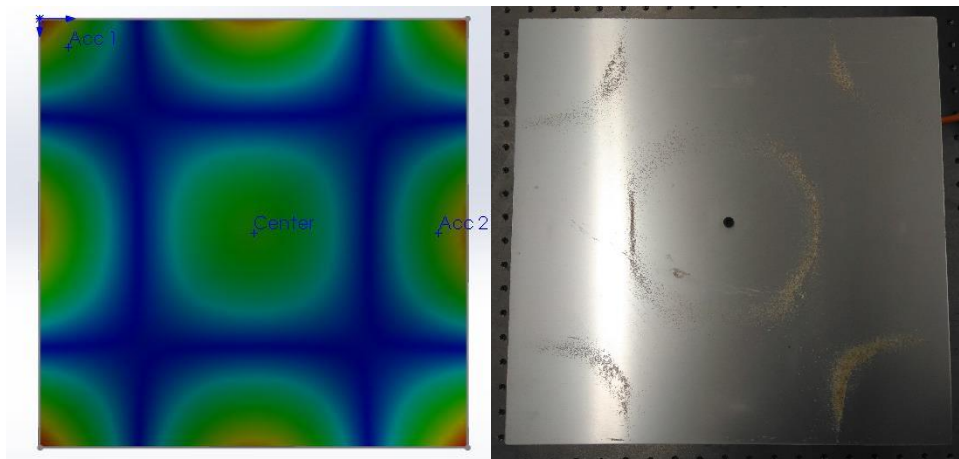


Figure 4.10 A

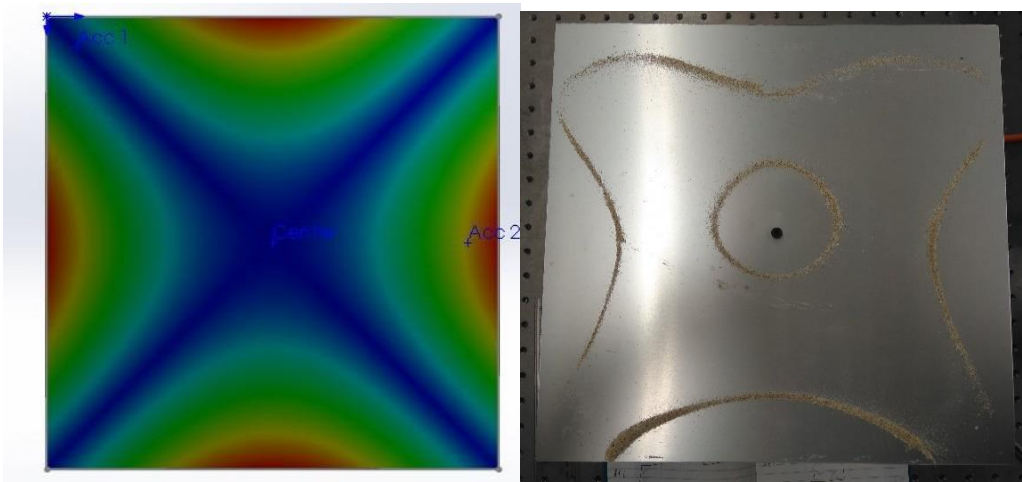


Figure 4.10 B

Figure 4.10 C

After some considerations, since mode shapes presenting a nodal area near the center were not easily visible (like shape in Fig 4.10 B) and all the frequencies were higher than the expected, it was clear that the problem should have been attributed to constraint: the central point, initially only considered as the point where force was exerted, was re-modelled as a proper clamping, the plate being constrained on the circular ring surfaces under the head of the screw on the upper side, and below the nut on the lower side (Fig 4.11).

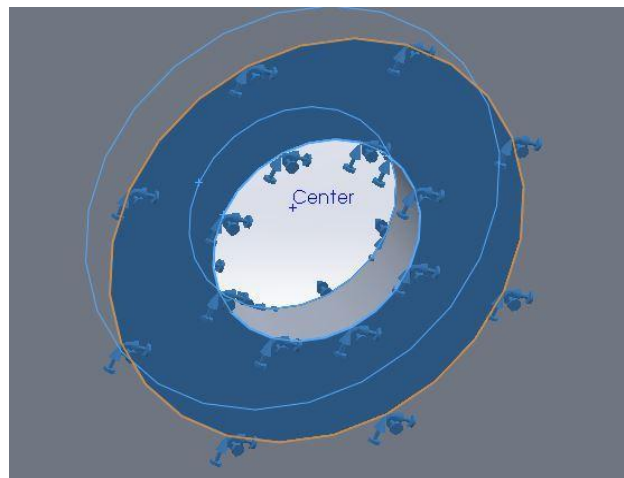


Figure 4.11 – constraint on one of the sides.

Frequencies and mode shapes expected from FE simulation, and their experimental visualization, are reported below (Fig 4.12-4.20). The frequency generator was used to progressively scan through frequencies, carefully listening to the increase in acoustic intensity to spot resonances, as most of them were not immediately evident just looking at the motions of the powdered material. Amplitude of vibration was adjusted manually at each frequency to create clear nodal lines, especially for mode shapes in which these lines pass through or near the center.

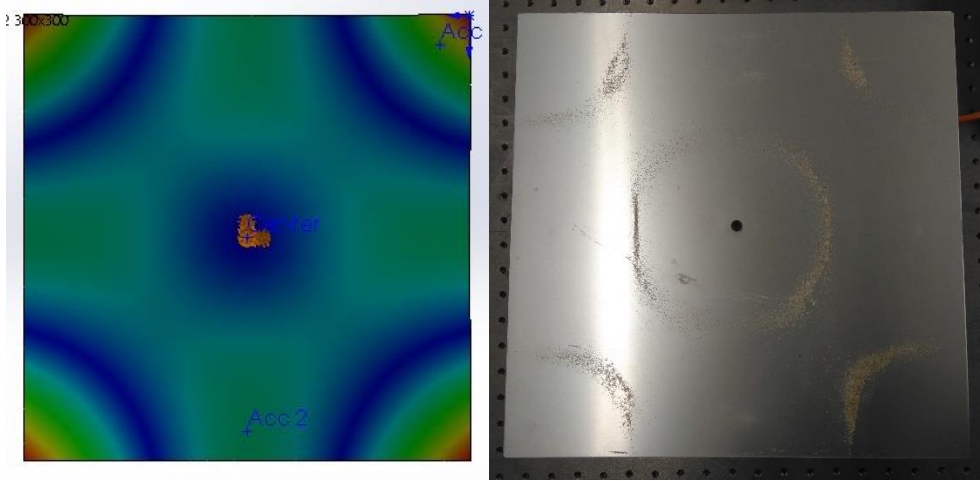


Figure 4.12 – 185 Hz

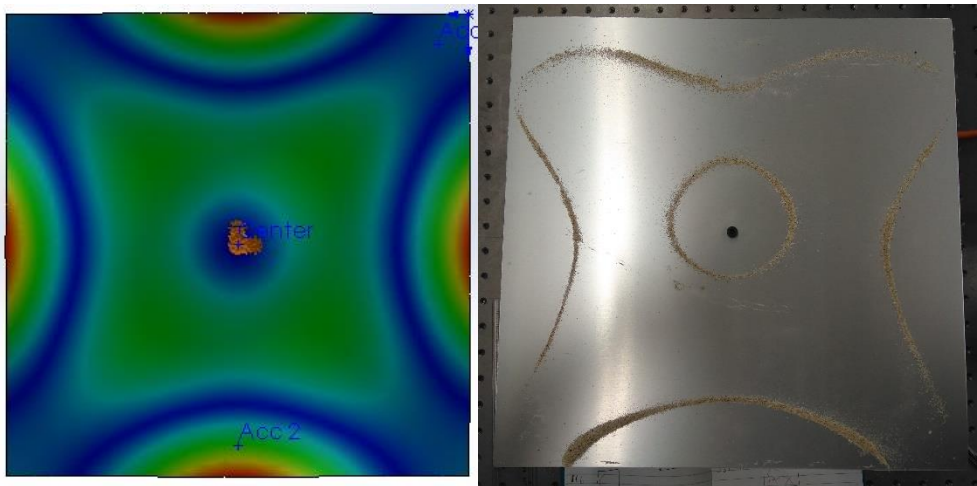


Figure 4.13 – 330 Hz



Figure 4.14 – 385 Hz

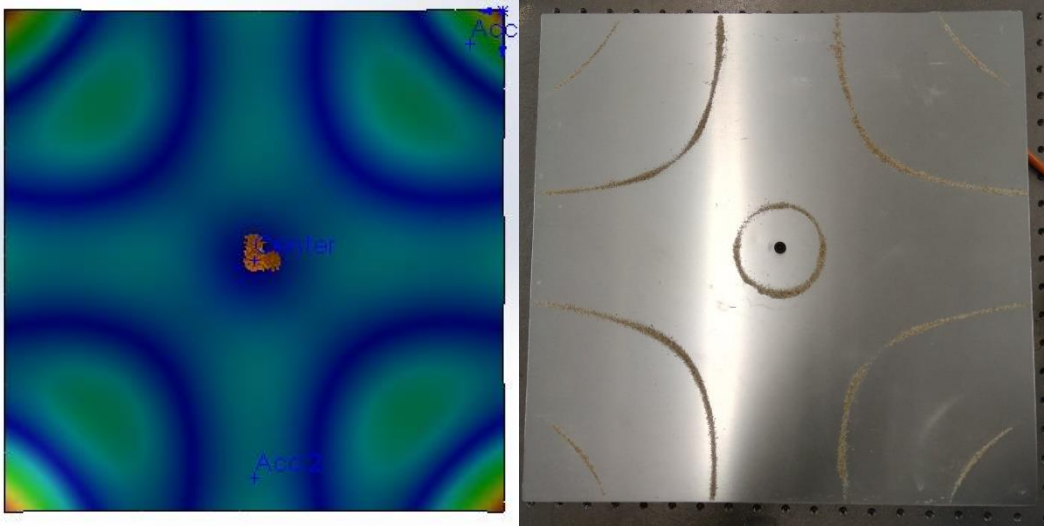


Figure 4.15 – 480 Hz

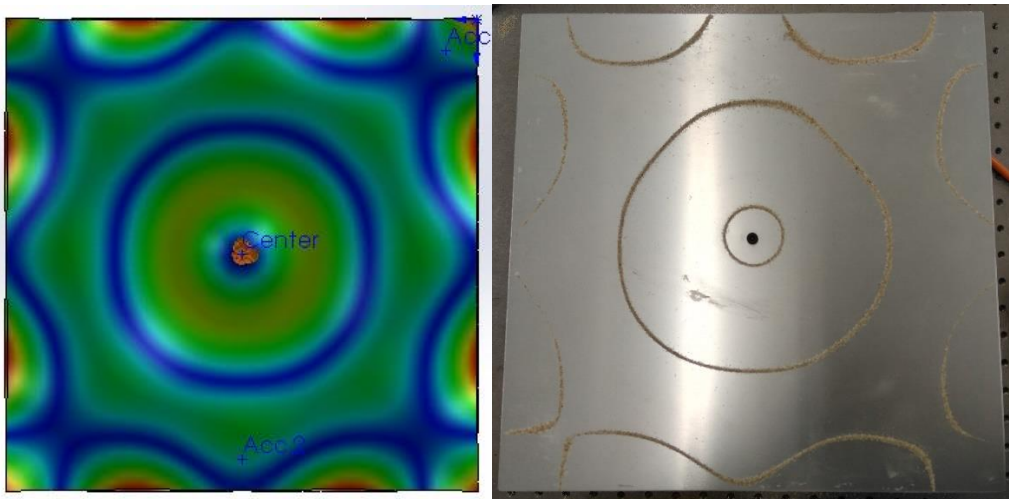


Figure 4.16 – 780 Hz

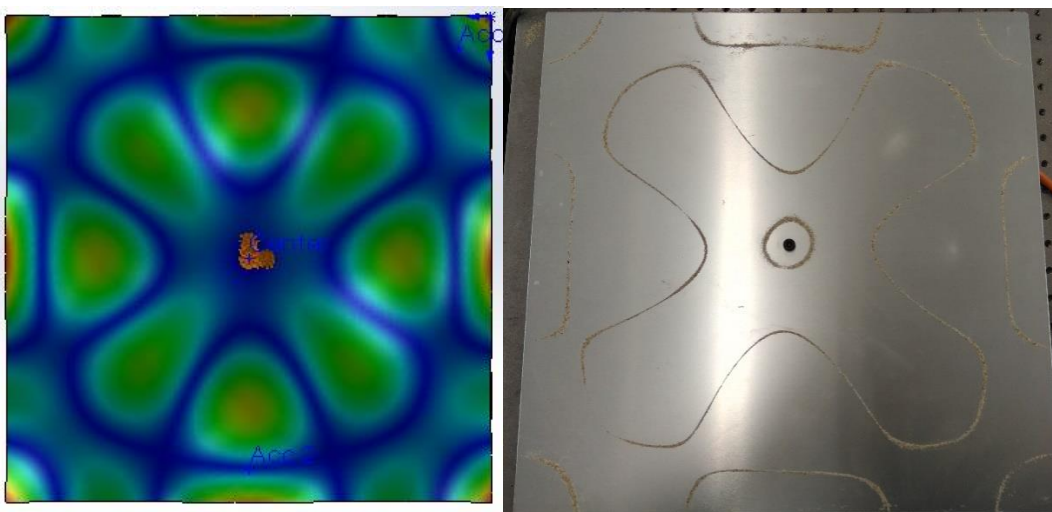


Figure 4.17 – 948 Hz

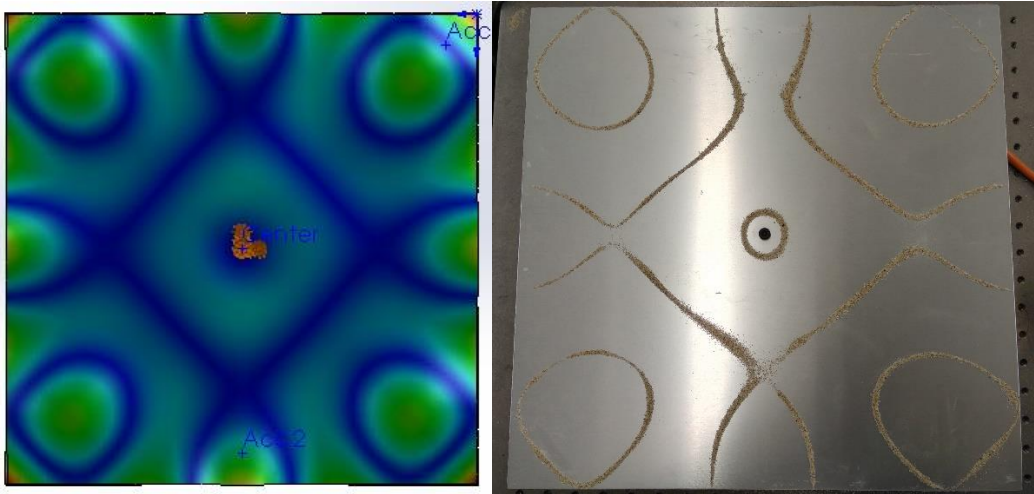


Figure 4.18 – 1048 Hz

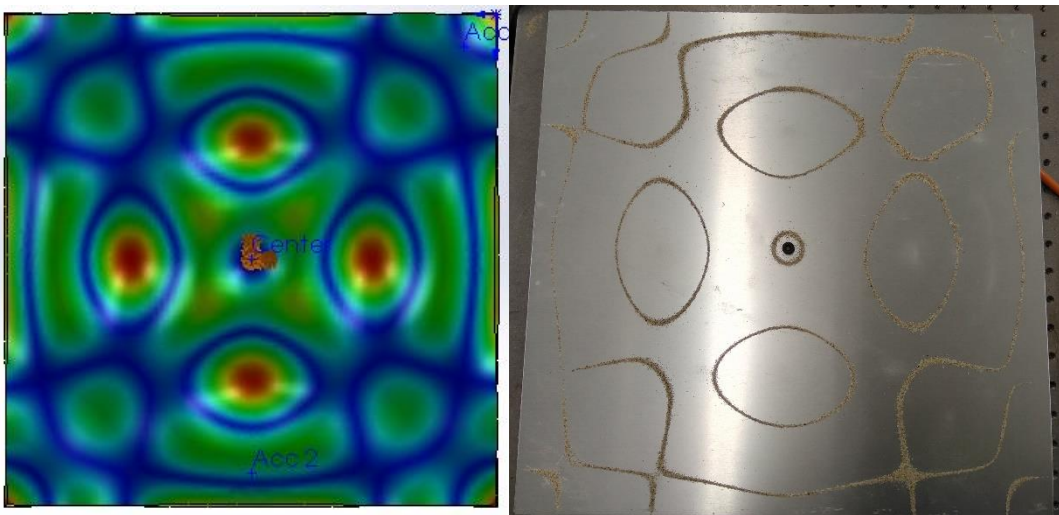


Figure 4.19 – 1693 Hz

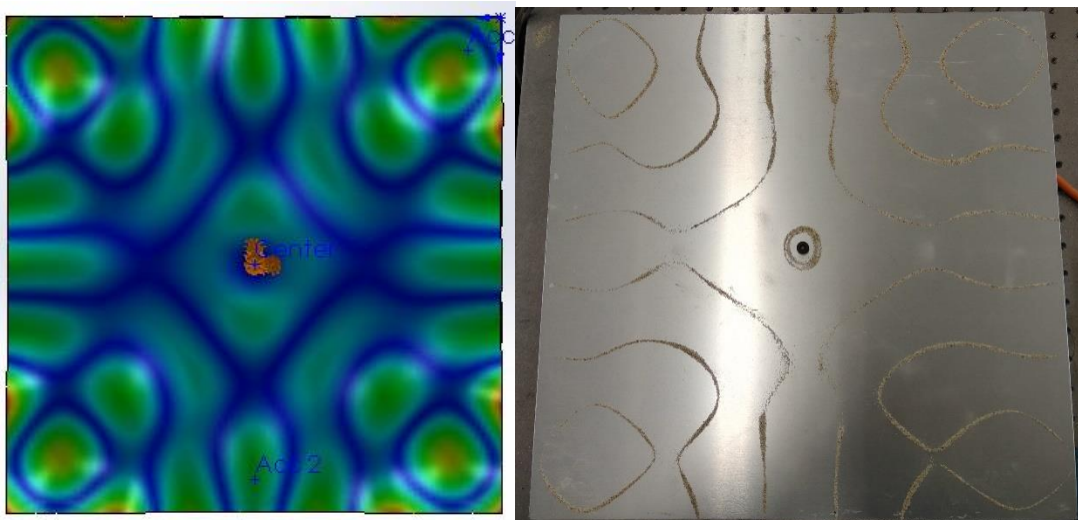


Figure 4.20 – 1865 Hz

The FE simulation proved to be accurate enough, with a lower error for higher frequency modes, and an average absolute error below 3% on the range of interest.

Table 4.1

Actual Frequency [Hz]	FEM Frequency [Hz]	FEM Frequency error
223	218	-2,24%
330	294	-10,91%
385	383	-0,52%
480	472	-1,67%
658	670	1,82%
700	700	0,00%
780	767	-1,67%
818	850	3,91%
948	958	1,05%
1048	1056	0,76%
1090	1112	2,02%
1280	1312	2,50%
1370	1382	0,88%
1376	1391	1,09%
1693	1728	2,07%
Mean Absolute Error		2,21%

A couple of resonant frequencies, especially in the lower part of the range, are less precisely predicted by the simulation; this is probably due only to constraint simulation, and computing the mean error without taking them into account, it decreases even more, to about 1,5%.

The first two mode shapes expected from simulation, with two nodal lines cutting through the center of the plate (Fig 4.21 on the left), and in general those which have complex nodal lines in the inner part of the plate, could not be highlighted, since the central excitation makes it difficult for salt grains to settle nearby the center; to excite this modes, force should be exerted on the periphery of the plate, like in the original experiment when a violin bow was used (Fig 4.20 on the right).

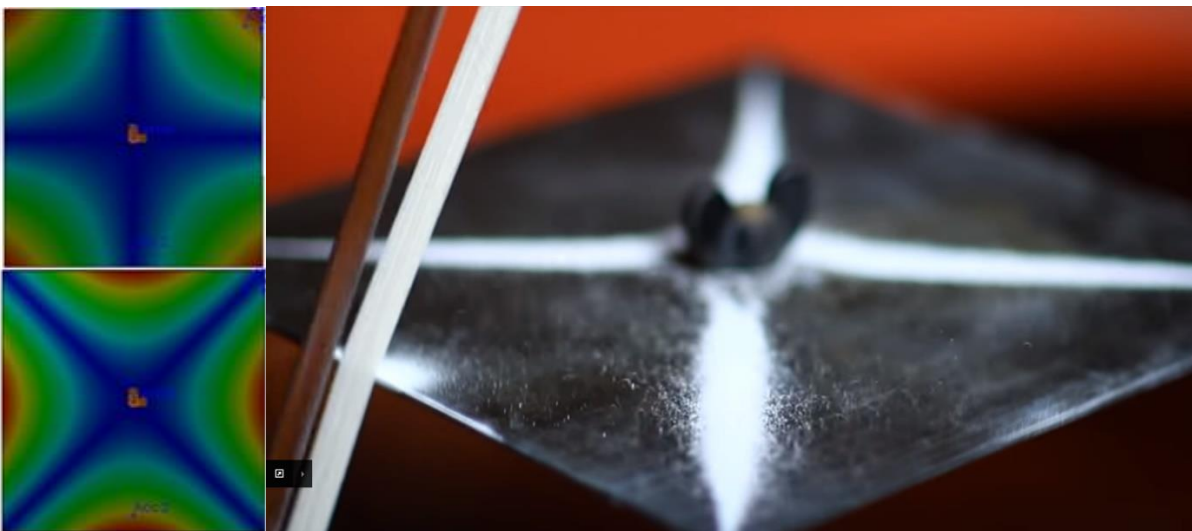


Fig 4.21 - On the left, first and second mode shapes obtained with FEM; on the right, the second one experimentally obtained using a violin bow.

4.2.2 PSD COMPUTATION - ACCELEROMETERS MEASUREMENTS

Two accelerometers, both with a mass of 2,4 grams, have been positioned on the specimen as illustrated in the drawing (Fig 4.22) The one near the midpoint will be referred to as ‘Track 2’ accelerometer, while the one near the vertex as ‘Track 3’ accelerometer, from the corresponding input port number on the analyzer.

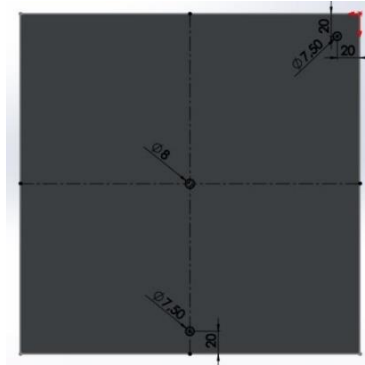


Figure 4.22 – Accelerometers positions.

The system is now excited (through the analyzer) in different ways, using linear and logarithmic sine sweep, and random noise, both with a frequency range from 20 to 2500 Hz to obtain a signal that, once processed through Fourier analysis, provides a Power Spectral Density spanning on the whole frequency range of interest.

Different measurements have been taken, changing the duration of the measurement itself; the following measurements have been selected among the other since they highlighted a clearer spectrum:

- Linear sine sweep, frequency range from 20 to 2500 Hz with 10 Hz/s speed, duration 248 s.
- Random noise, with a frequency content from 20 to 2000 Hz, duration 120 s.

Figures 4.23 and 4.24 show the PSD computed from these measurements (type of excitation and frequency range are specified for each image); blue curve refers to accelerometer nearby the edge’s middle point, while the red one refers to the accelerometer closer to the vertex.

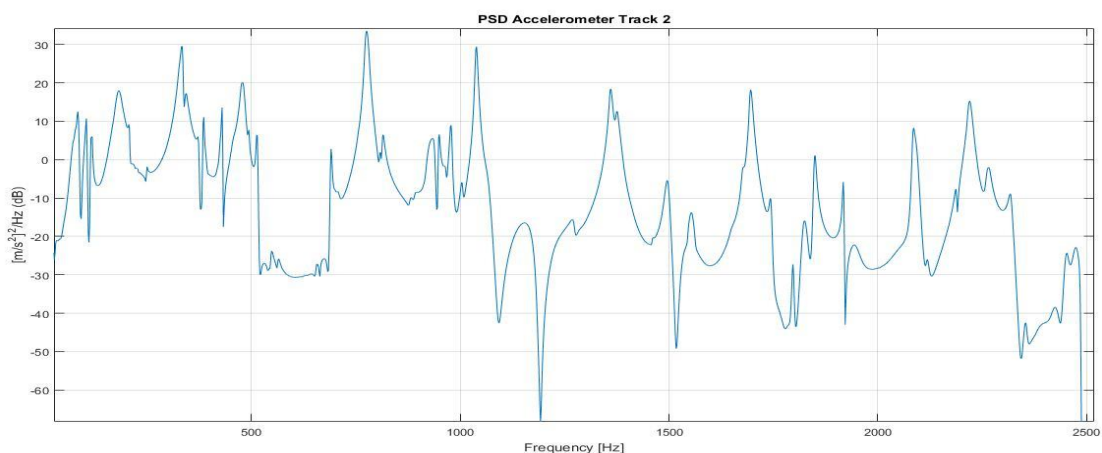


Figure 4.23 – PSD on the whole range of interest (from accelerometer on Track 2) showing main resonances and anti-resonances.

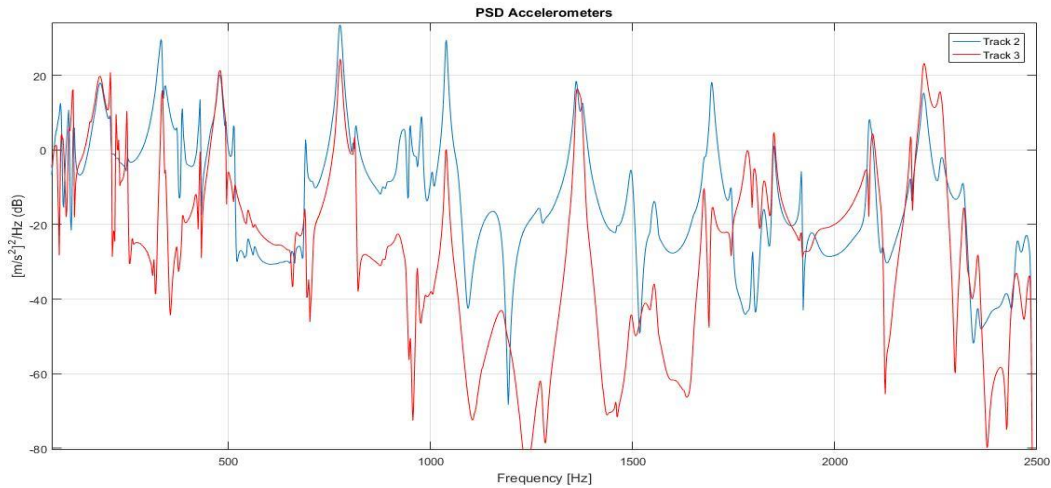


Figure 4.24 – PSD of both accelerometers signals superimposed.

Some considerations can be drawn from the analysis of the PSD:

1. The two accelerometers show different amplitudes; if, at a given frequency, the point they are placed in is above or near a nodal line, the signal will be very low, while if a peak is near the output will be higher. The point in using more than one accelerometer is actually describing the behavior of the specimen, as function of the frequency, with higher accuracy and differentiating between its points. Resonance and anti-resonance frequencies that would not be clearly seen with only one sensor, can be highlighted more easily (Fig 4.25)

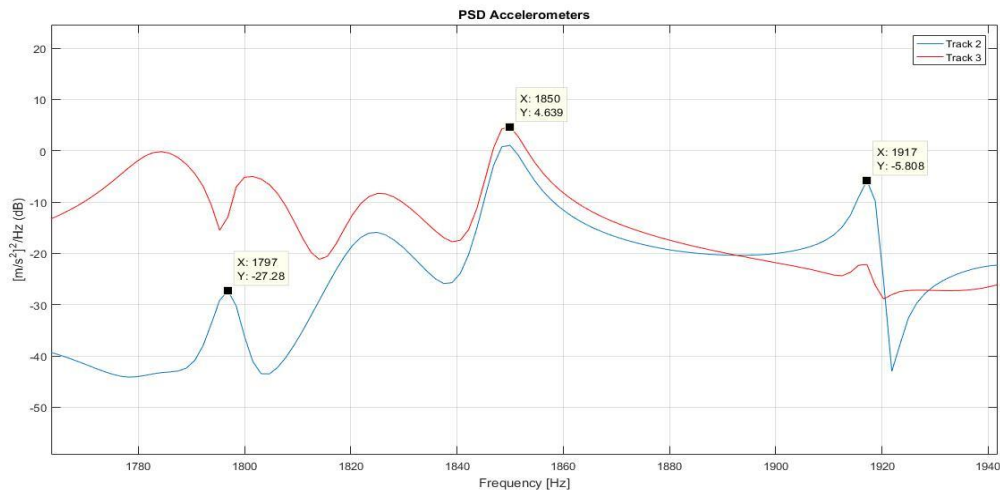


Figure 4.25 – Examples of the benefits in using more sensors: At 1797 Hz accelerometer on track 2 and 3 are on a peak and a node, respectively. At 1850 Hz resonance, both accelerometers have high response. Finally, the resonance and following anti-resonance at about 1920 Hz is slightly visible on the red graph, but very clear on the blue one.

2. A number of resonances can be spotted very clearly, and show a much higher amplitude in a wider frequency range compared to other resonances, that instead are less evident and occur only a very narrow frequency range (Fig 4.26). The first ones correspond to mode shapes that, during the Chladni experiment, produce a very distinct and clear shape, with a particularly strong increase in the sound; the second give mode shapes that are difficult to highlight using sand, because with a minimum change in frequency adjustment the shape would fade away or collapse into the closest, more stable resonance.

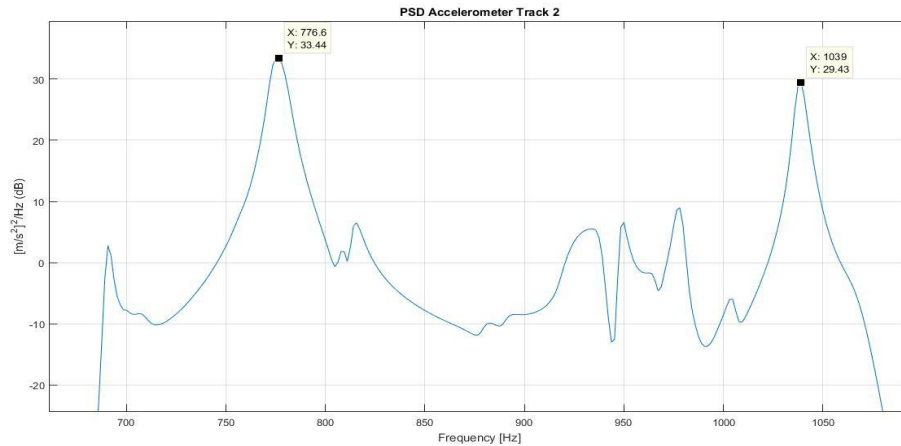


Figure 4.26 – Resonance peaks at 776 and 1039 Hz are more evident compared to smaller and narrower peaks in between.

3. Among the resonances mentioned in point 2), some are particularly close to each other, sometimes barely recognizable as separated; these frequencies often belong to ‘twin’ mode shapes, i.e. mode shapes that are identical but rotated of 90 degrees, and should theoretically appear at the very same frequency, the excitation position being determinant for which one actually occurs (as we have seen in 4.2.1). Because the plate’s edges are not identical in length, and because the central constrain, even if accurate, is not perfectly centered, these modes either show at very close frequencies or do not appear at all. In the example provided below, an enlargement of the spectrum shows the two very close peaks (Fig 4.27), then both the FEM distinct shapes and the experimental ones are provided (Fig 4.28).

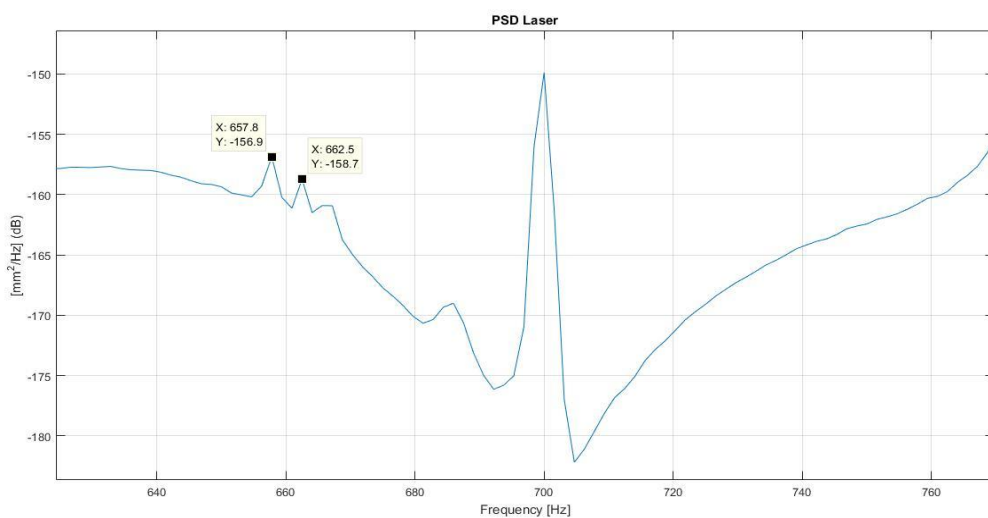


Figure 4.27 – Two very close natural frequencies at about 660 Hz.

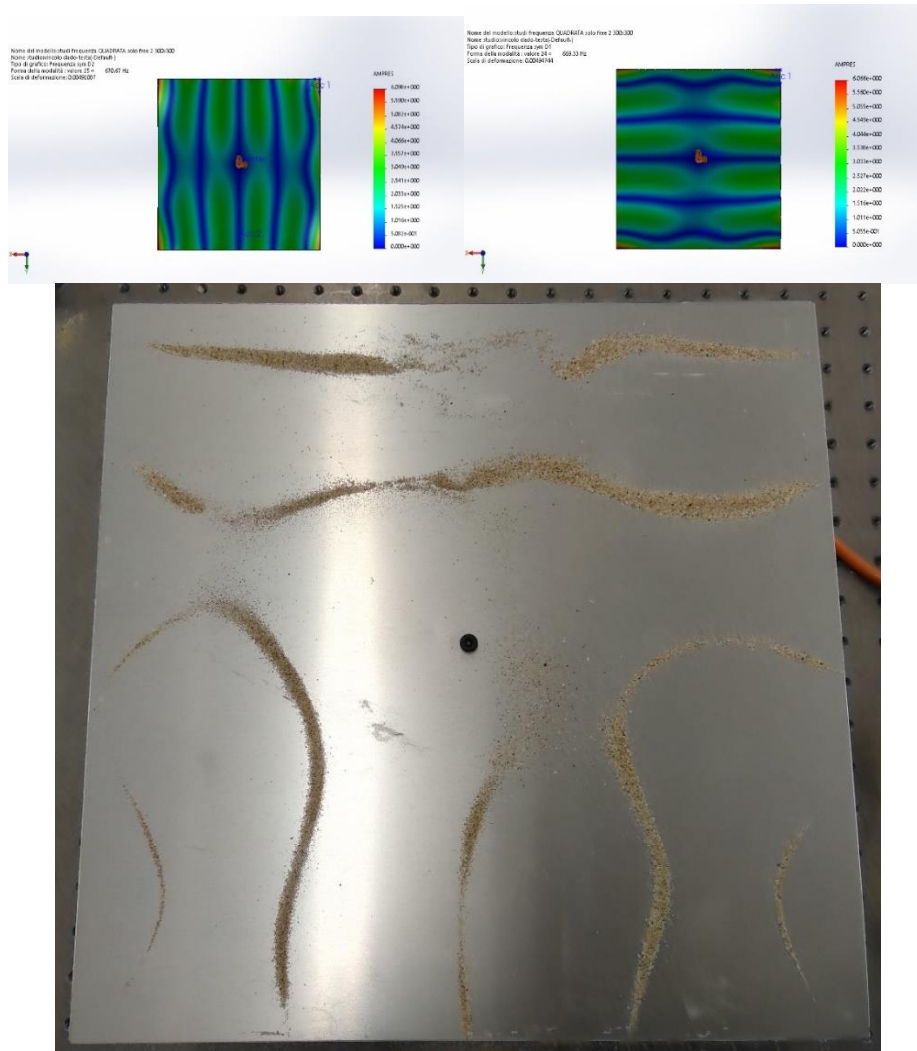


Figure 4.28 – Predicted mode shapes and the experimentally obtained pattern.

4.2.3 PSD COMPUTATION - LASER MEASUREMENTS

Laser sensors can be used to measure displacement or velocity when accelerometers are not suitable, for example if the surface can't be reached easily, or it is too hot causing the wax to melt, or if the specimen to be tested is so light that even the small accelerometers masses would modify its dynamic properties; the comparison between the results of this point and the previous one, shows that we are in this situation.

The laser head has been mounted on a structure and pointed towards the desired point (Fig 4.29).

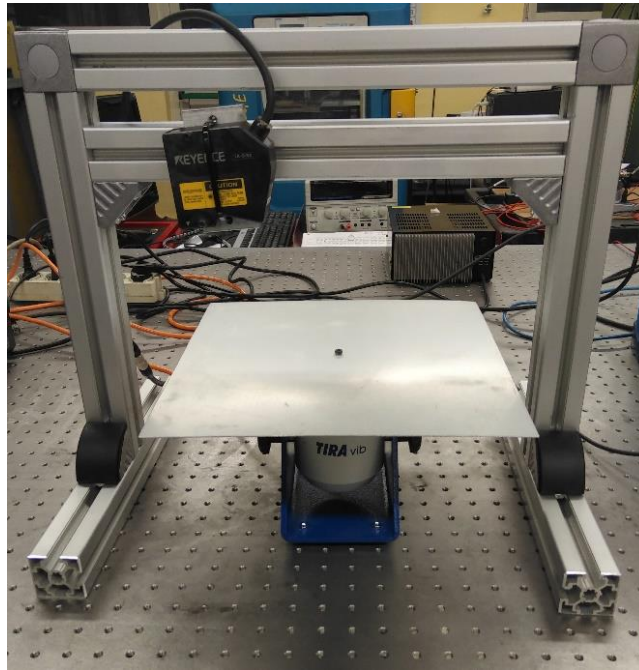


Figure 4.29 – Laser head support structure.

Measurements have been taken with the same exciting signals (random noise and sine sweep), and for the same duration as before.

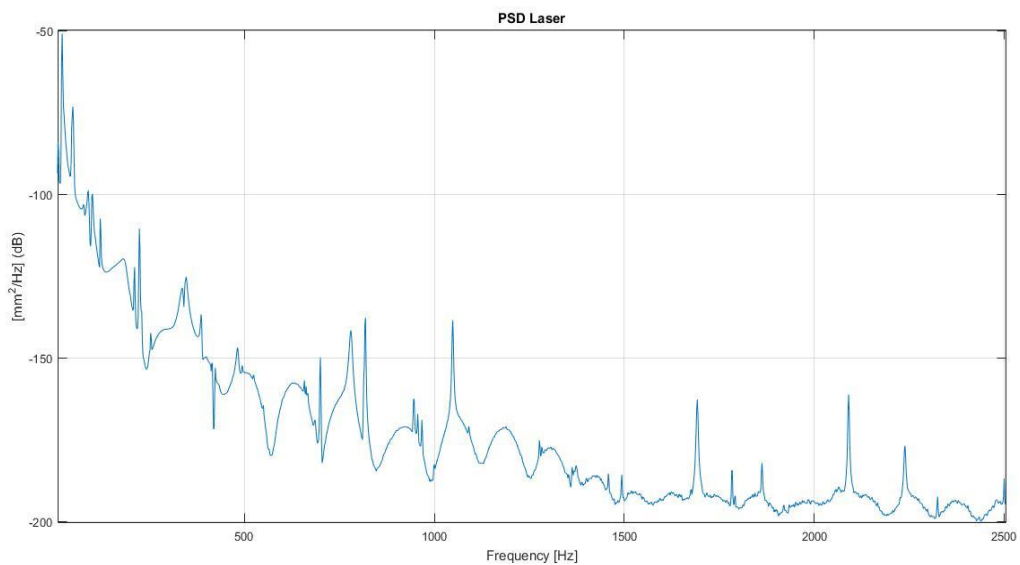


Figure 4.30 – PSD on the whole range of interest. Excitation is a sine sweep.

- 1) A significantly weaker signal can be noticed, as laser sensor measures displacement, that is lower than acceleration by a factor ω^2 (the difference is more evident with increasing frequency). In the last part of the spectrum, only resonances stand out clearly because of the too low signal to noise ratio.

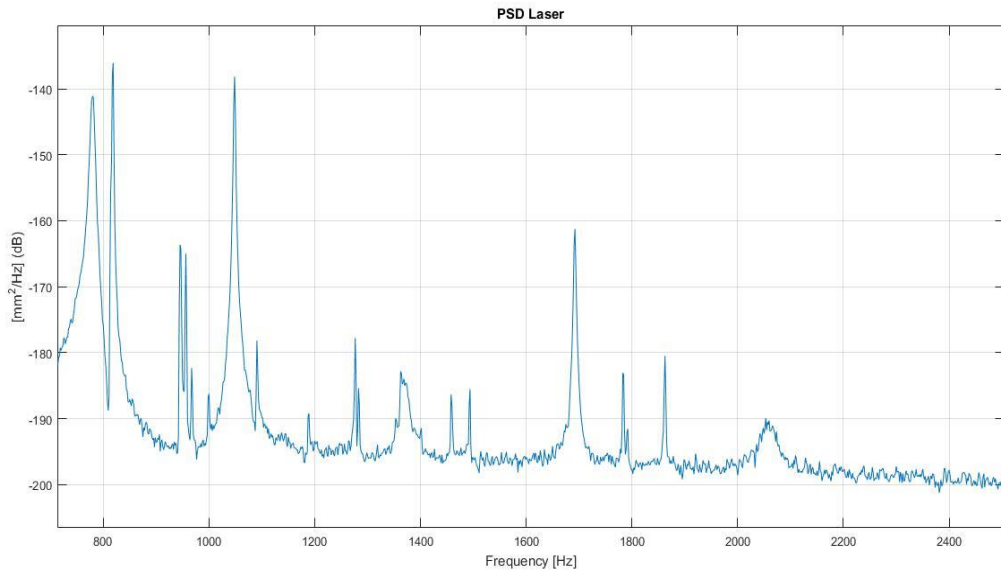


Figure 4.31 – Amplitude of signal decreasing significantly with frequency. It is particularly evident with random noise excitation.

- 2) Since the plate is not loaded with additional accelerometers masses, its resonant frequencies are higher, as can be seen from the comparison below (Fig 4.32 A and B). Even if the added masses are only 2,4 grams each, a small but non-negligible change is induced, being the plate itself very light.

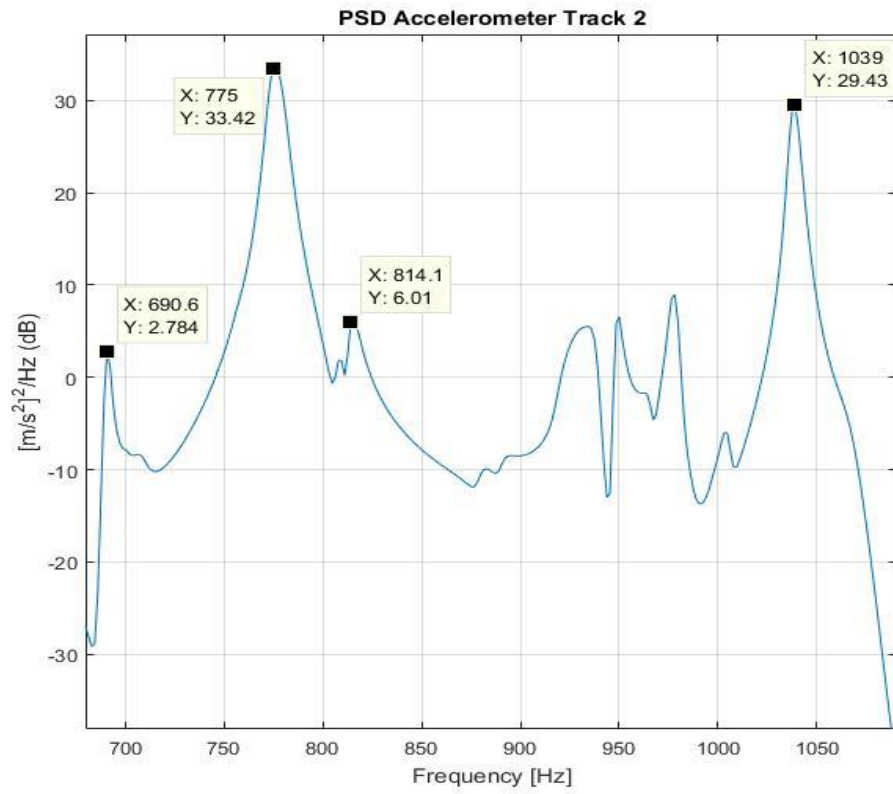


Figure 4.32 A

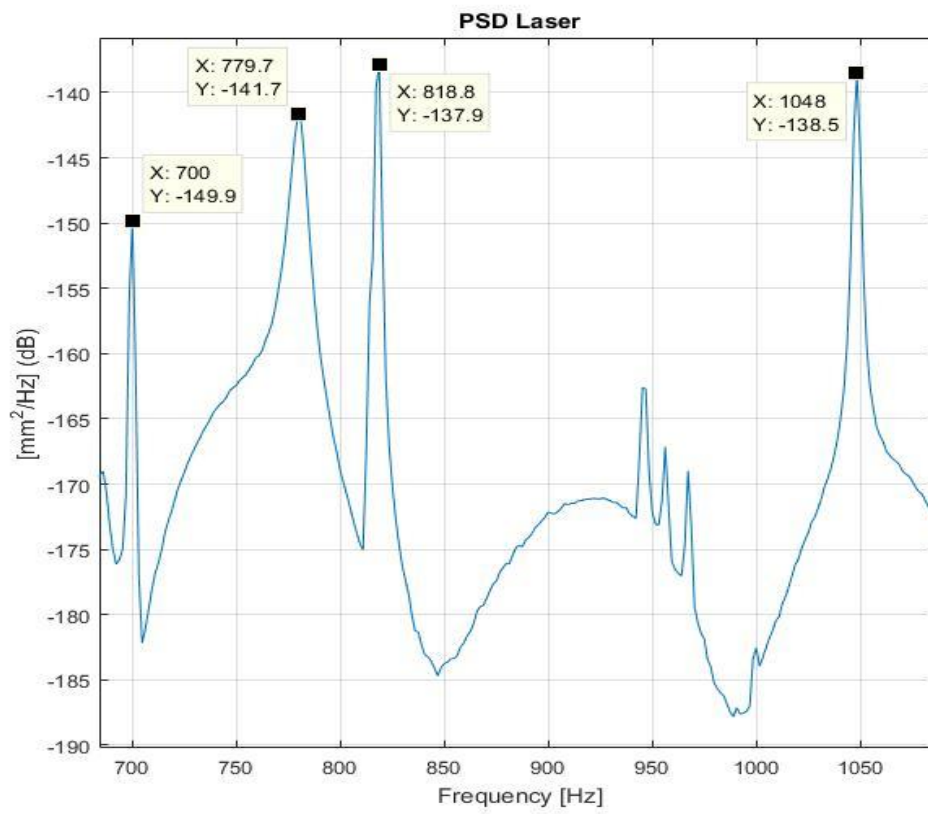


Figure 4.32 B

- 3) Damping factor for a given mode can be estimated using the -N dB method; according to this method, the loss factor β is:

$$\beta = \frac{1}{2} \frac{1}{\sqrt{n-1}} \frac{(\Omega_2 + \Omega_1)}{\omega_n} \frac{(\Omega_2 - \Omega_1)}{\omega_n}$$

where N is:

$$N = 20 \log_{10} \sqrt{n}$$

Since damping for a 1,25 mm thin aluminum plate is very low, resonant peaks in the spectrum are narrow, so to identify clearly points 1 and 2 we need to move downwards from peak of more than 3 dB (as it is usually done in more damped systems); in the following images (Fig 4.33), the points at -15 dB from the peak are highlighted; they are not at the very same amplitude because of the spectrum resolution.

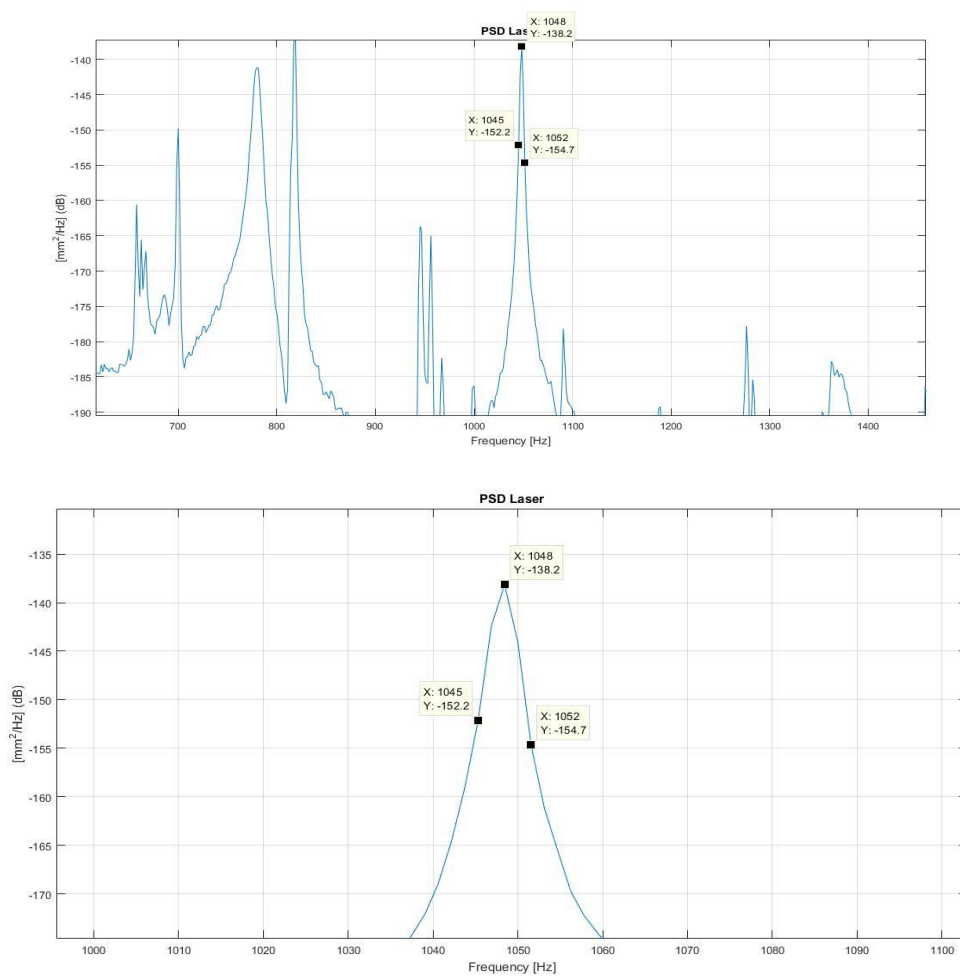


Figure 4.33

From computations, we have:

$$\beta = \frac{1}{2} \frac{1}{\sqrt{32-1}} \frac{(1052 + 1045)}{1048} \frac{(1052 - 1045)}{1048} = 0,0012 [-]$$

a very low value, as expected. It should be underlined however, that this is an estimation, since the -N dB method is accurate for values of damping neither too high, nor too small.

5 PROCEDURE FOR STUDENTS EXPERIENCE

A procedure with detailed operative instructions and safety measures has been obtained from the previous analysis, to guide students to replicate in the laboratory some of the results.

WARNING

Moving objects and fragile instrumentations are present in the test rig, then it is advisable to pay attention during the laboratory experience and carefully follow the provided instructions.

Preliminary operations

1. Make sure all the instruments are turned off, and check the status of their knobs and potentiometers, in particular:
 - Frequency generator: amplitude and frequency knobs should be set to zero, frequency range switch should be on the '200 Hz' position;
 - Shaker's power amplifier: both current and voltage knobs should be set to zero.
2. Turn on the frequency generator using the switch, set amplitude to a minimum value, set frequency at a low value (30-40 Hz).
3. Turn on the amplifier using the power button.

Chladni experiment – Visualization of mode shapes

1. Place the shaker, with the plate already bolted on it, above the square plastic base, which will gather the powdered material falling off the vibrating plate during the experiment.
2. Sprinkle some grains of salt or sand over the plate, trying to cover it homogeneously. This operation must be repeated from time to time since material will progressively fall down with vibrations.
3. Turn the voltage knob a few degrees past the position that produces a click sound. The shaker is powered and the plate starts vibrating at the frequency selected through the frequency generator.
4. Use the frequency knob on the generator to slowly move at the desired frequencies (see Table 5.1); when the frequency reaches the maximum value for the current range, the following range must be selected (to go beyond '200' choose '2k', to pass '2k' choose '20k'), making sure to set to zero both the voltage knob on the amplifier and the frequency knob on the generator, to avoid a sudden jump in the frequency of the excitation that could damage the shaker's internal spring system.

When approaching the suggested resonance frequencies, gently adjust the exciting frequency not to surpass the resonance. A further hint to recognize the resonance is to carefully listen to the increasing sound emitted by the plate. Once the plate is in resonance, it is suggested to adjust the voltage knob on the generator increasing the power if nodal lines are not clear enough, or decreasing the power if nodal lines are already evident, to avoid the sand jumping away from the plate.

Laser head positioning

1. **GENTLY** clean the plate from residual sand or dust using a cloth, without exerting pressure.
2. Place the structure supporting the laser head above the plate, paying attention not to hit the specimen; the plastic base can be left in position.

Laser vibrometer calibration (to be left to the supervisor)

WARNING: do not point the laser beam towards eyes.

1. Adjust the relative position of the structure and the plate, or slide the head along the horizontal beam, to aim the laser head towards the desired point.
2. Switch on the current generator to power the laser head; the control unit display will turn on, and the head will project a red dot on the plate. Since the laser head should be at a given distance from the target surface, adjust the vertical position of the horizontal beam (using screw and nut on the sides) until the control unit will display the displacement measure; if the head is too close or too far, the display will show 'FFFFF' or a fixed number.
3. Once the distance is set, press the 'zero' button on the control unit, and hit gently the plate to see if the measure on the display changes.

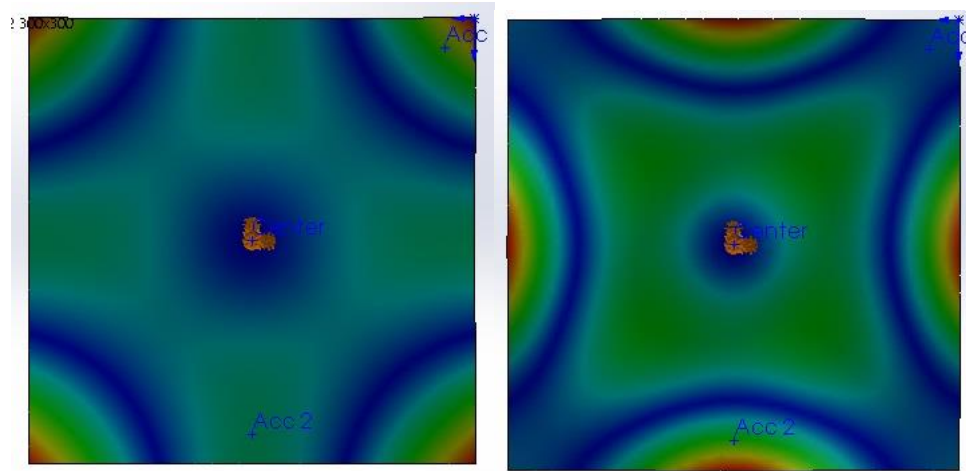
Considerations - signal amplitude and nodal lines

1. Once the laser head is working, the acquired signal can be visualized on the analyzer software; exciting the system with a sine sweep in a frequency range with several resonances (use the known resonances from table 5.1), it can be seen how the signal's waveform noticeably increases as one goes past a resonant frequency.
2. At any resonant frequency, pointing the laser head in different points of the plate, by simply sliding it on the horizontal rail (without moving the support structure), highlights how different amplitude of motion is; if a mode shape previously identified with the Chladni experience is selected, it can easily be observed that nodal lines have an almost null displacement compared to other areas.

Power spectral density

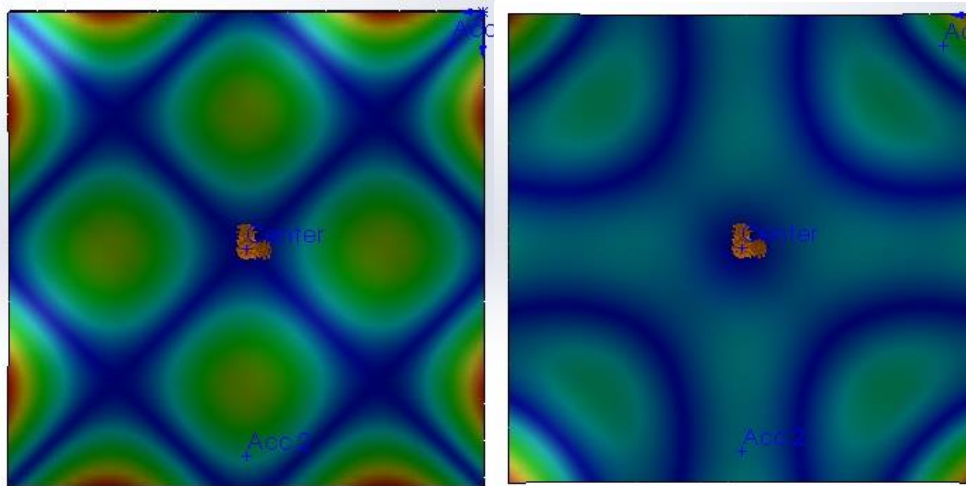
1. Define the excitation properties (sine sweep or random noise, frequency range, duration).
2. Run the measurement paying attention not to move the plate, nor the laser holder or the table.
3. Save and export the measured data as MATLAB file.
4. Run the provided script to load the measured file, processing it to compute and visualize the power spectral density.

TABLE 5.1 – MODE SHAPES AND NATURAL FREQUENCIES



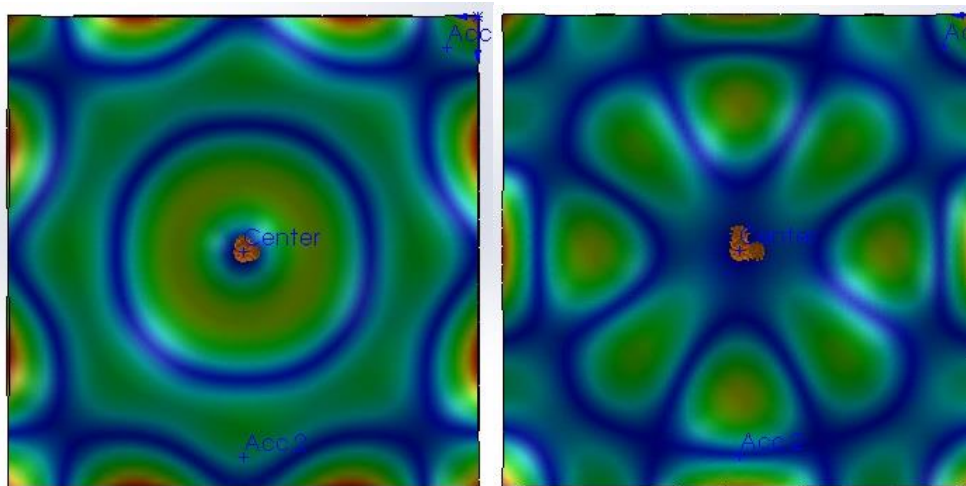
185-190 Hz

330-335 Hz



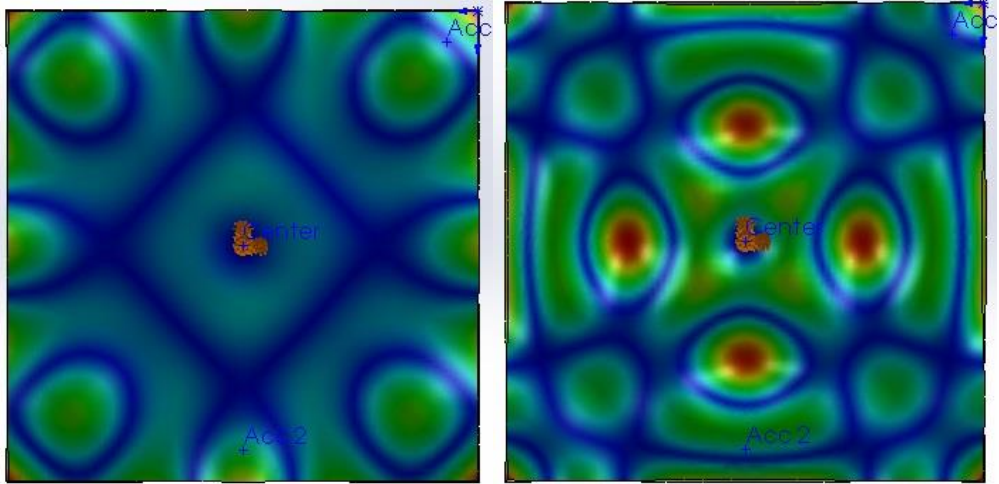
385-390 Hz

480 Hz



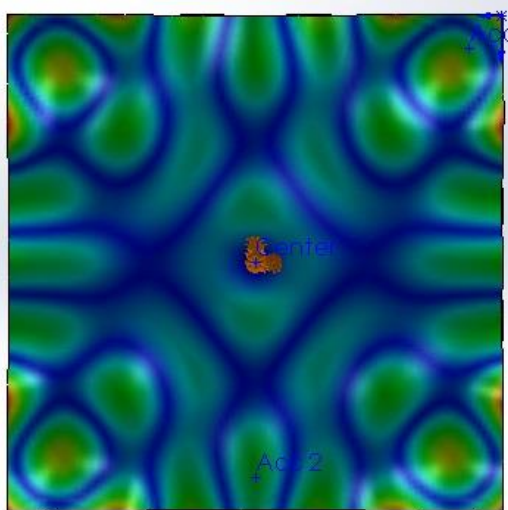
780 Hz

948 Hz



1048 Hz

1693 Hz



1865 Hz

PART II

The aim of this part is linking part I with a practical application, the design and manufacturing of the soundboard of a string instrument, namely an acoustic guitar.

After an introduction explaining the key role of the soundboard in the quality of the instrument sound, the change in the behavior of this component is analyzed using FEM simulation, with progressively increasing complexity of the model to mimic the manufacturing process.

Finally, results from several measurements taken in an anechoic chamber are compared, to describe the evolution of the soundboard acoustic properties.

1 GUITAR ANATOMY AND PHYSICS [4]

A brief description of the most important parts of the instrument is reported; Rossing, Thomas D., *The science of string instruments* provided useful information on the topic.

1.1 STRINGS

Guitar strings follow the taut string models, ruled by the following wave equation:

$$\frac{\partial^2 y}{\partial t^2} = \frac{T}{\mu} \frac{\partial^2 y}{\partial x^2} \quad (1.1)$$

where T is the applied tension, μ is the linear density, and the x axis is parallel to the string. Once the string is plucked, waves propagate in both directions with speed $c = \sqrt{T/\mu}$ and, when they reach the ends, are reflected; the interaction between the two waves creates a standing wave, which can be described by the superposition of normal modes:

$$Y = \sum_n (C_n \sin \omega_n t + \phi_n) \sin k_n x \quad (1.2)$$

where C and ϕ are the amplitude and phase of the n^{th} mode, and $k_n = \omega_n/C$ is the wave number. The actual motion of the string is a combination of mode shapes (Fig 1.1), and it depends on the point the string is plucked, too: for example, since even harmonics have a node at the center of the string, if it is plucked in the midpoint only the odd numbered harmonics contribute to the motion.

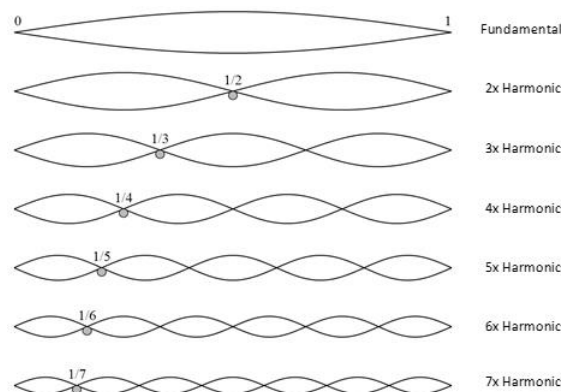


Figure 1.1 – Mode shapes from 1 to 7.

Strings frequencies depends on their gauge, material, length, applied tension; the fundamental frequencies of each string in standard tuning is reported below.

Table 1.1 –String fundamental frequencies in standard tuning.

String	Fundamental Frequency[Hz]	Pitch Notation
1	329.63	E4
2	246.94	B3
3	196.00	G3
4	146.83	D3
5	110.00	A2
6	82.41	E2

Since strings are very thin, the sound pressure produced is low and the sound produced is barely audible, therefore some kind of amplification is required.

1.2 COUPLED RESONATORS

In acoustic instruments, amplification is provided by a soundbox, and in particular by its top part, the soundboard, to which strings are connected through the so-called bridge (Fig 1.2); string vibration is so transmitted to the soundboard, that has a much larger surface than the string, moving more air and emitting a louder sound. It is worth underlining that it is not a proper amplification since, unlike electric string instruments, the system is supplied with energy only when strings are plucked.



Figure 1.2 – Detail of a guitar bridge; the upper profile of the saddle, in white in the picture, plays an important role, affecting the direction of the vibration component to be transmitted to the soundboard.

The price to pay to obtain this kind of amplification, is that the decay time of the string-soundboard system is shorter than that of the string alone, as energy is transmitted (and dissipated) more efficiently thanks to the soundboard, producing a vibration with higher intensity; in fact, guitar players say that acoustic instruments have a lower ‘sustain’ than their electric, solid-body equivalent, where the lack of a sound box allows the string to vibrate for a longer time, while amplification is obtained with electric power.

Moreover, the soundbox acts as a Helmholtz resonator (Fig 1.3), making the volume of air inside the hollow cavity resonate with the soundboard, in particular at its lower frequencies; its operating principle is based on the small pressure variation caused by the initial exciting force: the consequent increase in air pressure will make air exit through the soundhole, leaving an inside pressure lower than the outside one, thus inverting the direction of air, now entering the soundhole. The process

repeats, progressively damping out and causing the typical, slightly ‘wobbling’ sound, at low frequencies.

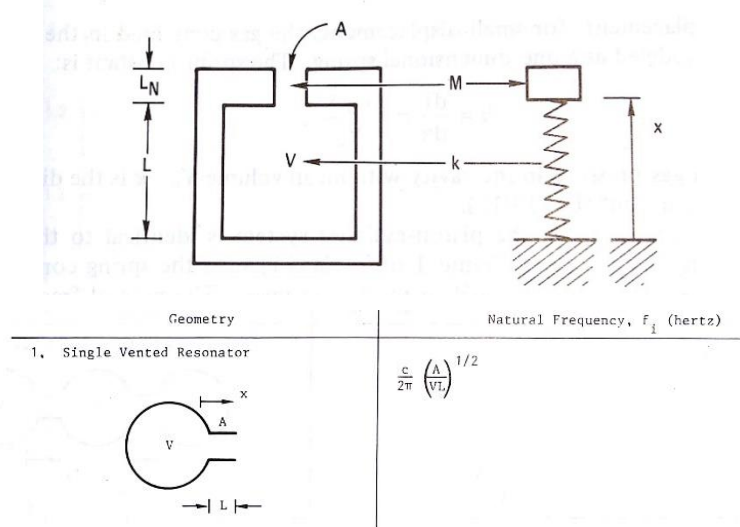


Figure 1.3 – 1 d.o.f. equivalent model of a Helmholtz resonator: the air cavity volume is modeled as a spring, the fluid in the neck as the mass; the natural frequency as function of geometry is also given (notice it is not dependent from the shape of the cavity).

As first approximation, a guitar can therefore be described as system of coupled resonator, i.e. soundboard and air cavity (2 d.o.f. model) or the formers plus the back plate (3 d.o.f plate), as the schemes in Fig 1.4 and 1.5 explain.

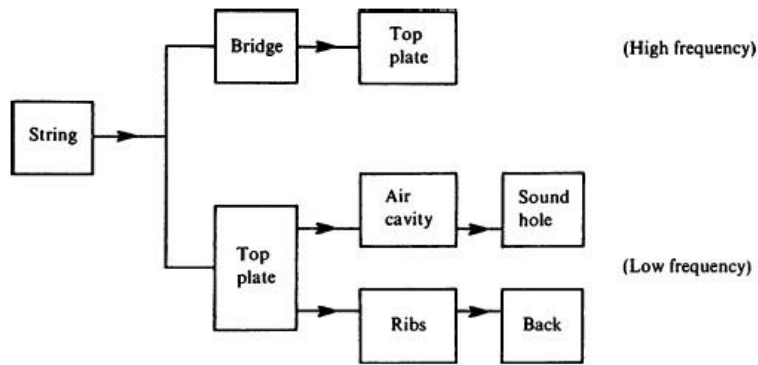


Figure 1.4– Schematic of the connections between guitar parts acting as resonators.

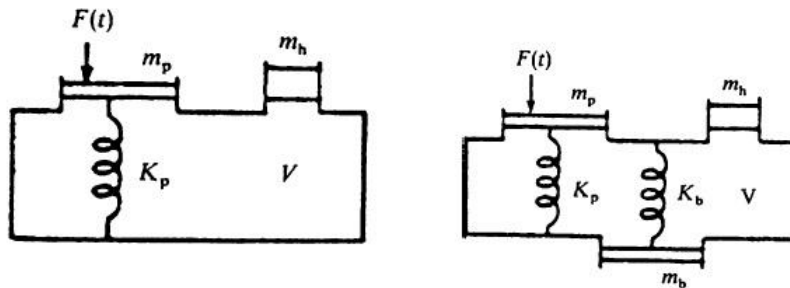


Figure 1.5 – 2 d.o.f. equivalent system, with the plate m_p and the air cavity m_h masses. On the right, the 3 d.o.f. model, with the additional back mass m_b .

The air cavity has an almost fixed volume, so Helmholtz frequency is not adjustable in the design process, and anyway it is relevant only at low frequencies; the back plate as well is considered of minor importance in the middle and treble bandwidth, since it mainly resonates with soundboard lower frequencies, and air cavity ones, creating the low frequency mode shapes of the instrument (Fig 1.6).

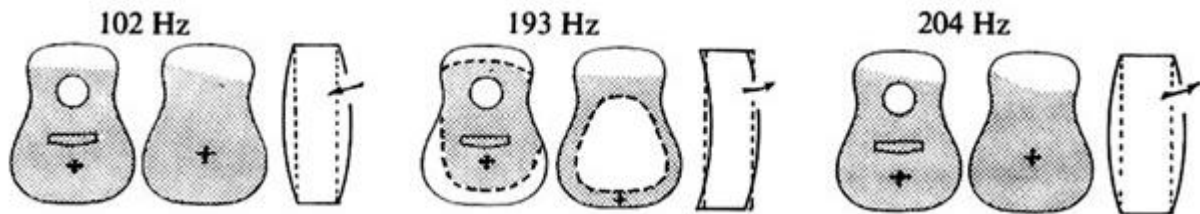


Figure 1.6 – Low frequency modes of the coupled top-air cavity-back system.

The middle-high frequency range, therefore, depends almost only on the soundboard properties, which will be discussed more deeply.

1.3 SOUNDBOARD

Since the soundboard has its own dynamic properties, its coupling with strings will amplify some frequencies more than others. The soundboard will affect not only the intensity of the sound but also its spectrum, giving what is called a timbre, i.e. that sound property that makes a note of the same intensity and pitch perceived as different if played by two different instruments. At this point, it is easy to understand that the soundboard is the critical component of a guitar, the one which differentiates a good sounding instrument from a poorly made one, providing it its peculiar sound. Tonewoods, wood types with particular acoustic qualities like spruce or cedar, are used to build the soundboard, that should be thick enough to withstand the string tension, still having good dynamic properties; a good result is usually achieved by using 2-3 mm thick soundboards, strengthened with wooden ribs on the inner side, to increase their stiffness without resorting to thicker wood plates, that would make the instrument not responsive; such a soundboard is referred to as 'braced'.

A first choice in selecting the range of frequency to be highlighted by the soundboard, is to select a body shape (Fig1.7); without providing too many details, a small waist parlor guitar (B profile in figure) has a better high frequencies tone than a large and wide dreadnought one (E profile), which instead is the most common and versatile body shape, with a solid low-middle response.

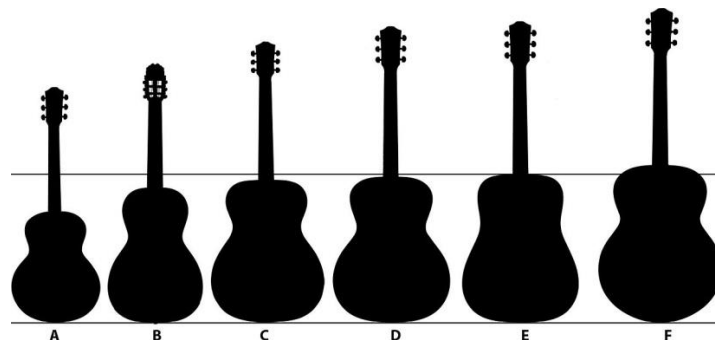


Figure 1.7- guitar body shapes: A. Range, B. Parlor, C. Grand Concert, D. Auditorium, E. Dreadnought, F. Jumbo.

Considering that both the thickness and the profile shape are fixed, the only way to change the soundboard natural frequencies, to make it accomplish its resonator function, is to adjust braces characteristics: layout, section shape and dimension, longitudinal profile.

1.4 SOUNDBOARD BRACING

1.4.1 LAYOUT

Wooden struts can be arranged in several patterns, the most common are the 'X' and ladder, but many others like double X and asymmetrical ones are possible (Fig 1.8).



Figure 1.8 – From top-left to bottom-right: ladder, 'X', double 'X', and an asymmetrical pattern.

It can be noticed that more complex ('X' and asymmetrical ones) bracing patterns are designed in order to provide larger, less stiff areas on the bass side of the bridge (right side of images above) and in the bottom part of the soundboard, when lower frequency modes are more prominent, while smaller and stiffer areas are defined on the treble side of the bridge (left side in previous images), and more generally along the narrow regions beside the soundhole, where higher frequency shapes are dominant.

Patterns provides additional stiffness especially along the horizontal direction, to compensate the fact that soundboard wood grains are instead oriented vertically; thicker struts have this structural function, while smaller ones are more oriented towards tone control, as it will be explained below.

1.4.2 SECTION SHAPE AND DIMENSIONS

As mentioned before, soundboard is braced to increase its flexural stiffness and avoid a dangerous deflection under the action of the high string tension; nevertheless, sufficient stiffness should be reached by adding the least quantity of wood, i.e. without adding too much mass to the system, thus reducing its responsiveness and worsening its dynamic behavior.

To achieve this scope, wooden struts should have a cross section with a high bending resistance module and the minimum area. So, not only they are slender, but often they are also shaved along their upper edges (Fig 1.9). Reducing the height and smoothing the edges of the struts using a chisel is exactly the way used by luthiers to tune the soundboard.

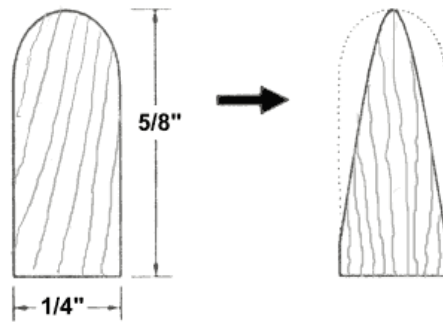


Figure 8: Cross section of a typical steel string guitar brace is shown at left. Author's brace, shown at right, has the same overall dimensions, but significantly less wood.

Figure 1.9 – The cross section on the right has a slightly lower bending resistance module, compensated by a much lower area.

1.4.3 LONGITUDINAL PROFILE

The principle of increasing stiffness while adding the minimum amount of mass is also present in the design of the longitudinal profile: a straight bracing would generally be too heavy, resulting in a 'overbuilt' guitar, while removing some mass to create the so-called scalloped profile would provide almost the same stiffness where the profile is high, still leaving a very light and responsive structure where the profile is lowered. Generally speaking, struts are left untouched in their part closer to the longitudinal axis of the soundboard, while they are lightened towards the periphery (it is a necessity for a correct joining with the sides the instrument, too); moreover, in between these two ends, a more complex profile can be developed (Fig 1.10).

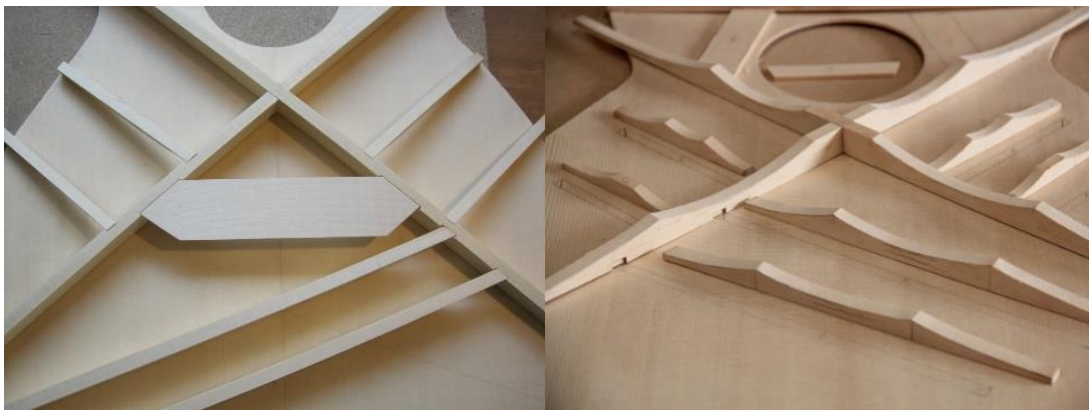


Figure 1.10 – Straight and scalloped braced soundboards; the difference in wood quantity is evident.

2 FEM SIMULATIONS

The aim of this chapter is to show the change in the dynamic behavior of a blank guitar soundboard after adding of bracing structure, and the following refinement when wood from the struts is progressively removed using the rationale explained so far.

The FEM models have been developed with accurate dimensions, taken from a real dreadnought guitar (Fig 2.1).

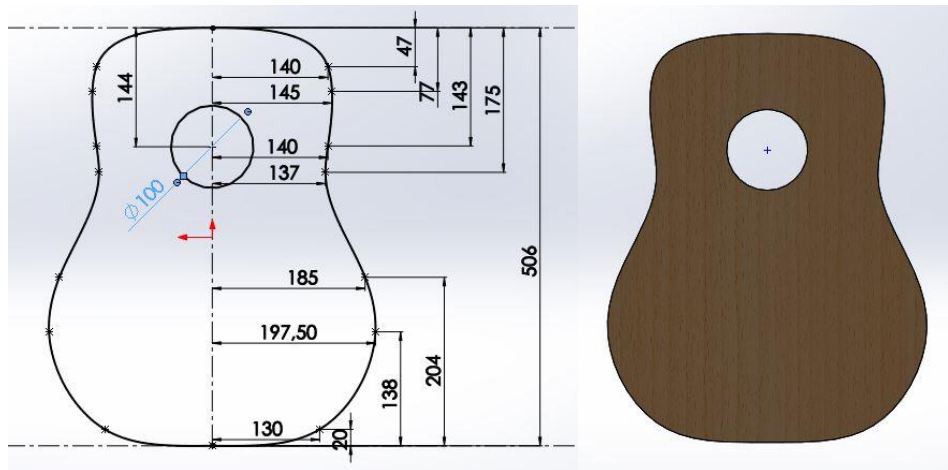


Figure 2.1 – Soundboard detailed dimensions.

A bracing pattern has been defined in every geometrical parameter (Fig 2.2); it is a simplified X bracing, actually used in practice, consisting of:

- A transversal cross brace, 15x15 mm cross section; it is larger than other parts, since it has basically a structural function.
- Two 10x20 mm struts, the actual ‘X’ brace; this adds stiffness in both directions, and along almost the entire length of the instrument.
- A tone bar in the lower part, 5x20 mm; the angle is different from the X brace, to create asymmetrical areas in the central part of the soundboard, for the reasons explained before.
- Two small finger bars, 5x20 mm, in lateral position; they will be lightened to a very reduced thickness, having the only purpose to obtain more uniform mode shapes.

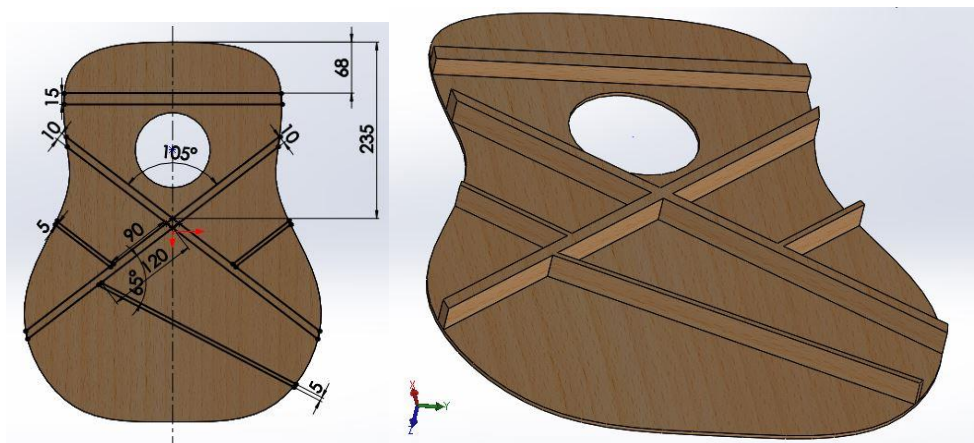


Figure 2.2

As geometrical features can be easily activated, deactivated or modified in the FEM model, this possibility has been used to obtain the mode shapes and natural frequencies for a set of different layouts, representing the various stages in the manufacturing of the soundboard:

1. Blank soundboard (Fig 2.3 A).
2. Soundboard with cross and X braces (Fig 2.3 B).
3. Fully braced soundboard, unrefined (Fig 2.4 A).
4. Braced, with lightened cross brace and X brace (Fig 2.4 B).
5. Braced, with lightened cross brace and X brace, scalloped tone bar (Fig 2.5 A).
6. Braced, completely finished with scalloped finger bars (Fig 2.5 B).

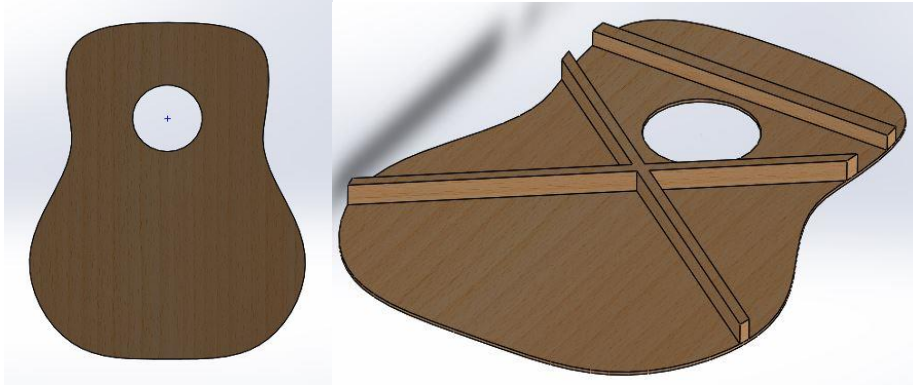


Figure 2.3 A and B

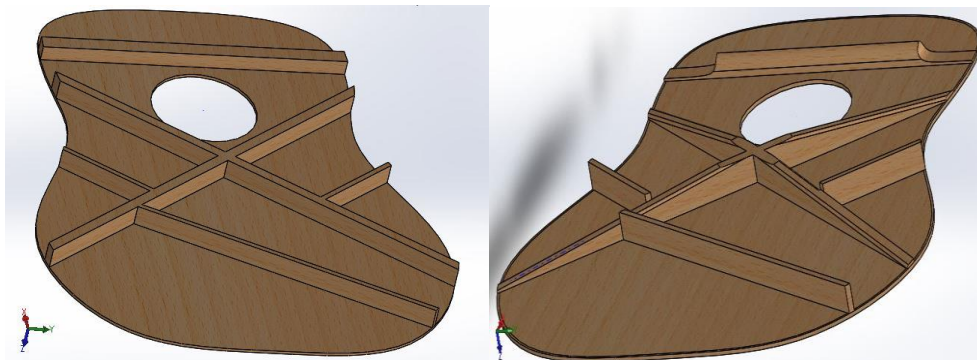


Figure 2.4 A and B

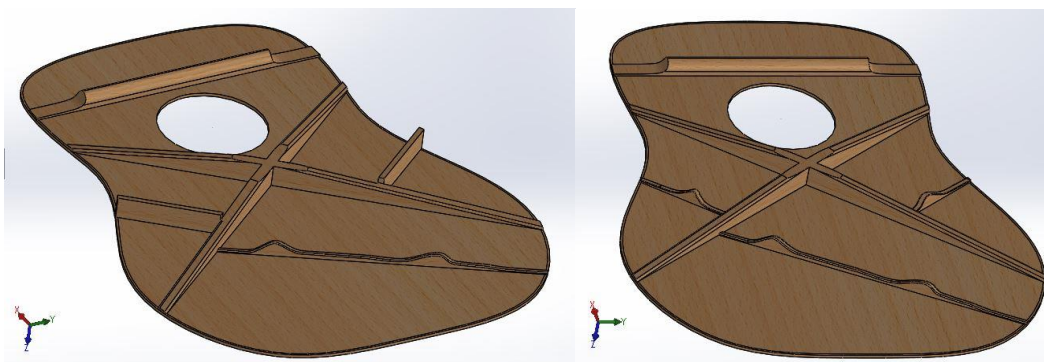


Figure 2.5 A and B

A comparison of both mode shapes and natural frequencies along this series of states can be performed.

2.1 MODE SHAPES

2.1.1 FROM BLANK TO BRACED SOUNDBOARD

Free mode shapes

The free soundboard shows mode shapes (Fig 2.6) resembling those of the plate seen in Part I, but of course they are even more complex because of the particular shape of the profile, and the presence of the 10 centimeters soundhole.

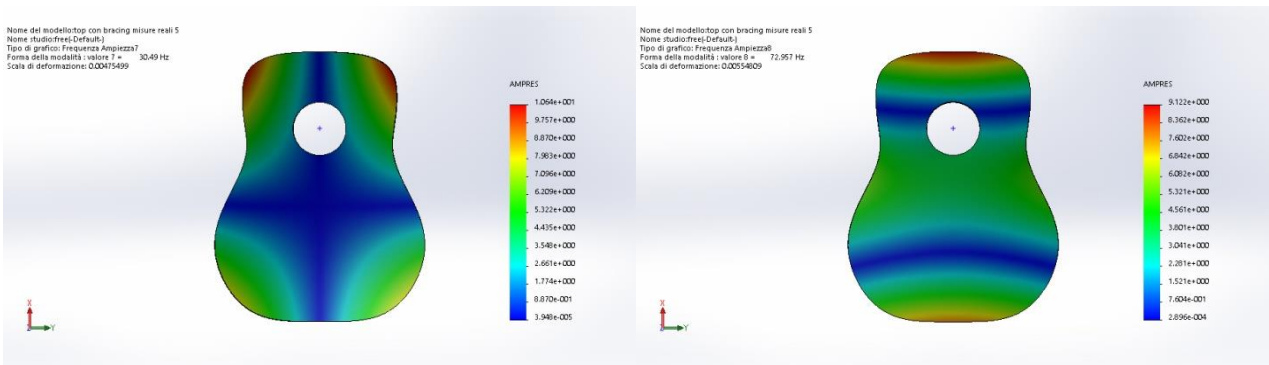


Figure 2.6 A and B

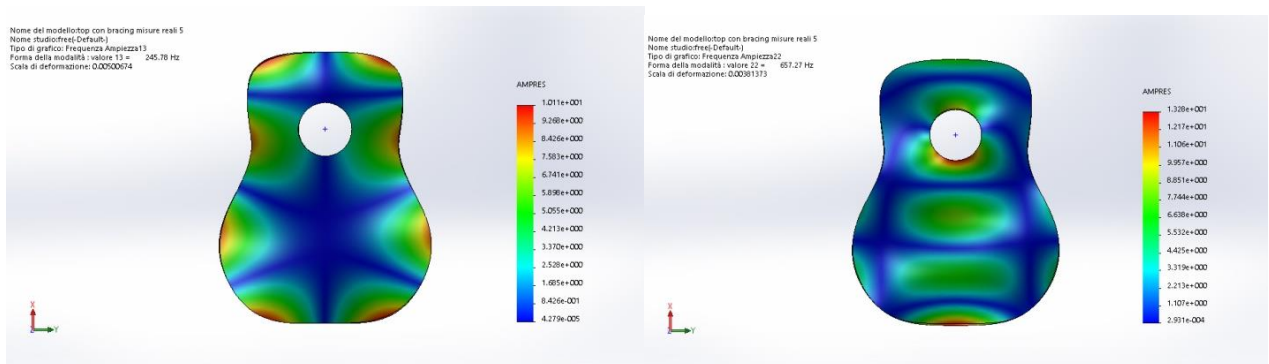


Figure 2.6 C and D

The blank soundboard is noticeably stiffened by adding the braces, which are much thicker and almost evenly disposed along the surface; as a consequence, even if mode shapes are still recognizable, their nodal lines now follow almost exactly the struts, thus defining different areas vibrating in phase or in counter phase (Fig 2.7-2.8).

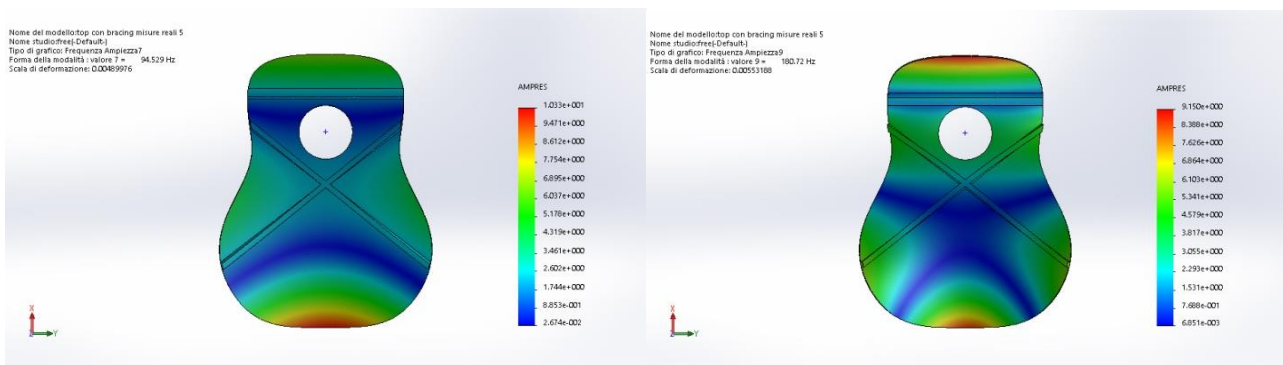


Figure 2.7 A and B – To be compared with 2.6 B and C to notice the shift of nodal lines.

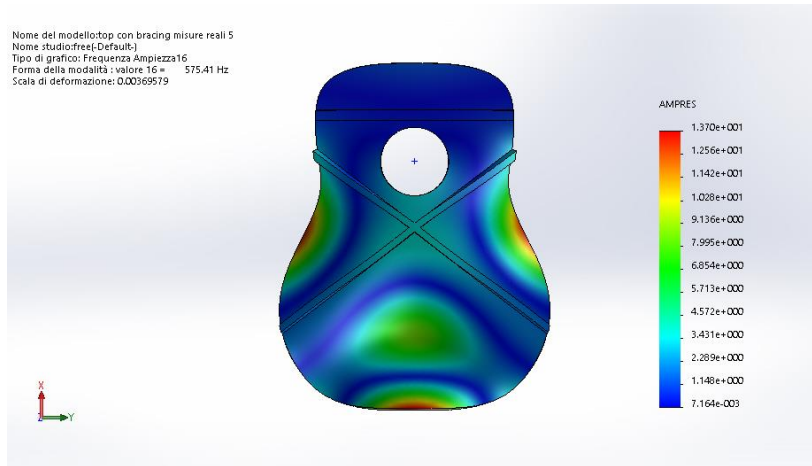


Figure 2.8 – An example of how the braces determine a mode shape.

The further addition of the diagonal tone bar creates asymmetry, while finger bars stiffen even more the sides (Fig 2.9).

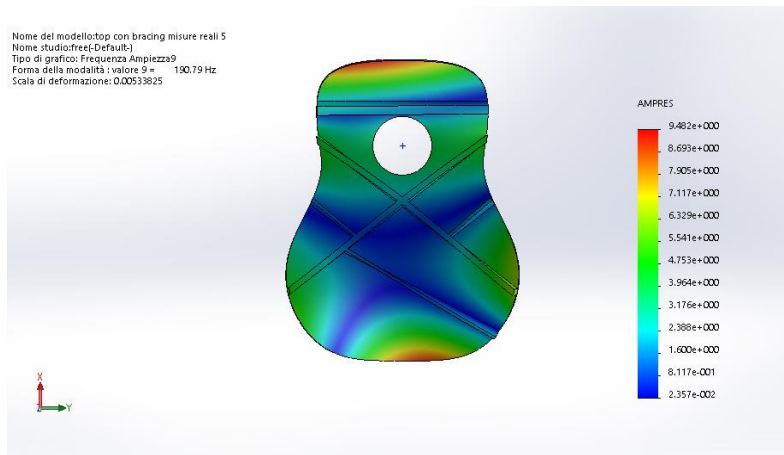


Figure 2.9 – To be compared with 2.7 B to notice the asymmetry.

Fixed mode shapes

When the soundboard is glued to the soundbox sides, it is constrained on its periphery; even if the constraint is not exactly a support nor a clamping, it has been modeled here as the latter. The effects of the bracing on mode shapes are even more evident with this boundary condition. Mode shapes for blank and partially braced top are reported below (Fig 2.10-2.12): modes shift downwards where the biggest area is described by the bracing pattern, and their nodal lines do not cross the struts in most of the cases.

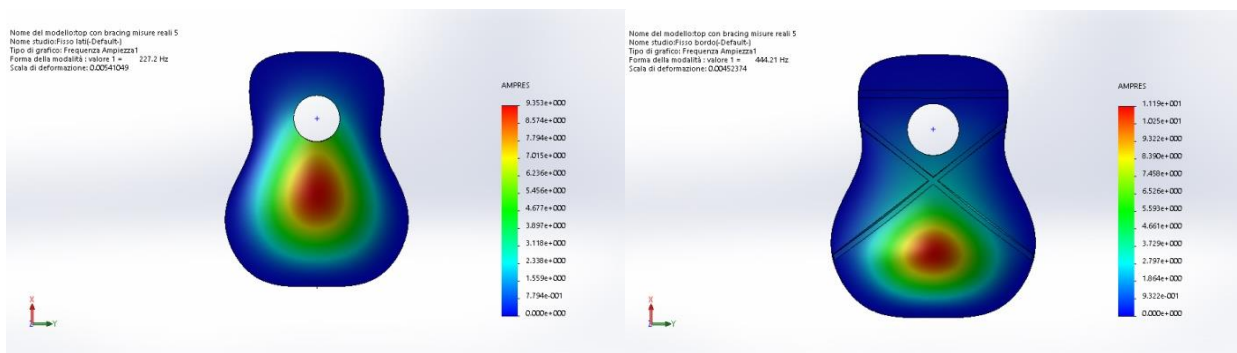


Figure 2.10 – Monopole in blank and braced case.

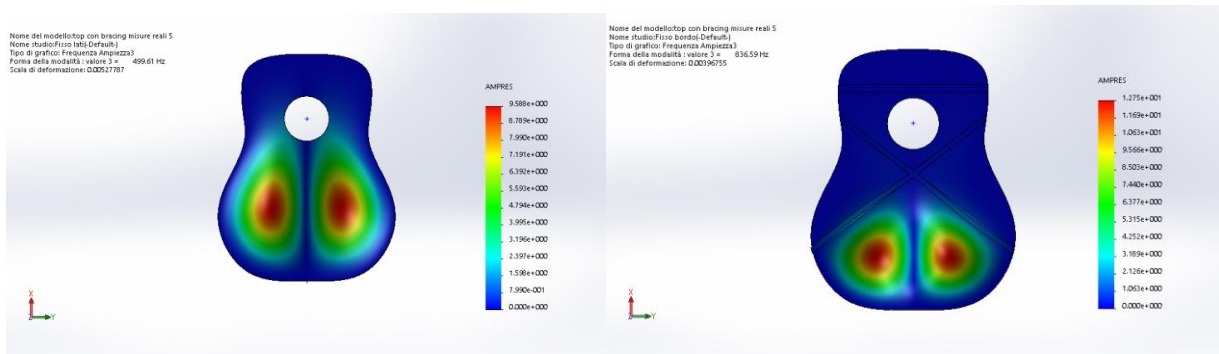


Figure 2.11 – Dipole in blank and braced case.

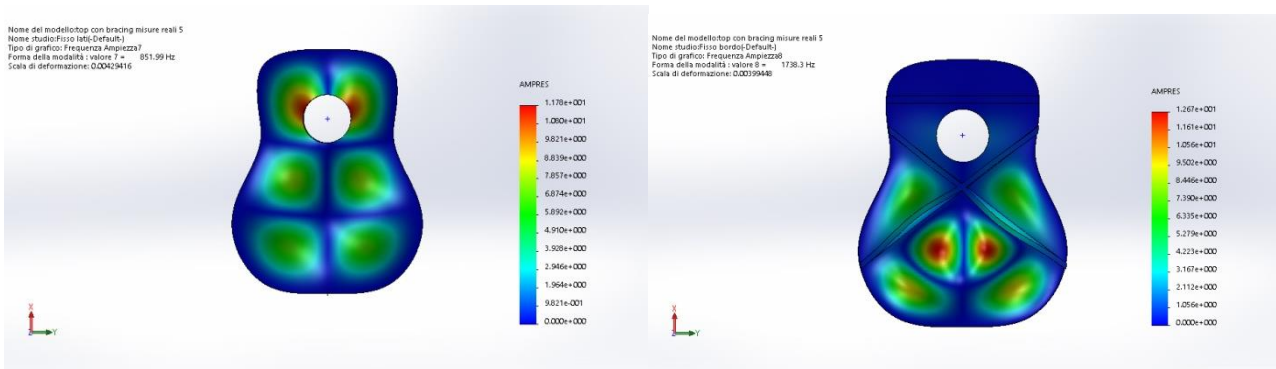


Figure 2.12 – The upper part of the soundboard does not vibrate as easily as in the blank configuration, because the thick cross brace and the smaller width make this part particularly stiff. Mode shape follows perfectly the areas delimited by the bracing.

As the diagonal tone bar is added, the lower area is split into two smaller ones, with most of the mode shapes changing accordingly (Fig 2.13).

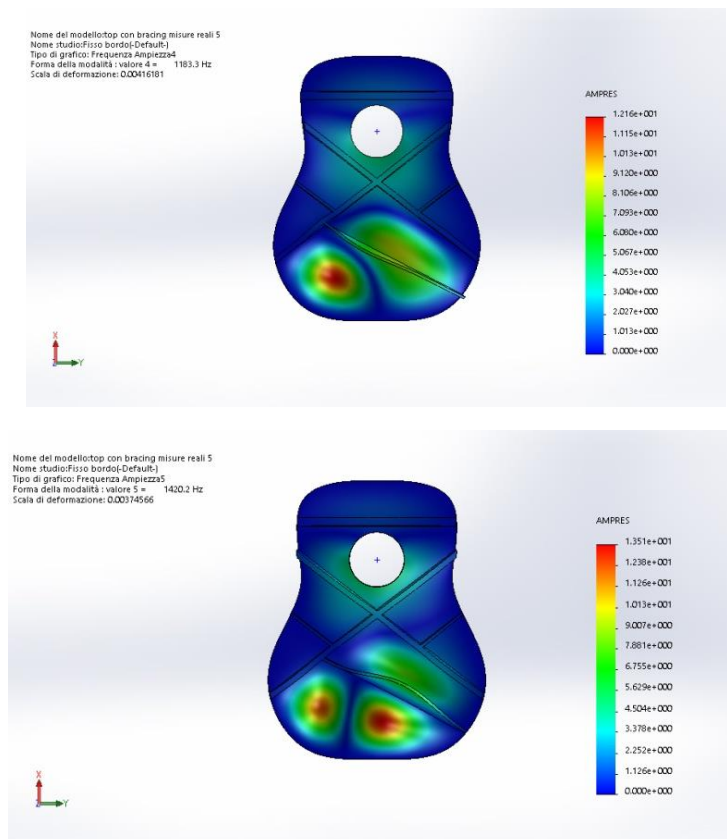


Figure 2.13 – Dipole and tripole follow the new layout.

The same happens to the two lateral parts, even if less evidently (Fig 2.14) because of their higher stiffness, due to finger braces and small extension.

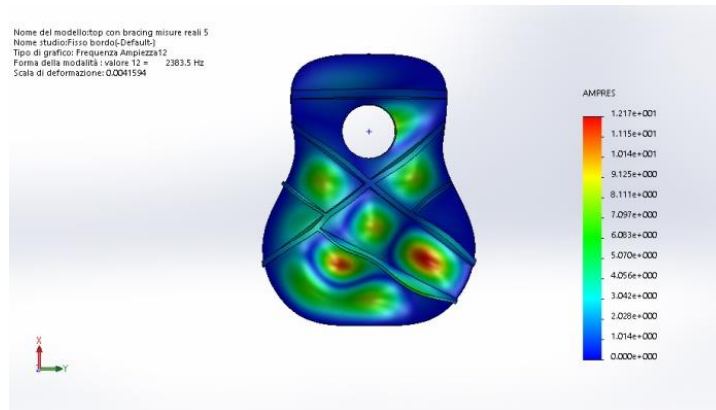


Figure 2.14

These points highlight the very essence of the bracing: the mode shapes are actually ‘modelled’ in the desired way, imposing a certain vibrational, and therefore acoustical, behavior.

2.1.2 MATERIAL REMOVAL

Free mode shapes

As material is removed from all the struts, nodal areas reduce, and mode shapes become more distinct (Fig 2.15).

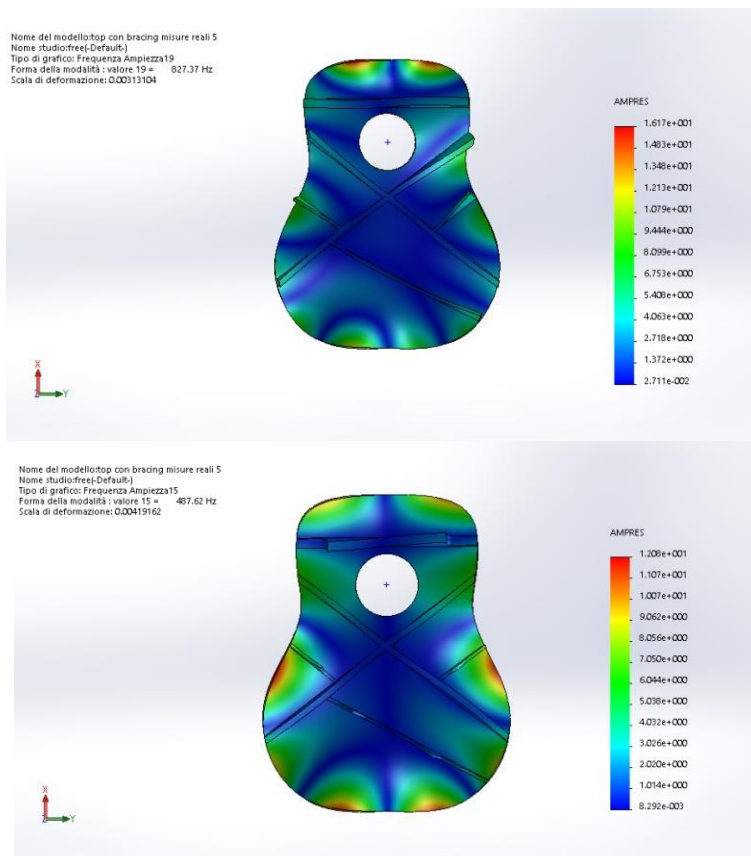


Figure 2.15 – An example of how the material removal from bracing creates a more responsive behavior.

Fixed mode shapes

The importance of lightening the bracing is much more evident in the constrained configuration. The first step consists in lightening cross and X brace (Fig 2.16), that are particularly stiff for structural reasons.

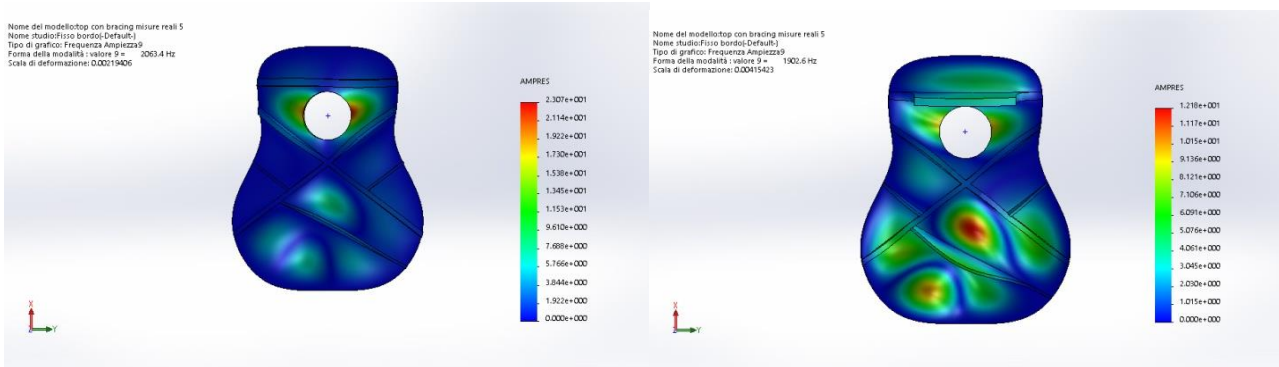


Figure 2.16 – Some mode shapes, barely visible before because of the excessive stiffness, are now clearer; a higher participation of the part above the sound hole can be seen, too.

In the next step, the ends and the central part of the tone bar are shaved, creating the so-called ‘scalped’ profile. The effects are very relevant, considering that the tone bar is one of the thinnest components of the bracing: besides having clearer mode shapes thanks to the general lightening of the bar, the material removal from its center reallocates the mass distribution, concentrating in the two ‘peaks’, each of them positioned at about one third of the length from the closest end. As a consequence, mode shapes’ areas in the two-bottom part can now cross the tone bar (Fig 2.18-2.20).

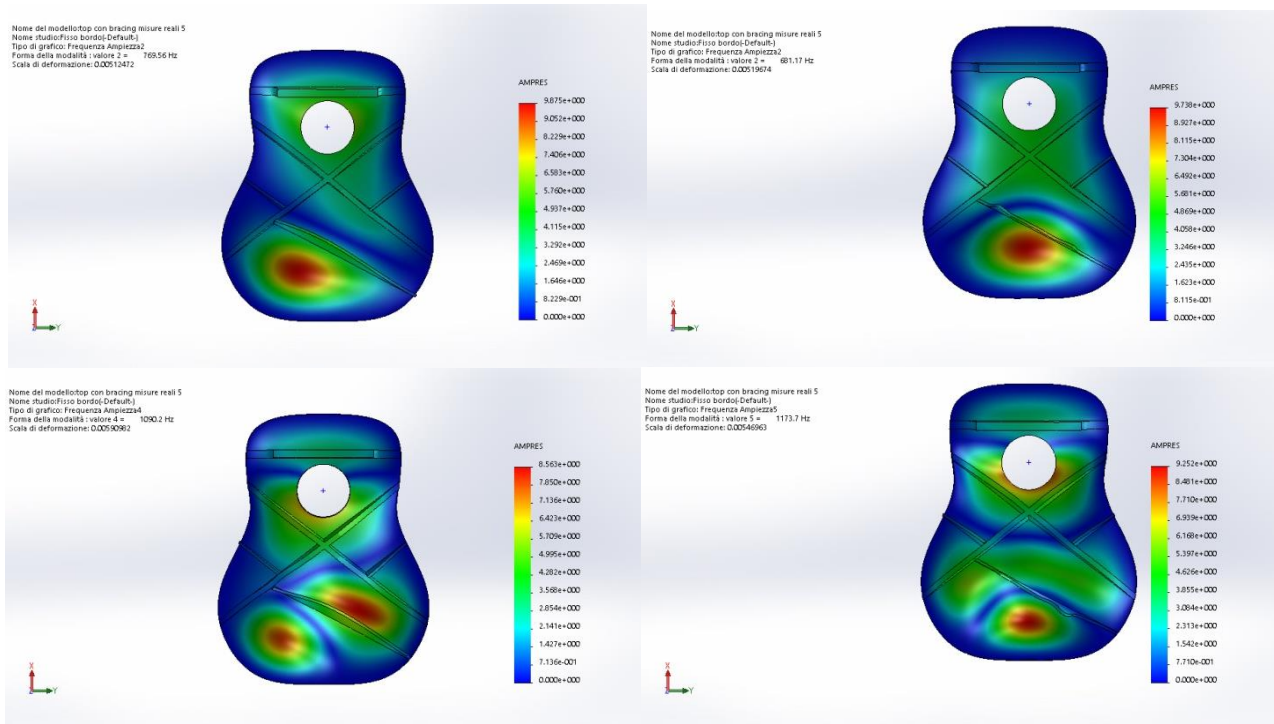


Figure 2.18– Untouched tone bar on left figures, scalped profile on right ones: removing mass from the middle of the tone bar moves, for certain modes, the maximum displacement areas towards the center of the soundboard, where the string sinusoidal force is exerted through the bridge.

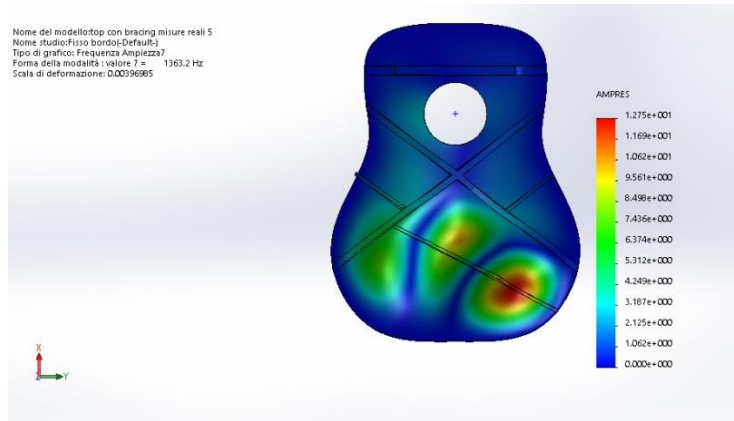


Figure 2.19 – Mode shape with nodal lines orthogonal to the tone bar; the unshaved mass near the right end acts as a peak, as the red color shows.

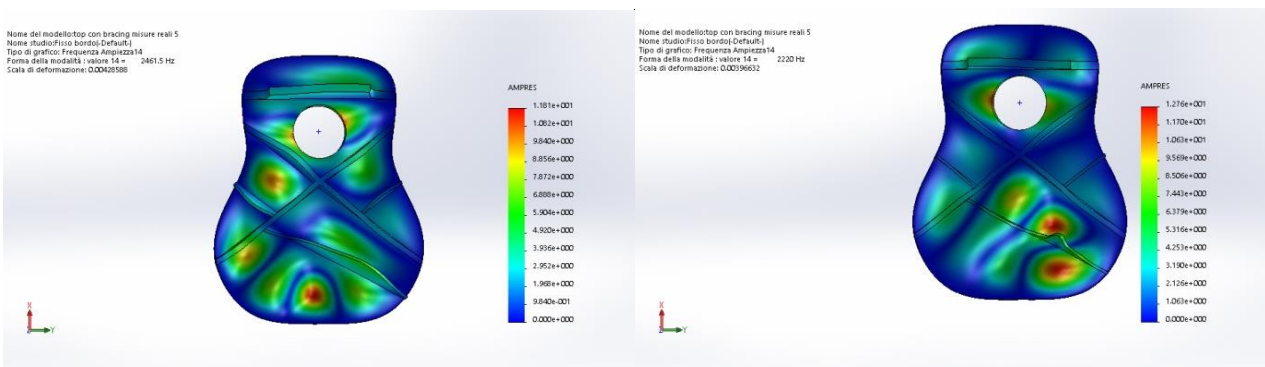


Figure 2.20 – Another example of how the nodal lines can now cut through the tone bar (scalped tone bar on the right).

The further material removal from finger bars affects almost only the two lateral areas, which can respond more freely (Fig 2.21).

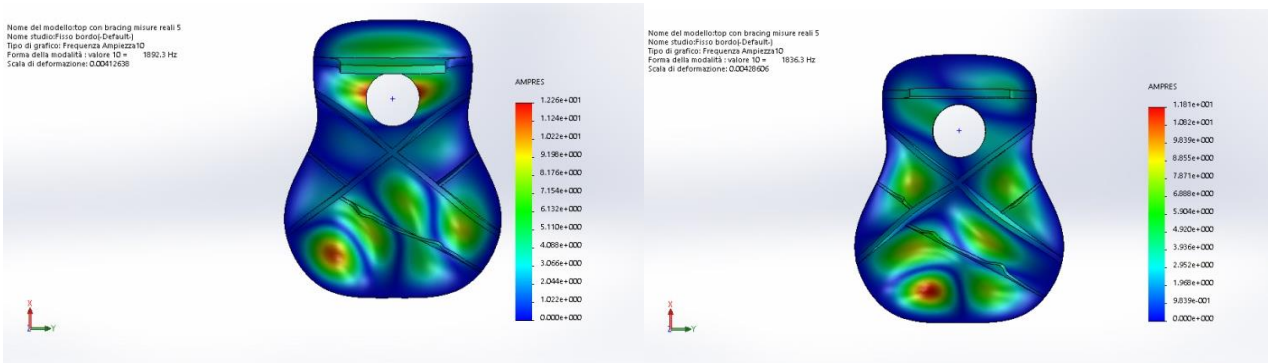


Figure 2.21– Higher displacement of side areas can be seen in the lightened finger braces case, on the right.

This part of the simulation highlights the very essence of the bracing: reinforcing the top, paying attention to every parameter of the pattern (geometric layout, struts thickness, final profile to be obtained) in order to get at the same time a light and responsive top, with a number of detailed mode shapes, essential to achieve the desired, complex sound spectrum.

2.2 NATURAL FREQUENCIES

For the reasons explained in chapter 1.4.2, the soundboard natural frequencies should match a particular spectrum, to create a responsive guitar. Precise guidelines about this target are difficult to find, as guitar makers often have their own design criteria, to provide guitars their ‘brand’ sound, that usually do not share. In general, however, the tuning process of the soundboard, often referred to as ‘voicing’, follows these steps:

- The soundboard is reinforced with bracing.
- As the braced top is definitively too stiff to have good dynamic properties, wood is removed from every component of the bracing, to noticeably lower natural frequencies.
- A subtler refinement is done, removing small amount of material especially from tone bar and finger braces.
- The last step is repeated, and after each passage some frequencies, in particular the fundamental one, are checked trough ‘tap tuning’, i.e. tapping the top with a finger in specific points and listen carefully to the obtained sound.

The FEM model, with its six steps (Fig 2.3-2.5) simulating the addition of the bracing and the following material removal, used to analyze the mode shapes variation, is now resorted to in order to follow the evolution of natural frequency throughout the process.

Natural frequencies for each state defined before is summarized in tables (Tab 2.1 for free soundboard, Tab 2.2 for fixed case).

Table 2.1 – Results for free soundboard. The relative shifts are referred to the previous column. The average of relative shifts is reported at the end of the column.

Mode	Blank soundboard	Cross and X brace		Fully braced	
	Frequency [Hz]	Frequency [Hz]	Relative shift	Frequency [Hz]	Relative shift
1	30,5	94,5	210%	96,8	2%
2	72,9	133,5	83%	142,2	6%
3	104,4	180,9	73%	190,8	5%
4	145,1	192,2	32%	211,5	10%
5	203,1	331,3	63%	345,5	4%
6	223,6	357,0	60%	365,8	2%
7	245,7	362,6	48%	436,6	20%
8	267,0	473,3	77%	487,1	3%
9	379,0	482,4	27%	518,0	7%
10	386,3	575,6	49%	660,0	15%
11	418,4	665,5	59%	670,5	1%
12	460,2	668,6	45%	688,5	3%
13	535,9	679,3	27%	827,4	22%
14	539,4	818,2	52%	843,8	3%
15	574,7	831,1	45%	904,4	9%
16	655,3	929,0	42%	949,1	2%
17	715,0	985,1	38%	1.012,9	3%
18	745,4	1.002,0	34%	1.051,2	5%
19	770,0	1.055,3	37%	1.089,4	3%
			58%		7%

Mode	Cross and X lightened		Cross and X bar lightened, Tone bar scalloped		Cross and X bar lightened, Tone and finger bars scalloped		Rounded edges	
	Frequency [Hz]	Relative shift	Frequency [Hz]	Relative shift	Frequency [Hz]	Relative shift	Frequency [Hz]	Relative shift
1	89,4	-7,7%	89,1	-0,3%	89,6	0,6%	89,7	0,1%
2	130,0	-8,6%	121,1	-6,9%	120,6	-0,4%	119,3	-1,1%
3	183,4	-3,9%	171,8	-6,3%	173,6	1,0%	170,0	-2,0%
4	199,9	-5,5%	186,5	-6,7%	184,9	-0,9%	184,8	0,0%
5	325,0	-5,9%	299,3	-7,9%	298,8	-0,1%	297,6	-0,4%
6	361,1	-1,3%	336,6	-6,8%	340,0	1,0%	338,5	-0,4%
7	412,3	-5,6%	359,1	-12,9%	356,4	-0,8%	351,5	-1,4%
8	475,9	-2,3%	466,6	-2,0%	468,5	0,4%	467,8	-0,1%
9	512,8	-1,0%	486,8	-5,1%	487,6	0,2%	481,4	-1,3%
10	614,5	-6,9%	603,3	-1,8%	571,9	-5,2%	569,8	-0,4%
11	650,9	-2,9%	609,1	-6,4%	608,6	-0,1%	604,7	-0,6%
12	670,6	-2,6%	646,3	-3,6%	647,4	0,2%	639,9	-1,2%
13	810,4	-2,1%	662,9	-18,2%	666,1	0,5%	660,8	-0,8%
14	822,2	-2,6%	819,7	-0,3%	818,6	-0,1%	797,7	-2,6%
15	842,7	-6,8%	841,1	-0,2%	838,1	-0,4%	836,1	-0,2%
16	936,3	-1,4%	877,1	-6,3%	877,3	0,0%	871,4	-0,7%
17	962,1	-5,0%	962,3	0,0%	929,9	-3,4%	926,6	-0,4%
18	986,5	-6,2%	969,4	-1,7%	974,6	0,5%	949,4	-2,6%
19	1.037,6	-4,8%	1.034,2	-0,3%	1.030,9	-0,3%	1.025,5	-0,5%
		-4,4%		-4,9%		-0,4%		-0,9%

Table 2.2 – Results for soundboard with clamped periphery.

	Blank soundboard	Cross and X brace		Fully braced	
Mode	Frequency [Hz]	Frequency [Hz]	Relative shift	Frequency [Hz]	Relative shift
1	227,6	447,3	97%	558,1	25%
2	383,6	683,5	78%	854,4	25%
3	500,3	833,6	67%	974,1	17%
4	563,0	1009,2	79%	1183,3	17%
5	705,2	1176,8	67%	1420,2	21%
6	768,0	1318,7	72%	1485,6	13%
7	852,1	1448,0	70%	1818,2	26%
8	881,7	1727,6	96%	2016,3	17%
9	1108,7	1755,5	58%	2063,4	18%
			76%		20%

	C + X scalloped		C+X+T scalloped		C+X+T+F scalloped		Rounded edges	
Mode	Frequency [Hz]	Relative shift	Frequency [Hz]	Relative shift	Frequency [Hz]	Relative shift	Frequency [Hz]	Relative shift
1	490,8	-12%	404,2	-18%	392,3	-2,9%	389,5	-0,7%
2	769,6	-10%	681,2	-11%	650,7	-4,5%	646,6	-0,6%
3	842,9	-13%	829,2	-2%	825,0	-0,5%	816,2	-1,1%
4	1090,2	-8%	835,2	-23%	833,8	-0,2%	819,9	-1,7%
5	1231,8	-13%	1173,7	-5%	1159,5	-1,2%	1154,3	-0,4%
6	1280,1	-14%	1226,9	-4%	1202,7	-2,0%	1196,8	-0,5%
7	1617,4	-11%	1363,2	-16%	1331,7	-2,3%	1322,4	-0,7%
8	1625,2	-19%	1577,4	-3%	1542,6	-2,2%	1540,0	-0,2%
9	1902,6	-8%	1620,9	-15%	1620,7	0,0%	1605,1	-1,0%
		-12%		-11%		-2%		-1%

Before discussing these results, it should be remembered that wood is orthotropic, with properties changing with a number of parameters; the engineered woods have even different characteristics. So, being difficult to find accurate data to correctly simulate wood behavior, a sample material (Balsa wood) has been chosen among those in the software library, being the one with a Young modulus closest to the average value found for birch plywood that will be used in experimental part. That said, the focus will be on the relative shift more than on the mere frequencies.

- As we can see, blank soundboard frequencies are strongly increased with the bracing, thus allowing their reduction through the following material removal. The cross and X braces have a higher contribution in the stiffening, because of their position and thickness.
- The negative shifts in frequencies caused by the lightening of cross and x brace, are almost equal to the one due to tone bar scalloping; this proves the importance of the latter, that can cause such an important change, despite its small dimension. Besides, the area where it is positioned seems to be, looking at modal shapes obtained in part 2.1, of major importance.
- Finger bars only show a limited influence on frequencies.
- A further, subtle refinement can be achieved rounding the edges; this is the actual way luthiers follow for the very last adjustments.

2.3 CONSIDERATIONS

FEM simulation proved to be an ideal tool, because it allows to uncouple the effects of single bracing component, thus understanding how each element contributes to the final result, and how a change in geometry could affect the vibrational behavior.

The reason behind each strut of the X bracing layout has been explored, discovering the complex behavior that the soundboard assumes after the addition of this relatively simple pattern, which possibly is the most common in acoustic guitars for that reason.

The analysis of mode shapes before and after the material removal helps to understand in detail the meaning behind the ‘voicing’ process, which is considered one of the most important, demanding more than the others the mastery of the luthier: removing the right amount of wood from a given spot, allows to modify the mode shapes and frequencies in a very progressive way, to soften the excessive stiffness of the bracing. The relationship between the amount and position of the wood to be removed, and mode shape and natural frequencies that are consequently modified, has been explained for each step of the simulated manufacturing process, but of course a detailed description is very difficult to be find, even if expert artisans claim to have found their own empirical way.

As this simulation has shown, the material removal has a significant impact on the vibrational behavior, and certainly adds further complexity to the soundboard sound; indeed, scalloped braced guitars are considered the state of the art of acoustic guitar.

3 EXPERIMENTAL MEASUREMENTS

3.1 BLANK SOUNDBOARD

3.1.1 EXPERIMENTAL LAYOUT AND CONSIDERATIONS

A soundboard made of birch plywood has been built with the dimensions of a real acoustic guitar, cutting it from a panel and then refining its profile.



Figure 3.1 – Blank soundboard.

Constraining the soundboard in a given point would have prevented some of the mode shapes from being measured so, to avoid using different constraints, the soundboard has been suspended with a wire instead, with the following advantages:

- the specimen is actually in a free condition, being the constraint due to the wire negligible.
- No holes are needed, and the specimen remains untouched, which makes sense for a component of a musical instrument.
- Excitation in different points is easily realizable with an instrumented hammer (Fig 3.2). Accelerometers are not suitable for measuring the system response in this case, both because of damping induced by their wires, and because the weight they add to the system, which is lighter than part I aluminum plate, resulting in an even more noticeable change in the dynamic properties. Since the system is free, free body motion occur when it is excited, making not feasible the use of the laser head as well (its camera would not be able to follow the laser dot). Therefore, the system's output has been acquired indirectly, with a intensimetric probe (Fig 3.2).



Figure 3.2 a) – Intensimetric probe and instrumented hammer.

To be sure of avoiding nodal lines, the soundboard has been excited on several points (Fig 3.3): a central point near the position of the bridge (C37), two lateral points beside it (L37, L39), and two points at the top and at the bottom (C28 and C13, respectively).

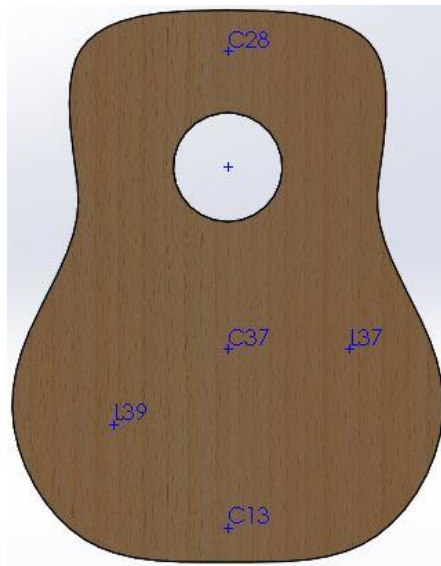


Figure 3.2 b) – Set of reference points on the blank soundboard.

Tests have been run in the anechoic chamber of the Department of Energy, Politecnico di Torino (Fig 3.4 a and b), to prevent the probe from measuring the environmental acoustic response, that would have altered the measured spectrum.

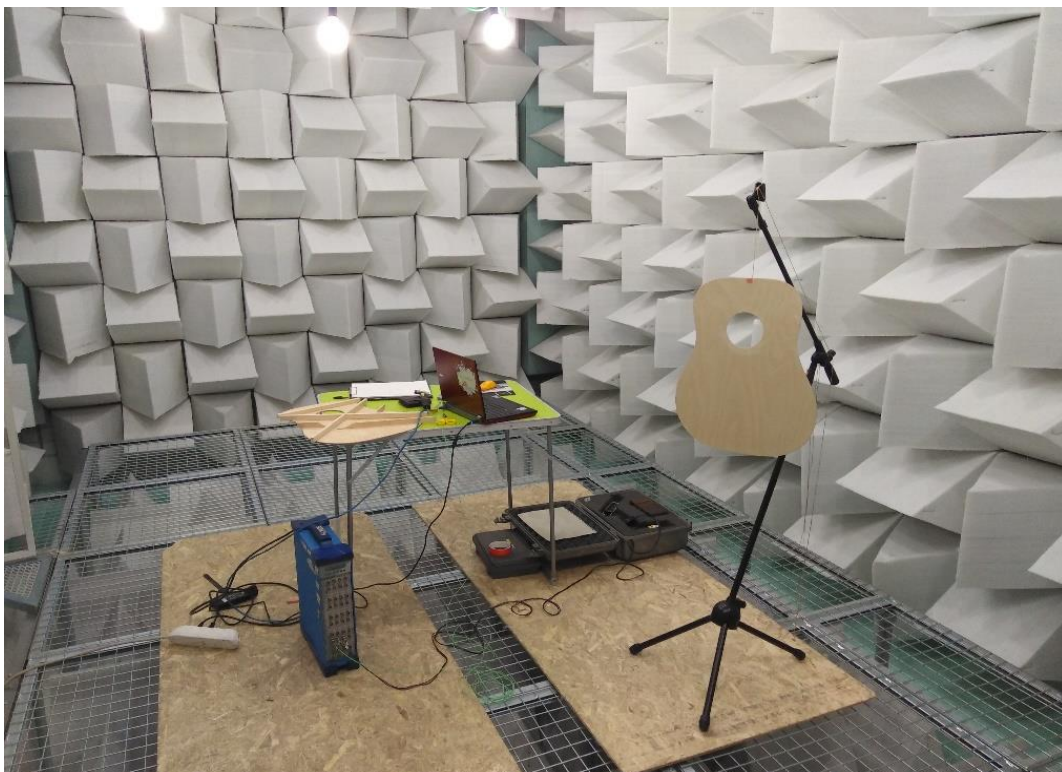


Figure 3.3 a) – The experimental setup in the anechoic chamber.
Thanks to Prof. Arianna Astolfi for having kindly allowed the use of the chamber.



Figure 3.3 b) – An example of the hammering and measuring during the tests.

Unlike Part I laboratory experience, where the power spectral density has been computed since only the output response of the system (measured by accelerometers) was available, the measurements of both input (through the instrumented hammer, connected to input port 1 in the OROS analyzer) and output (through the two probe microphones, connected to input ports 2 and 3) allowed the computation of the transfer function estimate.

Finally, it is important to remember that wood is an orthotropic material, with mechanical properties strongly changing along longitudinal, radial, tangential directions, with reference to fiber and annual rings orientation; besides, wood type, aging time, moisture content, cut direction from which it has been obtained, even the presence of knots, have a noticeable influence on its properties. When the so-called engineered woods (plywood, laminated board, etc.) are used, even manufacturing parameters must be taken into account, for example the number of layers, and their relative orientation. For that reason, Young's modulus for the used plywood couldn't be estimated, and a direct comparison between FEM and measured frequencies cannot be performed.

3.1.2 TRANSFER FUNCTION

A measure has been taken for each of the points in Fig 3.3, with the following procedure:

- Auto scale of the probe output with some repeated hits with the hammer.
- A 60 seconds measurement of the sound pressure level, hammering the given point.
- The computation of the system's transfer function from the exported input and output signals, through MATLAB.

The TF for central point 'C37' is reported below (Fig 3.4), with a data tip for the clearest resonances.

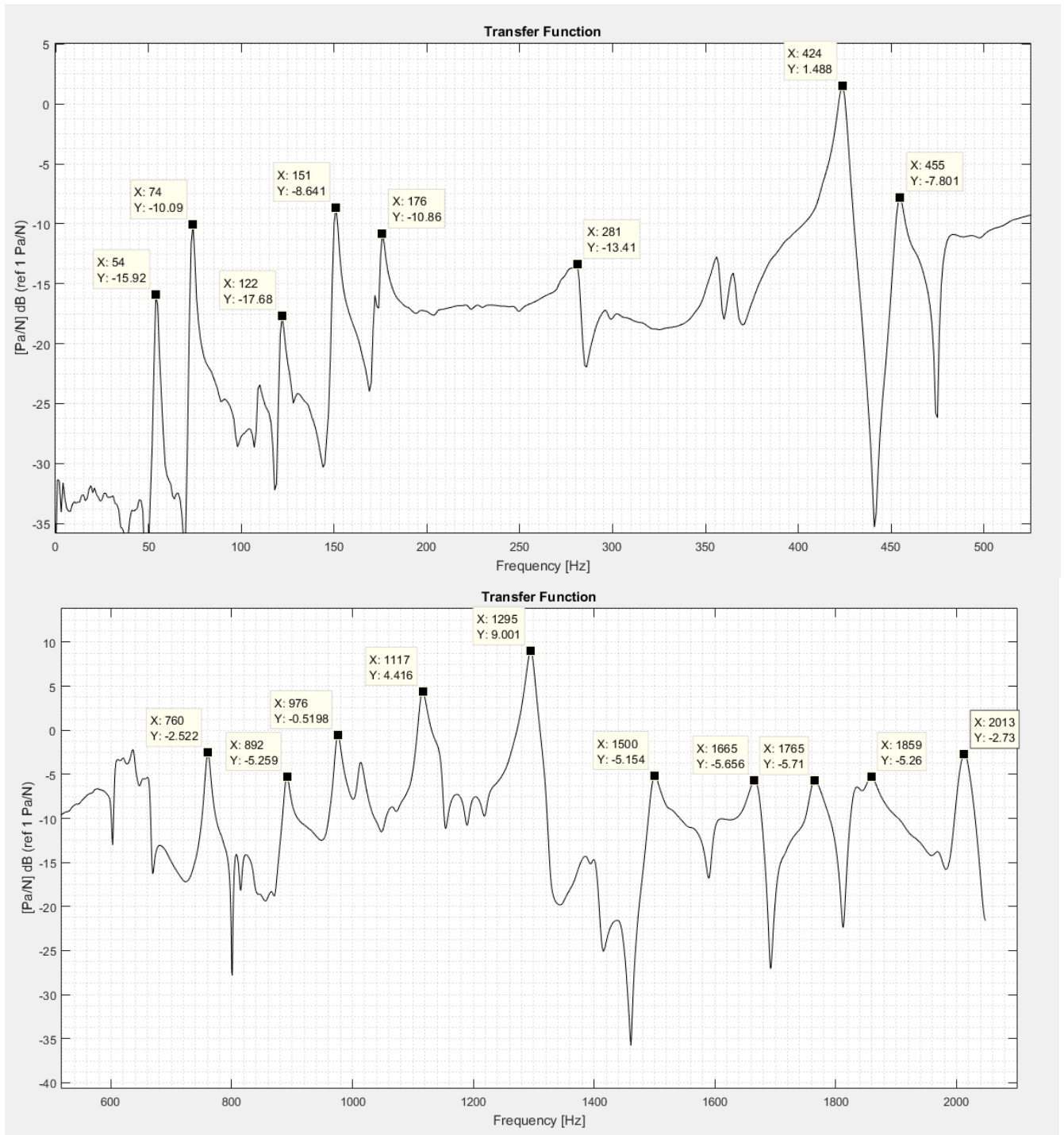


Figure 3.4 – TF of blank soundboard, excited in central point C37.

A number of natural frequencies can be easily seen, and other minor ones can be spotted in between them; anti-resonances frequencies are evident, too. There are a couple of frequency ranges in which the response is flatter, without clear resonances, for example 200-250 Hz and 500-700 Hz.

The previous transfer function plot is now compared (Fig 3.5) with the one obtained exciting the system in the point beside it, 'L37', and the one on the top of the soundhole 'C28'.

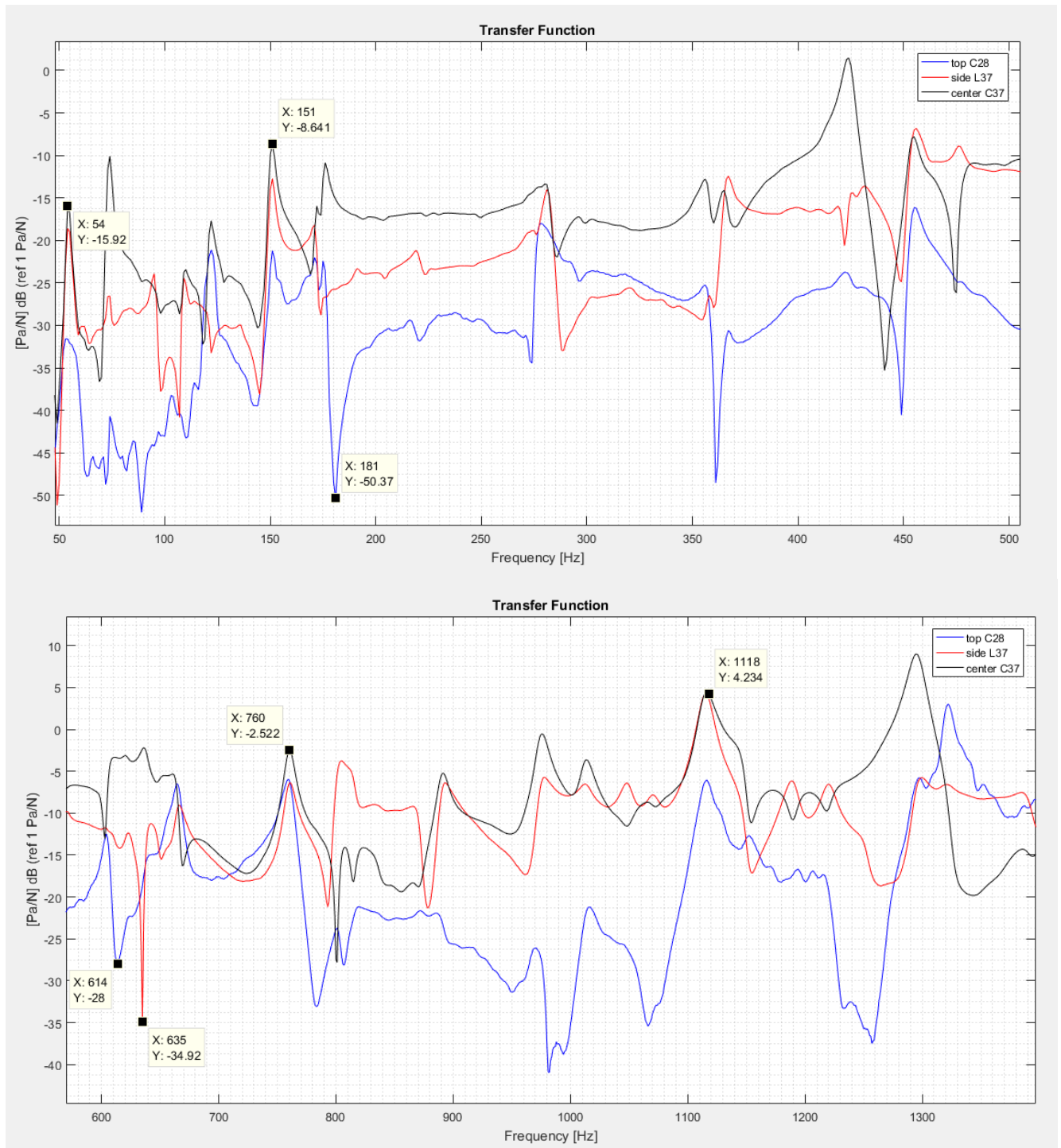


Figure 3.5 – Superimposition of TF of blank soundboard, excited in central point C37, L37 on the side and C28 above the soundhole.

As in part I, measuring the output in more than one point gives helpful information: main resonances are confirmed (54, 151, 760 Hz), while minor ones we couldn't be sure of, or ranges that

appeared flat, are now clarified by the presence of anti-resonances for side and top points response (for example 181, 361 Hz and the 600-700 Hz range).

A further comparison is done between the usual central point 'C37', and the more peripheral 'L39' and 'C13', respectively on the side and at the bottom of the board (Fig 3.6).

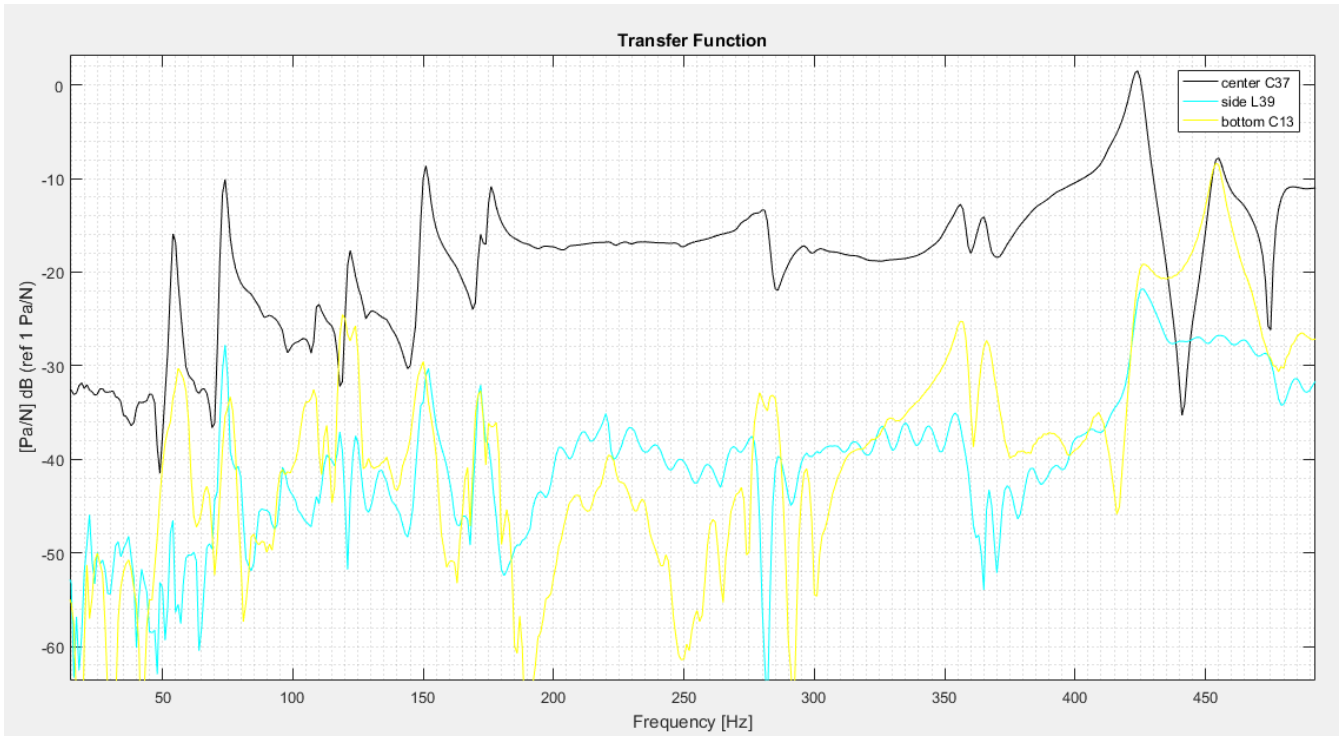


Figure 3.6 – Superimposition of TF of blank soundboard, excited in central point C37, L39 on the side, and C13 in the lower part.

The TF is much less clear, probably because hitting these points with the hammer caused the soundboard to swing and rotate, making necessary to stop it repeatedly during the measure to bring it back to its initial position, thus affecting the response. Moreover, a lower magnitude can be noticed, because these areas fall on nodal lines more likely than central ones (see Fig 2.6).

3.2 BRACED SUNDBOARD

Wooden struts with dimensions and thicknesses specified before, have been cut at the proper length and glued to the top, on which the bracing had been drawn, in several steps.



Figure 3.7 – Bracing pattern reported on the soundboard; a phase of the gluing.

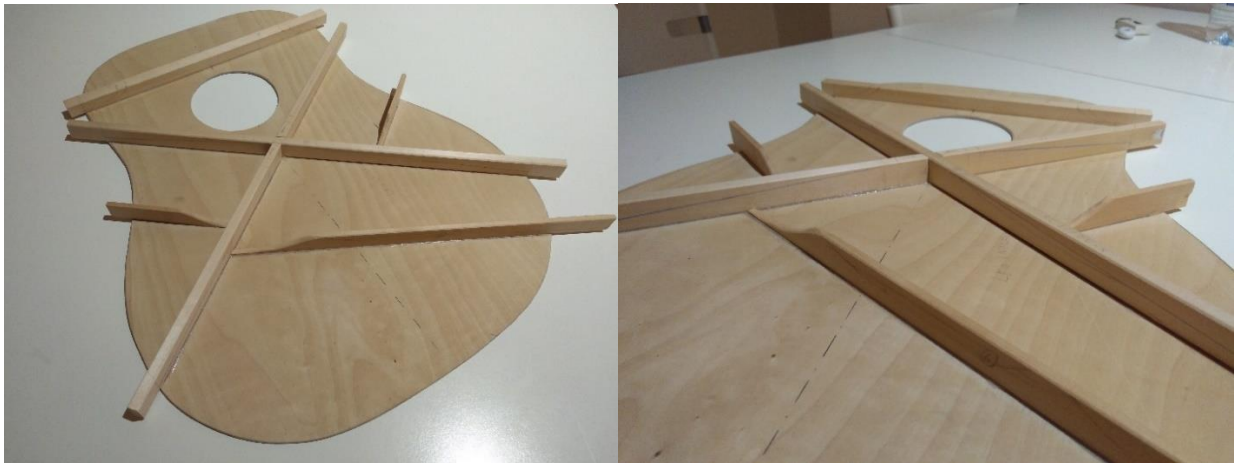


Figure 3.8 – The final braced top; the struts are protruding on the outside and already partially lightened on the inside only to ease the successive shaping with the chisel.

The soundboard, noticeably heavier and stiffer, has been tested in the anechoic chamber following the same procedure described for the blank top; this time, however, the higher complexity of the object (a different sound for each area described by the bracing could be perceived even by hear) required a higher number of measurement points, namely twelve (Fig 3.9), to fully describe its characteristics.

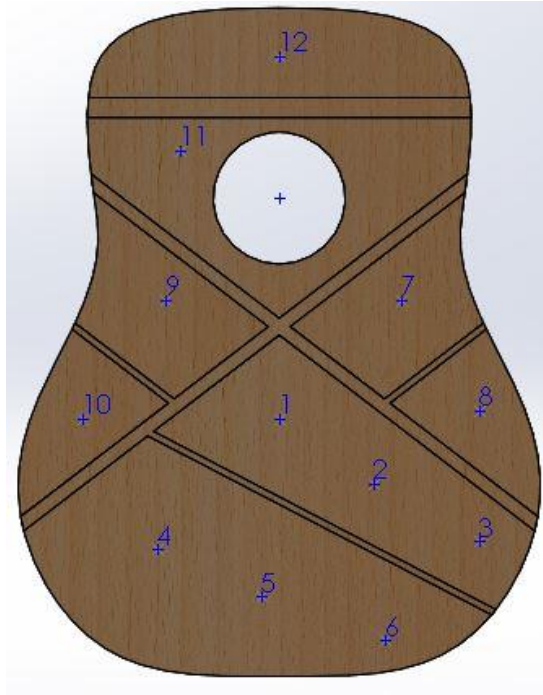


Figure 3.9 – Set of points taken as reference in the excitation of the braced soundboard.

The response of point 1 (Fig 3.10) will be taken as a reference, because of its central position, where the bridge should exert the string force.

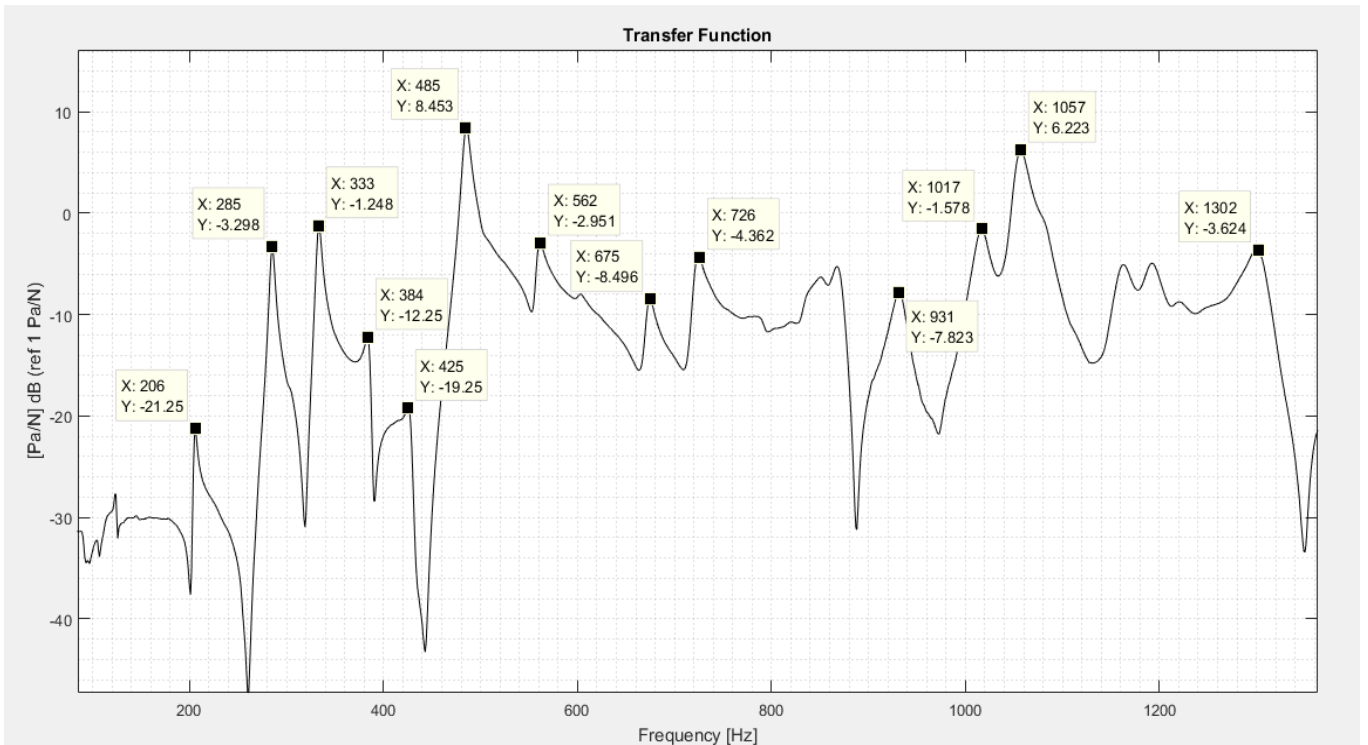


Figure 3.10 – TF of the braced soundboard, excited in central point 1.

Besides the usual presence of resonance and anti-resonances, it is useful to compare the transfer function of the braced soundboard with the blank one, in the analogous central point (Fig 3.11).

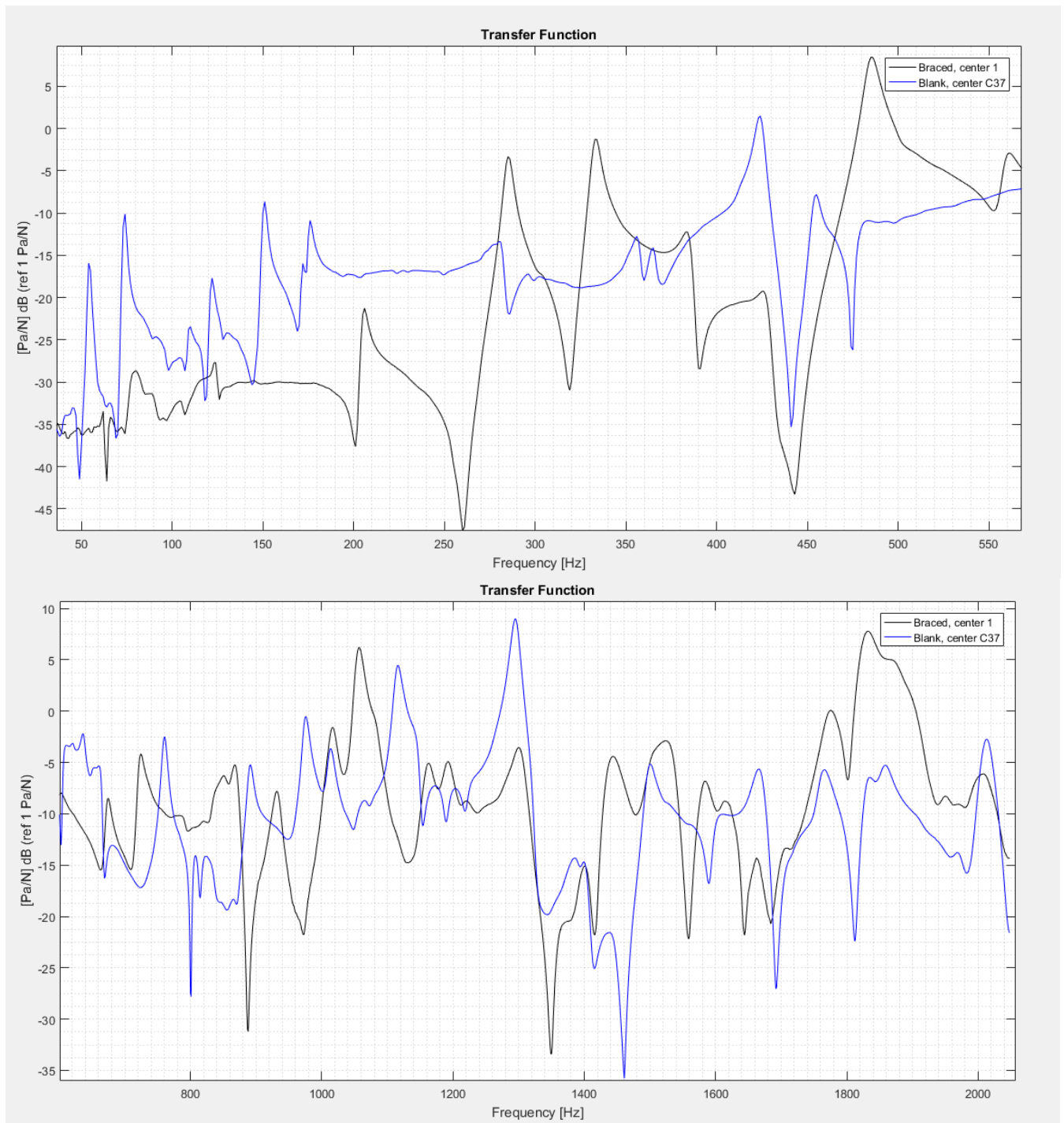


Figure 3.11 – Comparison between blank and braced soundboard TF, both excited in a central point.

From the comparison, we can notice that:

- Braced top response is generally higher than blank's one.
- Natural frequencies are higher, for example the range 50-200 Hz in which the blank soundboard has 5 resonances, is quite flat in the braced soundboard, with the first clear resonance at 200 Hz.

- The new transfer function, especially below 1200 Hz, has more distinct resonant frequencies, usually well separated by an anti-resonance; on the contrary, the blank top often has some less defined natural frequencies, or flat ranges with low response.
- Despite the strong geometric difference between the two boards, the response is rather similar in the range 1700-2000 Hz, aside from difference in magnitude; this is probably due to the fact that high frequency modes involve the movement of peripheric areas, smaller than the areas enclosed by the bracing branches, so less affected by them.

A comparison between the response of different points of the braced soundboard can now be proposed. The two areas delimited by the tone bar are rather large, so we expect the response to change within them; comparison between the TF of point 1, 2 and 3 is reported in Fig 3.12. Even if most of the resonances are visible in all the responses, the behavior between 500 and 1000 Hz becomes quite different, taking into account that these points are only a few centimeters apart. Points 4,5 and 6 show a similar trend.

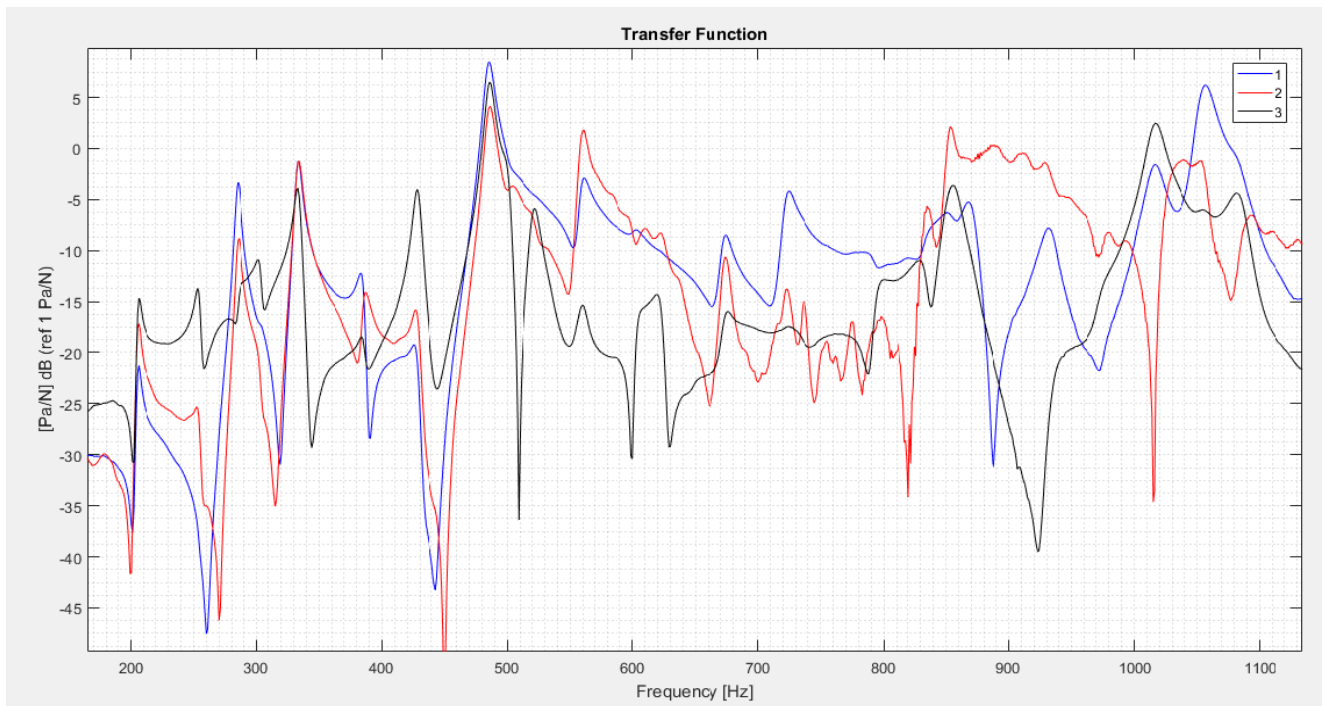


Figure 3.12 – TF of braced soundboard excited in point 1,2 and 3.

Comparing point 1 and 5 (Fig 3.13), both almost on the vertical axis on the soundboard, we can notice a much higher and evenly spaced response from point 5, almost in the whole range of interest, thus confirming the importance of larger areas of the soundboard in the sound emission.

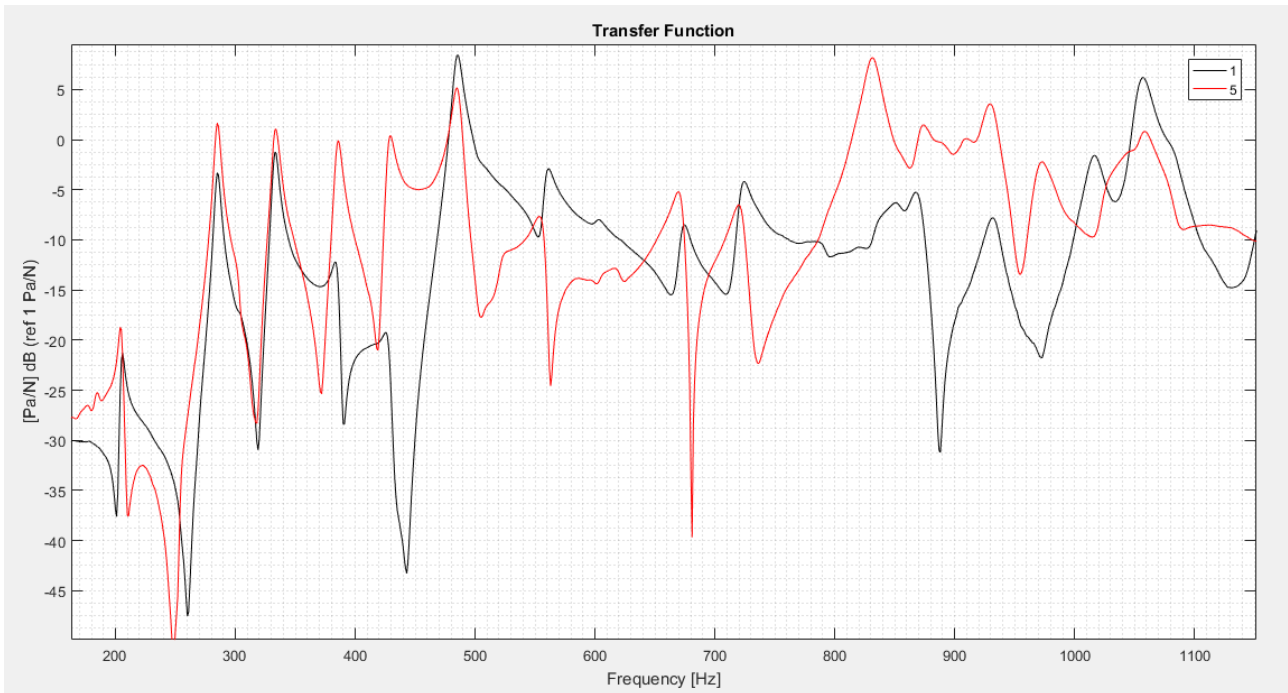


Figure 3.13 – Superimposition of TF of braced soundboard excited in point 1 and 5, both on the middle axis but at different heights.

A final comparison can be done between point 5 in the bottom part, point 7 in one of the lateral areas, and point 12 above the cross bar (Fig 3.14).

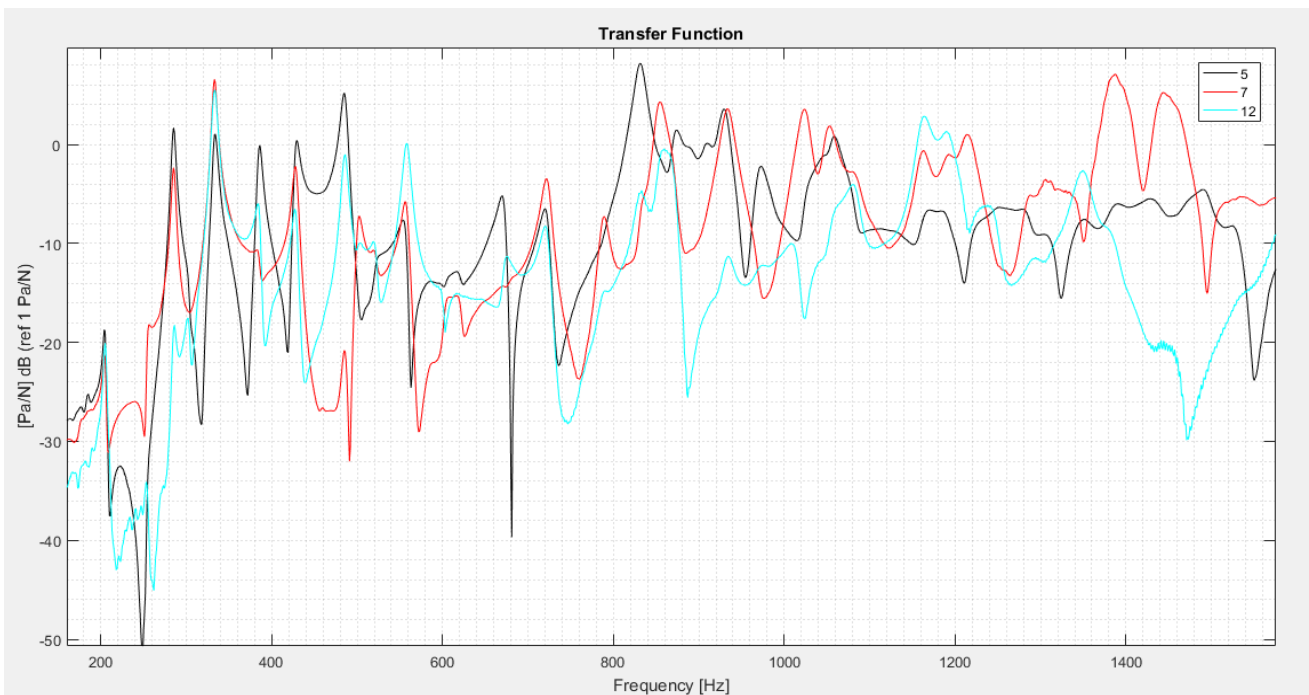


Figure 3.14 - Superimposition of TF of braced soundboard excited in central point 5, 7 on the side, and 12 above the soundhole.

Point 7 response integrates the lower response of point 5 above 1000 Hz, proving again the importance to have differently sized areas. Moreover, the top part of the soundboard, represented by

point 12, does not participate with more resonances nor with higher magnitude, confirming the minor importance of the area above the soundhole.

A second evidence that side areas are now more important, can be observed by looking at Fig 3.15, where transfer functions of side point L37 of the blank soundboard, and of side point 7 from braced one have been superimposed. We can easily see how the lateral point in braced case shows more resonances, without the flat areas that the blank soundboard has, besides of course having a higher magnitude in response.

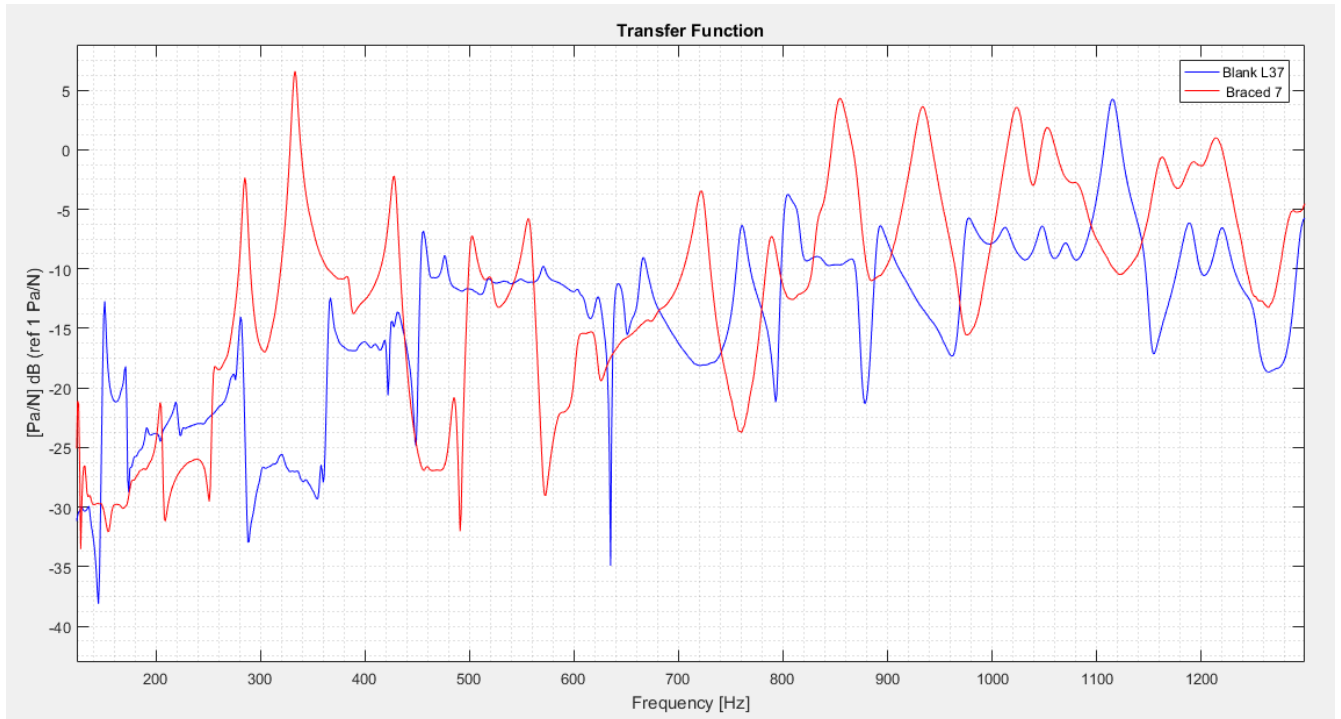


Figure 3.15 – Comparison of TF of the blank and braced soundboard, excited in lateral point L37 and 7 respectively.

3.3 LIGHTENED AND SCALLOPED BRACED SOUNDBOARD

Material has been progressively removed using a chisel and sandpaper, reaching the result represented in Fig 3.16. Since the soundboard is made of plywood, it is much stiffer than a wooden one and with bracing increasing its stiffness even more, it became evident, by simply tapping it, that a noticeable quantity of wood should have been removed.



Figure 3.16 – A detail of the scalloped bracing.

It is important to say that the previous measurements, on the blank and braced soundboard, were comparable also as far as amplitude is concerned, because they have been taken in the same measuring session; as the intensimetric probe has not been calibrated, these last measurements may not be perfectly comparable with previous ones, since they have been taken in a separate session, so with different environmental condition and surely with a different distance between the probe and the soundboard.

The different frequency content for different points can still be noticed: figure 3.17 compares points 1 and 5, while figure 3.18 adds the response of lateral point 9. Bottom point 5 and lateral point 9 confirm their higher contribution in low and high frequency range, respectively.

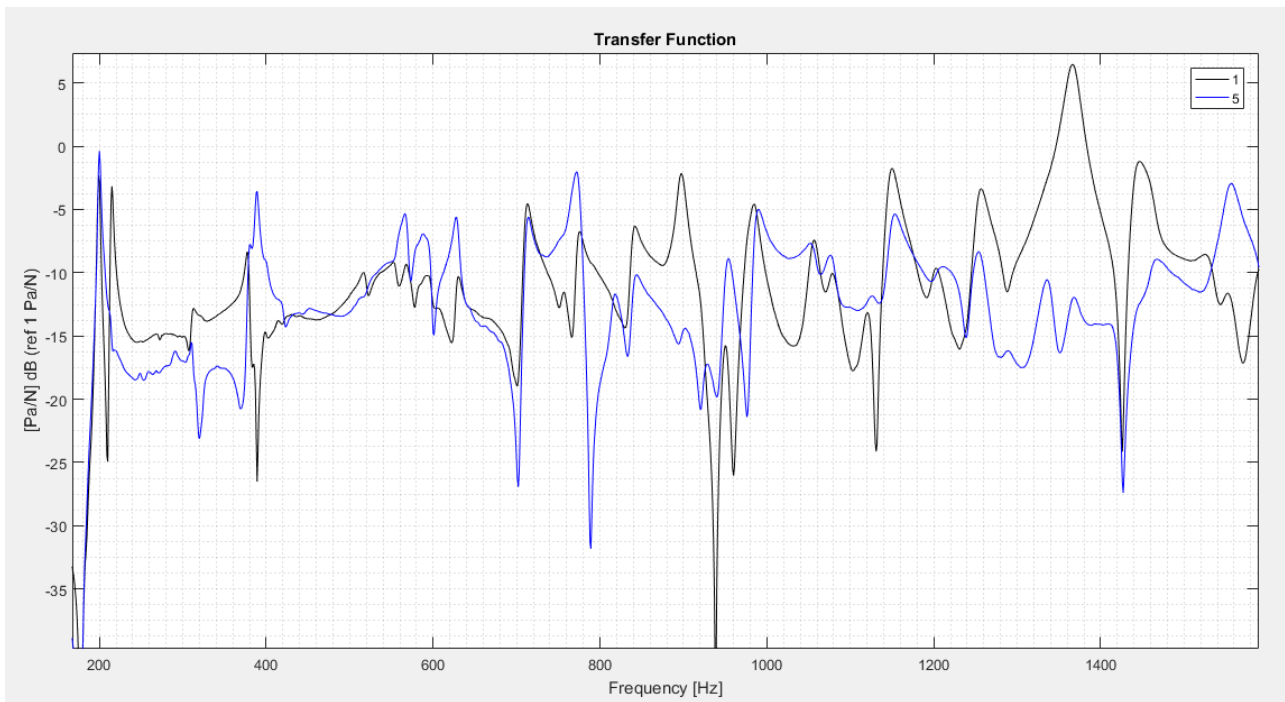


Figure 3.17 – Superimposition of TF of scalloped soundboard, excited in points 1 and 5.

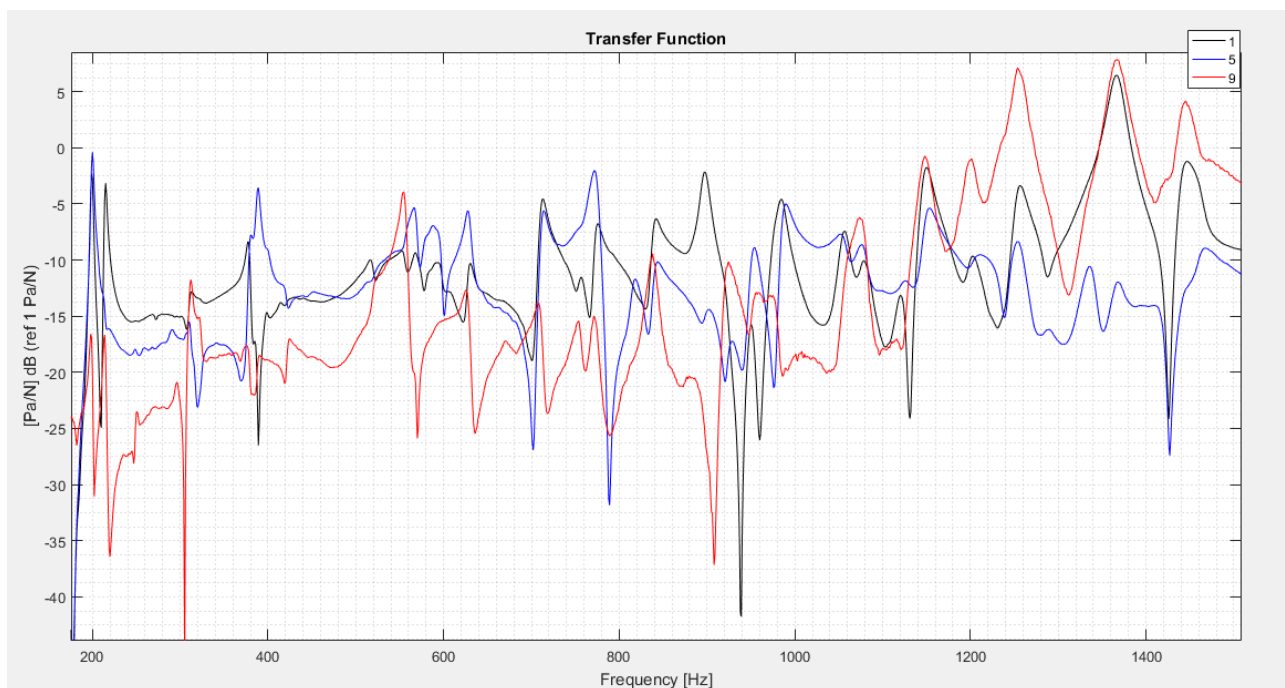


Figure 3.18 - Superimposition of TF of scalloped soundboard, excited in points 1, 5 and 9.

A comparison between the straight braced top and the scalloped one must be done too, to see how resonance frequencies changed; figures 3.19 A B and C compare the two soundboard responses in three different points.

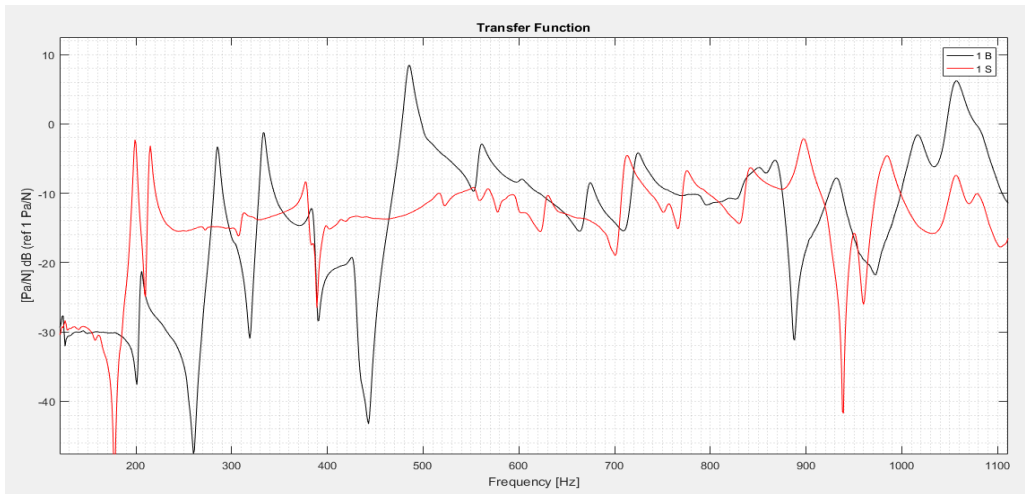


Figure 3.19 A – Comparison between braced and scalloped soundboard, both excited in point 1.

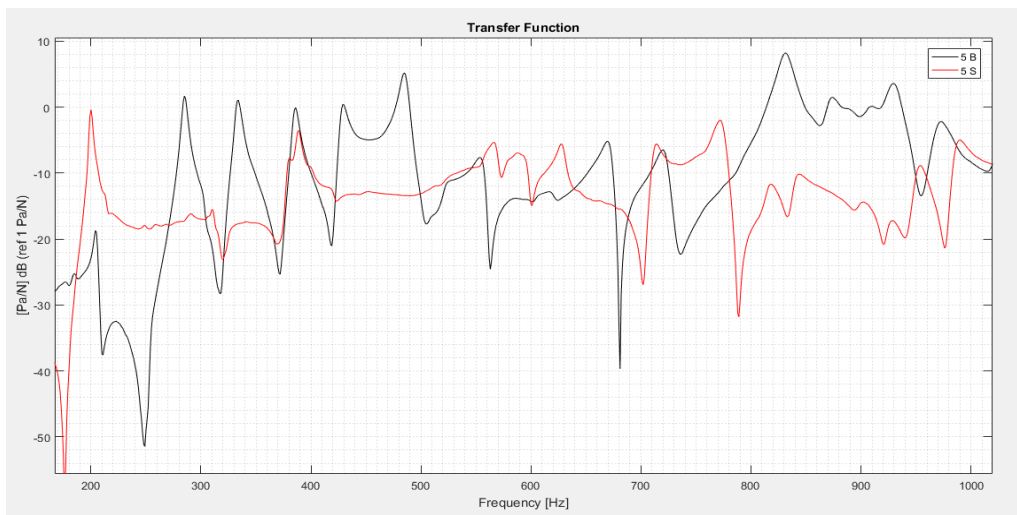


Figure 3.19 B - Comparison between braced and scalloped soundboard, both excited in point 5.

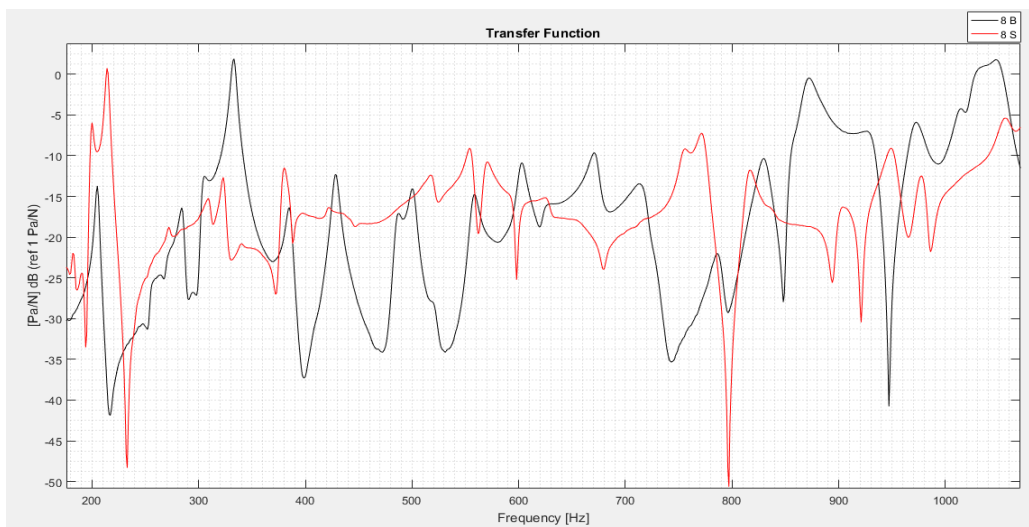


Figure 3.19 C - Comparison between braced and scalloped soundboard, both excited in point 8.

Two important conclusions can be drawn:

- Natural frequencies have shifted downwards, because stiffness of the plate has been strongly reduced. This is particularly evident for the fundamental frequency, as the process is mainly aimed to 'restore' a good response at lower frequencies, that the addition of the bracing weakened.
- Response in the straight bracing case is rather even, with resonance frequencies spread almost regularly in the whole frequency range (this is particularly evident in Fig 3.19 B and C), most of them only 70-80 Hz apart from the previous and subsequent ones. On the contrary, the scalloped bracing rearranged the natural frequencies spacing them apart, thus reintroducing some of the flat response areas that could be seen in the blank top behavior (range 250-350 Hz or 400-500 Hz in previous figures). The logic behind this is probably the following: to act as resonator, the soundboard should have a lively response in some given ranges of the spectrum more than in others, to emphasize only certain frequencies of the string vibrations; if, instead, the soundboard has a number of resonances almost in every frequency range, the very concept of resonator, i.e. something that strengthen some frequencies while removing others, stops making sense.

3.4 FINAL RESULTS AND CONSIDERATIONS

The evolution of the response through the three stages is summarized in figure 3.20.

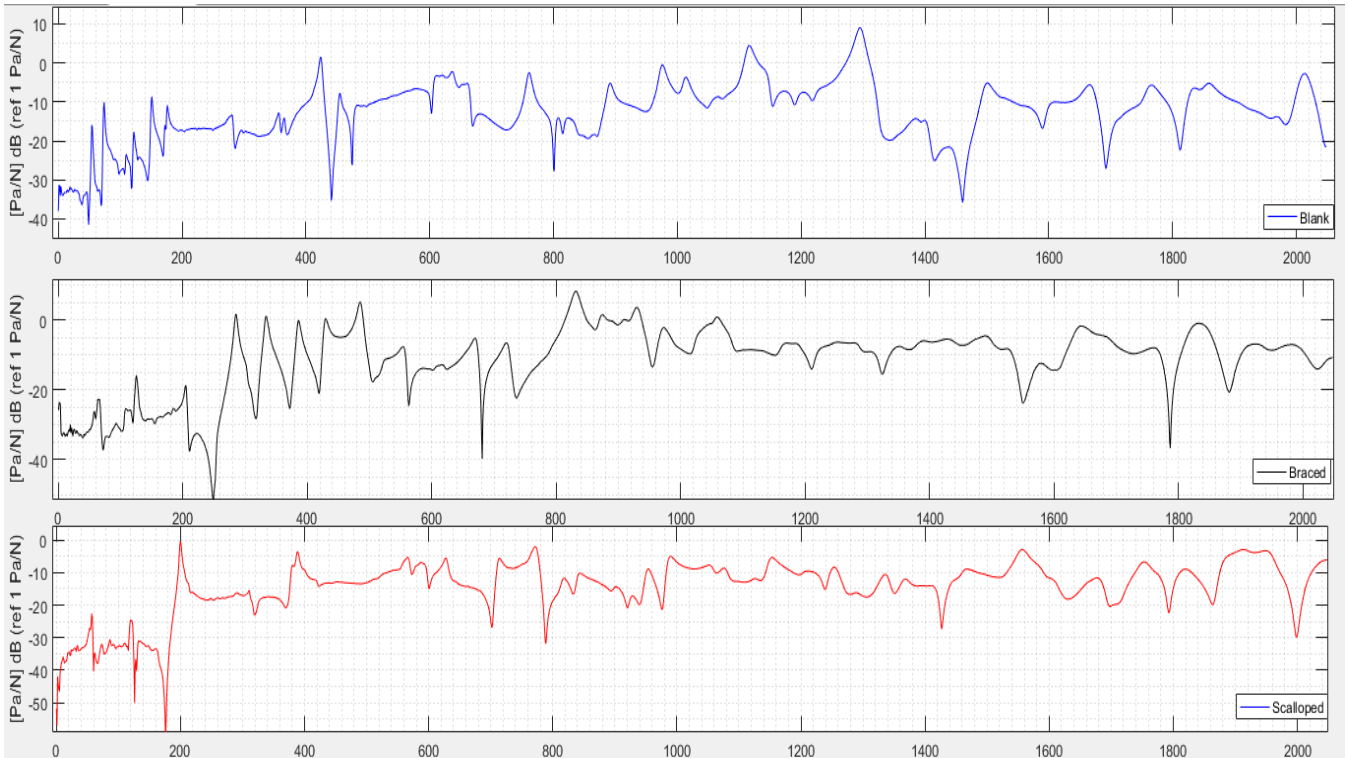


Figure 3.20 A – The tree transfer functions in the whole frequency range.

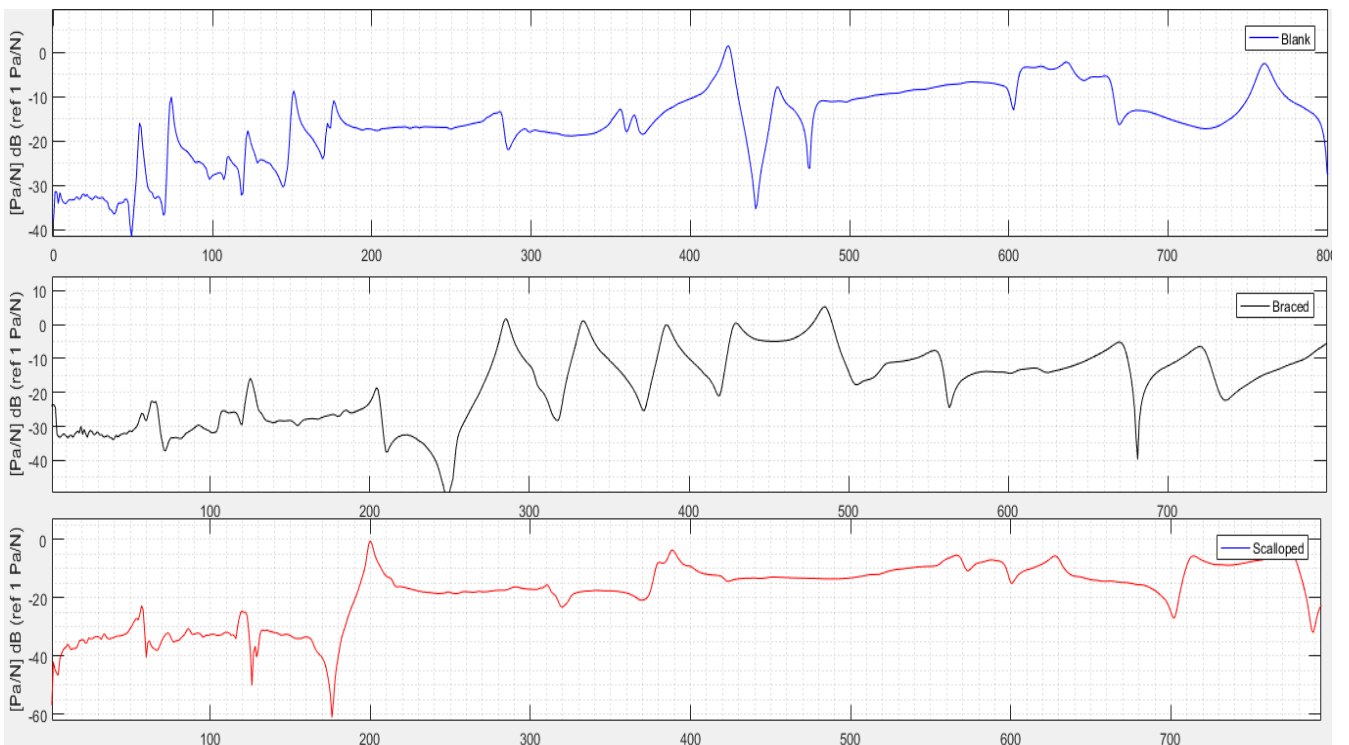


Figure 3.20 B – A detail of the lower range.

The frequencies of the most evident resonance peaks for the three cases are reported in Table 3.1.

Table 3.1 – Natural frequencies in [Hz].

Blank	Braced	Scalloped
54	285	200
74	333	214
122	386	389
151	429	628
176	486	713
424	555	772
456	722	843
761	829	898
891	932	949
975	1022	991
1116	1058	1151
1296	1388	1258

These final results can be used to recap the whole process and repeat conclusions we have reached. Blank soundboard had several natural frequencies in the low range (we can count five of them below 200 Hz in Tab 3.1), some flatter areas and then other noticeable peaks; this very flexible piece of plywood became much stiffer and heavier as bracing struts were applied, with a number of new resonances, almost evenly spaced (see Tab 3.1 or the TF detail in 3.20 B), in the range below 800 Hz, penalizing the low band as the first resonance occurs at 285 Hz.

Because the lack of the middle-bass response in the sound of a guitar (especially a dreadnought type) would create an incomplete, shallow sound, the fully braced soundboard must be enlightened and scalloped: the behavior under the 1000 Hz is strongly affected, as a glance at Fig 3.20 B can easily show.

Even though the upper part (above 1200 Hz) of the three transfer functions is not superimposable, the effect of the addition of the bracing and the following material removal is almost absent in this range, the explanation being that higher mode shapes are characterized by smaller areas, that are not affected by the regions delimited by the bracing pattern.

The practical difficulty of removing wood using the chisel, after a reduced thickness was achieved, acted as limiting factor, stopping the process with a fundamental frequency approximately tuned at 200 Hz, i.e. a $G\#_3$ note; an expert artisan working with proper tools, and a less fibrous, higher quality wood, would have allowed a further and certainly more accurate material removal, with a fundamental at around 100-110 Hz (i.e. a G_2 , more than an octave below). Besides, it must be remembered that plywood is much stiffer than a plate of fine tonewood, this being another strong factor preventing the achievement of low resonant frequencies.

4 CONCLUSIONS AND POSSIBLE APPLICATIONS

This part of the thesis showed how much the bracing addition and the successive voicing process has a substantial impact on the soundboard response, and this leads to some consideration about guitars manufacturing.

Laminated and solid soundboards manufacturing

A guitar with a plywood top is typically a very cheap, entry-level product, so the complex and time-demanding tuning process of the soundboard is not executed; a bracing structure is however required, and often the combination of high stiffness of the plywood and the thick, straight bracing, create a poorly sounding instrument, with very low soundboard response and a ‘boxy’ sound. A simple cure to this problem can be a more accurate design of the bracing, instead of its subsequent refinement piece by piece:

- because the laminated wood is already rather strong, struts can be much thinner and lighter than they usually are, avoiding ‘overbuilding’ the product only to be on the safe side; obviously, the structural resistance must be guaranteed in any case.
- If a scalloped predetermined profile is designed with modern tools (for example extensive FEM simulations, like those used in chapter 2), good compromise results can be achieved for mass-produced soundboards, taking into account also the fact that laminated wood mechanical properties are less variable than solid wood ones.
- The previous consideration, combined with the cost constraints for products of this level, oriented towards quantities and robustness, make the voicing process neither suitable nor reasonable.

It is rather unanimous that an acoustic guitar worth its name should have a solid tonewood soundboard, because, as explained in Chapter 1, the tonal quality of the material itself is fundamental for the roles that this component has in the instrument. The other side of the coin is the lower mechanical properties and their variability from one piece of wood to another, which makes the voicing of the soundboard so important.

Although a solid top with straight bracing would probably still sound way better than a laminated one, not scalloping and voicing it would be a waste of such a fine material, losing the chance to bring its acoustic qualities to life. So, if a proper design of bracing structure is enough for laminated soundboards, for solid ones it should be matched with the creation of scalloped profiles and the tuning of each soundboard.

Still, an advanced design of bracing pattern, comprehensive of geometric and dimensional detailed definition, would represent a huge advantage in the manufacturing of this instruments: the more the bracing characteristics are optimized, the less material should be removed in the tuning phase, thus speeding up the process, combining time and results with increased efficiency.

As it became evident, the industrial production of a musical instrument that, by its nature, needs a handcraft attention for each particular specimen, can achieve excellent results only if modern technologies, artisan knowledges, and industrial engineering solutions are cleverly combined.

An automation hypothesis

The problem of voicing a guitar soundboard is typically solved by luthiers with their own empirical methods, often changing from case to case, and with the only help of their experience. Their results are examples of the highest craftsmanship and excellent sounding musical instruments, according to many, not even comparable with any mass-produced guitar, even if it is a high range one. This statement is probably confirmed by the results of this study: the variability of wood mechanical properties, the number of geometric parameters to control, the need of great precision and the general complexity of the process, creates a problem that seems only solvable by a highly experienced and skilled artisan.

Despite these difficulties, in my opinion a complete and systematic study of the phenomenon may lead to its full comprehension, and possibly to the automation of the whole process, if each stage is designed with extreme attention. At that point, handmade guitars would still be the state of the art, and probably remain every player's dream, but factory-made ones would earn a huge improvement in sound quality that would certainly not remain unnoticed to the market, as the difference in price between an artisan instrument and a mass-produced one is so high, that the latter will certainly remain the only choice for most buyers.

In this second part of thesis, the effects of the bracing and the problem of soundboard tuning have been approached with scientific methods, as FEM simulation and transfer function analysis, trying to reach a more general knowledge of how the bracing geometry and material removal affect the dynamics of the soundboard.

These tools are certainly more powerful than human senses, and unlike them, they provide an objective, clear and repeatable results. The material removal process as well, however skilled the luthier performing it may be, is still not as repeatable as a CNC machine code.

In an ideal automated process, once the natural frequencies of the soundboard are obtained, an algorithm should identify them and decide where to remove material in order to change them, guiding a CNC milling machine to do so. Of course, the only relatively simple steps would be the frequencies measurements and the CNC operations, while the algorithm in between them should have the considerable duty to substitute, or anyway emulate, the luthier's knowledge, with difficulties that can be easily imagined.

If such a project should become feasible in the future, guitars could be manufactured industrially and still produce a sound close to the warm, vibrating and lively one that is now a prerogative of handcrafted instruments.

BIBLIOGRAPHY

- [1] Genta G, *Vibration of structures and machines*, Springer, 1999, chapter 2.3.
- [2] Blevins, Robert D., *Formulas for natural frequencies and mode shapes*, Van Nostrand Reinhold Company, 1979, chapters 11 and 13.
- [3] Fasana A., Marchesiello S., *Meccanica delle vibrazioni*, Clut, 2006, chapters 4 and 5.
- [4] Rossing, Thomas D., *The science of string instruments*, Springer, 2010, chapters 2 and 3.